AD-A074 738 ARMY MILITARY PERSONNEL CENTER ALEXANDRIA VA F/G 13/13
STRUCTURAL PROPERTIES OF NB3SN DIFFUSION LAYERS FABRICATED ON S--ETC(U)
SEP 79 J F DEBROUX

UNCLASSIFIED NL

1 OF 2
ADA 074738

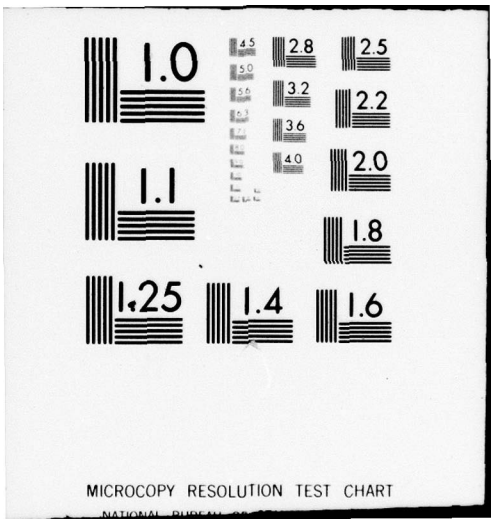
1.0
1.1
1.25
1.4
1.6
1.8
2.0
2.2
2.5
2.8
3.2
3.6
4.0
4.5
5.0
5.6
6.3
MICROCOPY RESOLUTION TEST CHART

STRUCTURAL PROPERTIES OF Nb_3Sn DIFFUSION LAYERS FABRICATED ON SINGLE CRYSTAL Nb SUBSTRATES

by

JAMES FREDERICK DeBROUX

S.M. Final rept., 9/79

4 Sep 79

147 p.

SECURITY CLASSIFICATION OF THIS PAGE (When Data Entered) UNCLASSIFIED

REPORT DOCUMENTATION PAGE

READ INSTRUCTIONS BEFORE COMPLETING FORM

1. REPORT NUMBER

2. GOVT ACCESSION NO.

3. RECIPIENT'S CATALOG NUMBER

4. TITLE (and Subtitle)
STRUCTURAL PROPERTIES OF Nb_3Sn DIFFUSION LAYERS FABRICATED ON SINGLE CRYSTAL Nb SUBSTRATES.

5. TYPE OF REPORT & PERIOD COVERED
Final report: 4 SEP 79

6. PERFORMING ORG. REPORT NUMBER

7. AUTHOR(s)
James F. DeBroux

8. CONTRACT OR GRANT NUMBER(s)

9. PERFORMING ORGANIZATION NAME AND ADDRESS
Student, HQDA, MILPERCEN (DAPC-OPP-E)
200 Stovall Street
Alexandria, VA 22332

10. PROGRAM ELEMENT, PROJECT, TASK AREA & WORK UNIT NUMBERS

11. CONTROLLING OFFICE NAME AND ADDRESS
HQDA, MILPERCEN, ATTN: DAPC-OPP-E
200 Stovall Street
Alexandria, VA 22332

12. REPORT DATE
4 September 1979

13. NUMBER OF PAGES
143

14. MONITORING AGENCY NAME & ADDRESS (if different from Controlling Office)

15. SECURITY CLASS. (of this report)
unclassified

15a. DECLASSIFICATION/DOWNGRADING SCHEDULE

16. DISTRIBUTION STATEMENT (of this Report)
Approved for public release; distribution unlimited.

17. DISTRIBUTION STATEMENT (of the abstract entered in Block 20, if different from Report)

18. SUPPLEMENTARY NOTES
This document is a thesis submitted to the Massachusetts Institute of Technology in partial fulfillment of the requirements for the Degree of Master of Science.

19. KEY WORDS (Continue on reverse side if necessary and identify by block number)
Structure-Superconducting Materials
Diffusion Layer Properties
Nb_3Sn

(or 1 to 17 micrometers)

20. ABSTRACT (Continue on reverse side if necessary and identify by block number)
The structural properties of Nb_3Sn diffusion layers fabricated on oriented single crystal Nb substrates exhibit systematic behaviors based on substrate orientation which result from interactions between the substrates and A15 overlayers. Preferred orientation of the diffusion layers is confirmed by X-ray and electron diffraction measurements. Within the bulk of a specific Nb(hkl) substrate layer, the preferred orientation appears to be a function of layer thickness for the range of thicknesses studied. (~1 to 17 μm).

DD FORM 1 JAN 73 1473 EDITION OF 1 NOV 65 IS OBSOLETE

UNCLASSIFIED

SECURITY CLASSIFICATION OF THIS PAGE (When Data Entered)

Block 20 cont.

It is believed to develop over distance due to a competition between the growth region orientation at the advancing interface (required by lattice registry of the bcc and A15 lattices) and the tendency of Nb_3Sn layers toward a natural growth direction, A15(100); this competition is moderated by in situ annealing of the Nb_3Sn as growth advances. Consistent with this model is the fact that surface preferred orientation of a diffusion layer on a given Nb(hkl) substrate, both for as-grown surfaces and for internal surfaces exposed by etching, appears to be a function of net layer thickness.

Layer thickness regimes have been identified and associated with variations in diffusion layer properties according to the orientation of the underlying Nb substrate. These thickness regime behaviors and the A15 preferred orientation dependence on substrate (hkl) suggest that a diffusion layer on a given Nb(hkl) substrate orientation has a specific "personality profile". Trends in T_c and lattice parameter as a function of layer tin composition suggest the possibility of orientation effects in Nb-Sn nucleation and growth kinetics, perhaps also with implications for phase equilibria and the ordering effects of in situ annealing.

Scanning electron microscopy shows microstructural variation among diffusion layer samples of differing A15 layer thicknesses on the same niobium substrate orientation, between layers on differing substrate orientations fabricated under the same conditions and to the same thickness, and between samples of different substrate geometry. Also observed is a similarity between the microstructures of the thinnest layer's surface and the advancing interface of the thickest layer.

The existence of differences in properties of diffusion layer Nb_3Sn exhibiting preferred orientation arising from the influence of niobium substrate orientation, and observations that these differences show variation with processing conditions, suggest that the tradeoffs between fabrication and layer quality are dramatic.

STRUCTURAL PROPERTIES OF Nb_3Sn DIFFUSION LAYERS FABRICATED ON SINGLE CRYSTAL Nb SUBSTRATES

CPT James F. DeBroux
HQDA, MILPERCEN (DAPC-OPP-E)
200 Stovall Street
Alexandria, VA 22332

Final report - 4 September 1979

Approved for public release; distribution unlimited.

A thesis submitted to the Massachusetts Institute of Technology in partial fulfillment of the requirements for the degree of Master of Science.

STRUCTURAL PROPERTIES OF Nb_3Sn DIFFUSION LAYERS FABRICATED ON SINGLE CRYSTAL Nb SUBSTRATES

by

JAMES FREDERICK DeBROUX

B.S., United States Military Academy
(1973)

SUBMITTED IN PARTIAL FULFILLMENT
OF THE REQUIREMENTS FOR THE
DEGREE OF

MASTER OF SCIENCE

at the

MASSACHUSETTS INSTITUTE OF TECHNOLOGY

September 1979

Signature of Author. . . . . James F. DeBroux . . . . .
Department of Physics, September 4, 1979

Certified by . . . . Margaret MacVicar . . . . . .
Thesis Supervisor

Accepted by . . . . . .
Chairman, Department Committee

STRUCTURAL PROPERTIES OF Nb_3Sn DIFFUSION LAYERS FABRICATED ON SINGLE CRYSTAL Nb SUBSTRATES

by

JAMES FREDERICK DeBROUX

Submitted to the Department of Physics on
September 4, 1979 in partial fulfillment of the
requirements for the Degree of Masters of Science.

ABSTRACT

The structural properties of Nb_3Sn diffusion layers fabricated on oriented single crystal Nb substrates exhibit systematic behaviors based on substrate orientation which result from interactions between the substrates and A15 overlayers. Preferred orientation of the diffusion layers is confirmed by X-ray and electron diffraction measurements. Within the bulk of a specific Nb(h k ℓ) substrate layer, the preferred orientation appears to be a function of layer thickness for the range of thicknesses studied (~1 to 17 μm). It is believed to develop over distance due to a competion between the growth region orientation at the advancing interface (required by lattice registry of the bcc and A15 lattices) and the tendency of Nb_3Sn layers toward a natural growth direction, A15(100); this competition is moderated by in situ annealing of the Nb_3Sn as growth advances. Consistent with this model is the fact that surface preferred orientation of a diffusion layer on a given Nb(h k ℓ) substrate, both for as-grown surfaces and for internal surfaces exposed by etching, appears to be a function of net layer thickness.

Layer thickness regimes have been identified and associated with variations in diffusion layer properties according to the orientation of the underlying Nb substrate. These thickness regime behaviors and the A15 preferred orientation dependence on substrate (h k ℓ) suggest that a diffusion layer on a given Nb(h k ℓ) substrate orientation has a specific "personality profile". Trends in T_c and lattice parameter as a function of layer tin composition suggest the possibility of orientation effects in Nb-Sn nucleation and growth kinetics, perhaps also with implications for phase equilibria and the ordering effects of in situ annealing.

Scanning electron microscopy shows microstructural variation among diffusion layer samples of differing A15 layer thicknesses on the same niobium substrate orientation, between layers on differing substrate orientations fabricated under the same conditions and to the same thickness, and between samples of different substrate geometry. Also observed is a similarity between the microstructures of the thinnest layer's surface and the advancing interface of the thickest layer.

The existence of differences in properties of diffusion layer Nb_3Sn exhibiting preferred orientation arising from the influence of niobium substrate orientation, and observations that these differences show variation with processing conditions, suggest that the tradeoffs between fabrication and layer quality are dramatic.

Thesis Supervisor: Margaret L. A. MacVicar
Title: Associate Professor of Physics

To Ann

TABLE OF CONTENTS

LIST OF FIGURES

LIST OF TABLES

ACKNOWLEDGEMENTS

First, I would like to thank my advisor, Professor Margaret MacVicar, for her guidance and support throughout the course of my thesis work. I would also like to thank Professor Judy Bostock for her interest and helpful suggestions.

My thanks go to Dr. Jim Gregory and Mr. Irvin Puffer for sharing with me their technical expertise and taking the time to teach me many valuable laboratory techniques. I would also like to thank Dr. Prabha Tedrow, Dr. Stuart Cogan, Walter Zwirble, Susie Arney, Joe Boisvert, and Mike Levy for many interesting and useful discussions on physics, material science and life in general. Their friendship has made my M.I.T. experience most enjoyable.

A special thanks to Dr. Vicky Diadiuk for her encouragement, advice and generosity in allowing me to use her samples and data to help my study.

Finally, I want to extend my deepest thanks to my wife Kathy and my sister-in-law Ann for their love and moral support. Without their continual optimism, understanding and encouragement, this work would not have been possible.

This research was supported in part by the U.S. Department of Energy.

I. INTRODUCTION

The mechanical properties of superconducting materials have been of interest and concern to researchers in the field of superconductor technology since the discovery of high field superconductors about two decades ago.[1] The inherent brittleness of many of these high field superconductors, specifically the A15 crystal structure materials, requires the development of unique processing and fabrication techniques for the manufacture of practical conductors. Diffusion-processed A15s are currently being investigated for use in multifilamentary composite wires and tapes, as well as for the linings of high energy accelerating structures.[2] The A15 materials have proven to be very attractive for these applications because they are characterized by high superconducting transition temperatures, T_c, (as high as 23K for Nb_3Ge) high critical current densities, J_c, (e.g., 2×10^{10} a/m^2 at 3T for Nb_3Sn) and high upper critical magnetic fields, H_c (24T for V_3Si). See Table 1.

Recently research efforts have been directed at investigating the important influence of microstructure on the superconducting parameters as well as on the mechanical behavior of these A15 materials. The key roles of stoichiometry, long range order and crystal perfection to the enhancement of superconducting properties have been widely accepted, although still under active investigation.[13,4,14,15,6] But interest is also turning to establishing the effects of substrates on the fabrication of the overlying A15

TABLE 1

Compound	T_c(°K)	Ref	J_c(A/m^2)	H_{c2}(0) (T)	Ref
V_3Ga	15.4	3	2.5×10^{10} at 4T	25.0	9
V_3Si	17.1	4		24.0	9
Nb_3Sn	18.3	5	2.0×10^{10} at 3T	28.0	9
Nb_3Al	18.9	6	5.0×10^{9} at 10T	33.0	10
Nb_3Ga	20.3	7	1.0×10^{8} at 15T	38.0	11
Nb_3Ge	23.0	8	1.8×10^{10} at 0T and 13.8K	38.0	12

TABLE 1 -- Typical High Field A15 Compounds

material, for example, the utilization of a substrate compatible with that of Nb_3Ge to determine the influence of epitaxial growth on the final physical properties of this high T_c A15.[17,18]

From a more microscopic point of view, crystalline orientation effects have been observed in the properties of high T_c type-II transition metal superconductors including the A15 materials and elemental Nb. Two specific examples which are well documented are the existence of anisotropy in both H_{c2} and the superconducting energy gap, Δ_o.[19] Initially these anisotropies were viewed as fundamental properties of the material, but as evidence accumulates the case for the intrinsic nature of anistropy is less than convincing. Bostock has pointed out, for example, that the experimental evidence supporting energy gap anisotropy is tenuous at best;[20] similarly, although H_{c2} anisotropy is more widely accepted, its magnitude and its effects on such phenomena as grain boundary flux pinning are still under debate.[21,22,23,24] Other microscopic effects in A15s which are demonstrably important include the grain size dependence of J_c[11] and the structural transformations of some A15s at low temperatures.[25]

The material of immediate interest in this research is diffusion-processed Nb_3Sn (T_c=18.3K, $H_{c2}(0)$=28.0T). The high critical current density ($2.0 \times 10^{10} A/m^2$ at 3T) and relative stability of its A15 phase have made Nb_3Sn the subject of extensive studies, both as an A15 structure in itself and as it relates to fabrication

technologies.[2] Nb_3Sn layers which are grown on a textured surface, whether by diffusion, sputtering, CVD, or coevaporation, might be expected to exhibit texturing themselves. A directional relationship between a clean Nb(110) substrate and Nb_3Sn diffusion layer was first reported in 1969 by Jackson and Hooker.[26] However, few studies of preferred orientation and lattice registry effects of A15 diffusion layer materials (V_3Ga and Nb_3Sn) have been done to date.[27,28,29] A characterization by Diadiuk of the surface properties of Nb_3Sn grown by Sn vapor diffusion indicates a definite relationship between the crystallographic direction of the niobium single crystal substrate and the properties and behavior of the surface region of the overgrown Nb_3Sn.[29] Specifically, there is a marked degradation of the superconducting properties of layers grown on the Nb(111) substrate orientation compared to those grown on non-Nb(111) orientations.

The goal of the present research is to investigate the preferred orientation effects, structural and behavioral, in the bulk of Nb_3Sn diffusion layers as a function of the substrate crystallographic direction. The evolution of preferred orientation effects from the Nb_3Sn surface towards the Nb_3Sn-Nb interface the the nature of the Nb_3Sn-Nb interface itself are a particular emphasis of this investigation. The results of this investigation can be expected to be of immediate application to applied superconductor technology as it relates to diffusion-processed wires, tapes and microwave cavities.

This thesis is organized as follows:

Chapter 2 presents a background to understand the nature of this project in the context of the overall research effort in the study of A15 materials, in general, and diffusion-processed Nb_3Sn, in particular. A brief description of the various experimental techniques utilized in the research, with their respective advantages and limitations, will also be presented.

Chapter 3 is a review of the actual experimental equipment and techniques used to prepare and analyze the samples.

Chapter 4 is the presentation of experimental results. These are presented in terms of the particular investigative technique employed and the crystallographic orientation of the niobium substrate. Also included is discussion of the experimental results in the context of previous and ongoing research in the area of superconductivity.

Chapter 5 summarizes the conclusions drawn from this research effort and makes recommendations for directions of further research beyond the scope of this thesis.

II. BACKGROUND

High field superconducting materials have been the source of many interesting and perplexing questions concerning their microstructure, superconducting properties, and mechanical behavior. Among the topics currently receiving attention is the interaction between the substrate and an A15 layer fabricated on it as it relates to structure and to both the physical and superconducting properties of such material. From a technological point of view, superconducting composites (wires, tapes, and ribbons) and cavities for high energy accelerating structures use diffusion processes in the formation of A15 material layers on various substrates. Thus, knowledge about the influence of these substrates on surface and on layer properties and structure is crucial to the successful commercial utilization of Nb_3Sn and other A15 alloys. For example, Nb_3Sn composite wires under tensile stress often exhibit fiber breakages which initiate due to Kirkendall voids at the Nb_3Sn-bronze interface where the Nb-Sn diffusion reaction takes place.[30,31] Also superconducting microwave cavities coated with a Nb_3Sn diffusion layer exhibit high rf losses and degraded Q values at regions thought to be characterized by excessive stress concentrations.[32,33,34,35]

The relationship of substrate-layer interaction to layer stoichiometry, long range order and crystalline perfection provides the impetus for investigation in this area by those pursuing basic superconductivity research.

Interest in a theoretical explanation of the phenomena of superconductivity led after many years to the Bardeen, Cooper, Schrieffer (BCS) microscopic theory of superconductivity which successfully accounts for the second-order phase transition, the observed electrical properties (no measurable resistance), and the observed magnetic properties (perfect diamagnetism plus a Meissner effect) of the superconducting state.[36] The BCS theory links the state to the existence of an energy gap in the excitation spectrum of electrons due to an attractive electron-phonon interaction resulting in a paired electron boson state.

The BCS theory and its strong-coupling extensions[37] predict that, given: $N(0)$, the electronic density of states near the Fermi surface; an average $\langle\omega\rangle$ and a mean square average $\langle\omega^2\rangle$ of the phonon frequencies; an average of the electron-phonon coupling matrix element over the Fermi surface $\langle I^2\rangle$; and an appropriately renormalized effective Coulomb pseudo-potential, μ^*, one can accurately calculate the superconducting transition temperature, T_c, for most metals.[38,39] The parameter λ, the electron-phonon coupling constant can be introduced to reduce the number of required parameters to three, since

$$\lambda = \frac{N(0)\ \langle I^2\rangle}{M\ \langle\omega^2\rangle} \qquad \text{where } M = \text{ion mass}$$

The formalism works very well for describing superconducting behavior in s-p band metals.[39,40]

However, an explanation of the superconducting behavior

of transition metals and alloys has proven more elusive.[41,42] Concern centers on those d-band alloys which form in the A15 structure. (See Figure 2.1.) This structure has the stoichiometric composition A_3B where the A atom is a transition metal. If the B are transition metal atoms, the A15 generally has a moderate-to-low T_c (<10K), while for non-transition metal B atoms, the A15 may be a high T_c superconductor (T_c>15K). The A atoms form three mutually orthorgonal, nonintersecting chains and sit in the tetrahedral sites on the faces of a body-centered cubic lattice of B atoms. The highest T_c A15s have been formed with Nb or V as the transition metal A atom; interestingly, Nb and V are among the elements with the highest T_c's and are the only elements which are type-II superconductors.[43] The A15 structure normally can form over a range of compositions close to and including A_3B. In particular, the A15 phase field of Nb_3Sn extends between 18 and 28 atomic % Sn[44] and is quite stable. See Figure 3.5 for the Nb-Sn binary phase diagram.

Ashkin and Gavaler have observed a definite relationship between T_c, stoichiometry and A15 phase stability in the Nb_3X series where X is Sn, Al, Ga, Ge or Si.[15] For a given alloy of this series the A15 phase has the highest T_c, and within the A15 phase the composition closest to A_3B stoichiometry has the highest T_c. Additionally, the more ordered the material, the higher its T_c. Furthermore, T_c increases in the series as the size of the X atom decreases. The integrity of the Nb chains appears to be

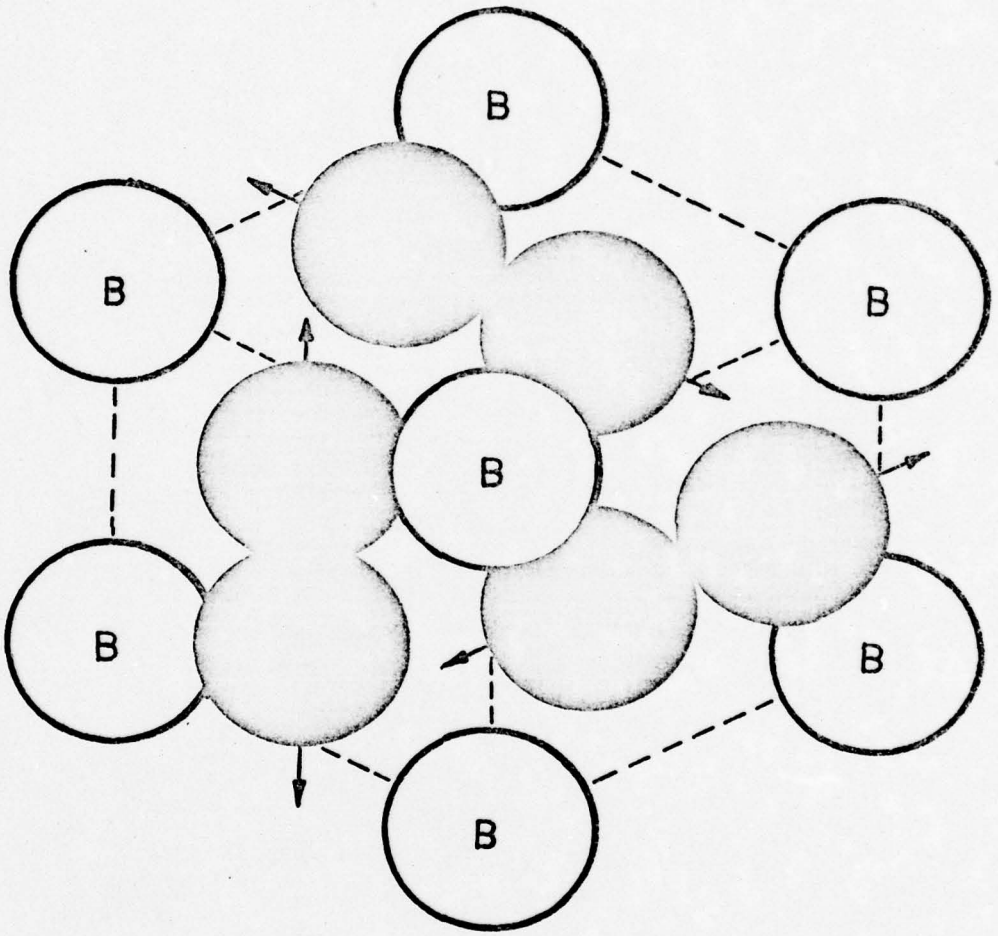

2.1 A15 UNIT CELL -- The A atoms form three mutually orthogonal chains on the cell faces. The B atoms are on the body-centered cubic cell positions.

critical to maintaining high T_c's. The importance of these chains is attributed to the overlap of the d-electron orbitals along the chains, contributing to a high density of states near the Fermi surface and pseudo-one dimensional character to the electronic properties.[15,4,14,45] Thus disorder in the chains where X atoms replace the Nb is thought to destroy the one dimensionality and d-electron localization, thus degrading T_c.

Additionally, phase instability arises as the X atom size decreases. In particular, the ordered stoichiometric A15 Nb_3X phases of lower atomic number become less stable and therefore increasingly more difficult to prepare. For example, single phase, high T_c Nb_3Ge can only be formed by sputtering, CVD, or electron-beam coevaporation onto heated substrates[15] as compared to normal metallurgical processes (arc-melting, etc.) used to form Nb_3Sn. Smaller X atoms in the Nb_3X A15 compounds appear to lead to the highest T_c's, but also result in an unstable lattice configuration. Impurity stabilization appears to one solution to the fabrication difficulties of such compounds as illustrated by the apparent role of oxygen in stabilizing A15 Nb_3Ge.[46,47,48]

The pseudo-one dimensionality of the d-electron chains might also be expected to contribute to a marked anistropy in the upper critical field, H_{c2}, through Fermi surface anisotropy and Fermi velocity.[49] (Note: H_{c2} is also temperature and impurity dependent.)[49] Anisotropy in H_{c2} has been investigated extensively as it relates to grain boundary flux pinning in A15 compounds.[50,51,21,23]

Free energy differences (whose potential sources include inherent strains, impurity clusters or structural anomalies) across the grain boundaries result in an orientationally dependent free energy which is linked to anisotropy in the upper critical field, H_{c2}.[51] Actual measurements of H_{c2} anisotropy in V_3Si by Kramer and by Foner have produced different conclusions about the magnitude of the anisotropy (Kramer finds a value of approximately 16% while Foner sees only about 3%). Thus, the importance of the role of H_{c2} anisotropy in flux pinning is unclear.[21,23] However, the importance of impurity effects is clearly demonstrated in de Haas-van Alphen measurements on single crystal Nb_3Sn by Arko, et al., which shows an increasing H_{c2} anisotropy with increasing sample impurity.[52] Because the observed relationships of H_{c2} to grain boundaries, strain fields, and impurities are directionally dependent, one might expect preferred orientation effects to manifest themselves in a detectable H_{c2} anistropy.

An example of the effect of microstructure on the superconducting properties of A15s is the dependence of the critical current density, J_c, on grain size. It has been demonstrated that J_c can be enhanced by grain size refinement and by the addition of fine precipitates of non-superconducting materials.[11] It is not clear whether it is the precipitates themselves or their effect on the grain size which increases J_c.

Many A15 phase materials exhibit anomalous elastic

behavior and structural instabilities. Ultrasonic experiments for both V_3Si and Nb_3Sn show a softening of the lattice upon cooling which is arrested as the material passes through a structural transformation temperature. ($T_m \sim 21K$ for V_3Si and $T_m \sim 43K$ for Nb_3Sn).[53] The structural changes are cubic-to-tetragonal martensitic transformations, however, the transformation does not occur in all samples of a given material for, as yet, unknown reasons.[53] A similar structural transformation in Laves-phase ZrV_2, a C15 material, has been attributed to an electronic instability possibly associated with internal-local-stress distributions.[54] Martensitic transformations have also been observed in other high T_c A15's such as V_3Ga[55] and $Nb_3Al_{.75}Ge_{.25}$.[56]

Before proceding with the discussion of diffusion-processed A15's, it is germane to define some of the terms which will be used extensively. Each grain of a polycrystalline aggregate has a crystallographic orientation different from that of its neighbors. Considered as a whole, the orientation of all the grains may be randomly distributed in relation to some selected reference frame, or they may tend to cluster to a greater or lesser degree about some particular orientation or orientations. Any aggregate characterized by the latter condition is said to have a preferred orientation or texture, which may simply be defined as a condition in which the distribution of grain orientations is nonrandom.[57]

The importance of preferred orientation lies in the effects

it has on the overall macroscopic properties of materials. Given the premise that single crystals are anisotropic, i.e., have different properties in different crystallographic directions, it follows that an aggregate having preferred orientation must also have directional properties to a greater or lesser extent. Such properties may or may not be beneficial, depending on the intended use of the material.[57]

Preferred orientation can be produced by the fabrication process itself, such as rolling or swaging, or it can result from forming the material on or in a structure which is highly textured by previous plastic deformation or by virtue of being a single crystal itself. When forming diffusion layers on the latter, the substrate is perfectly ordered resulting in layers being grown on specific crystallographically oriented substrates. In this thesis research single crystal niobium substrates have been utilized in two geometries, rods and discs, (see Figure 3.3 for specific configurations) to take advantage of the availability of orientations around the rod circumference and the larger planar area of an oriented disc.

Epitaxy is a special case of preferred orientation. Epitaxial growth refers to the ordered growth of a material on a single crystal substrate where both substrate and overlayer have compatible crystalline structures and very similar lattice parameters.[58] Heteroepitaxy is the growth of a material which

differs in structure and composition from its underlying substrate on a single crystal substrate (as opposed to homoepitaxy -- same structure and composition). Heteroepitaxial growth leads to an interfacial misfit strain which is due to the difference in the lattice parameter between the overgrowth and substrate. Up to a critical thickness of the overgrowth, which can vary from 50 Å to 8 μm, this strain at equilibrium conditions is accommodated by purely elastic deformation and beyond, by misfit-relieving dislocations.[59]

The value of this thesis research effort lies in its contribution to a comprehensive systematic investigation of the relationship of the microstructural and behavioral properties of diffusion-processed Nb_3Sn overlayers to the orientational nature of the substrates.

In the first study of possible orientational effects in Nb_3Sn Jackson and Hooker, in 1969, performed LEED studies on tin films evaporated onto Nb(110) surfaces and heated to diffuse the tin into the niobium. The authors noted that the first few surface monolayers of the Nb_3Sn film differed orientationally from the film's bulk and concluded that true epitaxial layers of Nb_3Sn could be made on clean Nb(110) surfaces.[26] However, in 1975, Strozier, et al., in a similar study [a LEED and AES investigation of tin evaporated onto Nb(110) and Nb(100) surfaces] did not

observe a true epitaxial growth of the Nb_3Sn on the Nb(110) and Nb(100) surfaces.[60] Rather, the Nb_3Sn grew in small crystallites which were oriented in the plane of the Nb surface but randomly oriented about an axis perpendicular to the surface. (This arrangement is referred to as a fiber texture).

Jacobson, et al., have studied the microstructure of electron-beam deposited Nb_3Sn to investigate relations between structure, composition, morphology and superconducting properties.[61] They found that Nb_3Sn grows as fibers or columns, with grains varying in size from 250 Å to 2000 Å (finer grains result from higher growth rates). Of notable interest is the observation of a strong texturing suggesting a Nb_3Sn<200> preferred growth orientation. When excess tin was observed in the form of Nb_6Sn_5 (body-centered orthorhombic structure), it appeared as dome-shaped cones protruding above the film surface and surrounded by an inhomogeneous, irregularly-sized A15 grain structure exhibiting twins and faults.[61]

Diadiuk's characterization of Nb_3Sn diffusion layers grown on single crystal Nb substrates seems to indicate a very strong influence of the Nb substrate orientation on both the layer surface and interior bulk layer properties. This work will be discussed in more detail later in this chapter.[29]

In discussing diffusion-processed A15s, it is important to recognize that diffusion-processed A15s are of keen interest

to researchers because of their numerous practical applications and because of the interesting complexity of the diffusion process itself. Great effort is being directed at multifilamentary composite wire fabrication by the bronze process, the external tin process and the hollow tube method.[2] In all three fabrication techniques Nb_3Sn is formed by solid state diffusion at elevated temperatures. Thermal contraction mismatch between the Nb_3Sn filaments and the respective matrix induces compressive strains in the Nb_3Sn which must be overcome by the application of a tensile stress to maximize its superconducting properties.[62,63] However, the thermal mismatch between Nb_3Sn in contact with Nb is less significant. Considering only thermal expansion, Nb_3Sn made by diffusion at 1000 °C on a Nb surface would be subject to a mean tensile strain of only about 1% upon cooling to room temperature.[64]

In addition to the attention given to composite wires, much effort has been devoted to the study of lining cavities with diffusion-processed Nb_3Sn.[32,33,65,66,67,34,35] The linings of such cavities are made by the process of a heating the pure Nb lining in a saturated tin vapor resulting in a Nb_3Sn diffusion layer, the thickness of which generally follows a parabolic growth equation.[68,65,66,67,34,35,69] The resultant growth equation is:

$$x = k\, t^{0.5}$$ where x = layer thickness

t = reaction time

k = diffusion coefficient.

However, difficulties have been encounted as the result of "bad spots" in the Nb_3Sn layer having effective $T_c \leq 1K$ and unacceptably high rf losses.[70,67,34,71,72] The origin of these quasinormal regions is not clearly understood, although several indicators point to stresses possibly casued by oxygen impurities and/or by stresses inherent in registry of orientations of the Nb and the Nb_3Sn layers, especially the Nb(111) orientation.[29,72,73]

A study by Dickey, et al., of thin films of Nb_3Sn on Nb [tin evaporated onto thin polycrystalline Nb foils and the Nb (110) face of a niobium single crystal, and heated to react the tin] indicated a sensitivity of film properties to post-fabrication heat treatment. The authors attributed this to competition between diffusion of the tin into the sample and re-evaporation of tin from the sample surface.[74] In optimizing formation, the authors chose temperatures between 800 and 900°C to achieve a delicate balance between loss of tin and sufficiently rapid formation of well-ordered Nb_3Sn.

The kinetics of Nb_3Sn growth in niobium-tin diffusion couples (a diffusion couple is an assembly of two materials in such intimate contact that each diffuses into the other[75]) was studied by Old and Macphail.[76] They found that the Nb_3Sn growth was not determined solely by a diffusion mechanism (the .5 exponent of reaction time in the previously mentioned growth equation), but rather a combination of diffusion and solution deposition mechanisms

caused by the presence of liquid tin which depends on thermal gradient mass transfer of niobium ($x = k\ t^{0.36}$). Easton and Kroeger determined a similar growth equation ($x = k\ t^{0.32}$) while investigating the effects of Kirkendall voids in bronze-processed Nb_3Sn multifilamentary composite wires.[30] Kirkendall voids form at the filament-matrix interface because Sn diffusion into the Nb filament is accompanied by vacancy flow in the opposite direction. The vacancies coalesce and nucleate as voids and have been related to reduced mechanical properties, thermal instabilities, and crack initiation in Nb_3Sn multifilamentary conductors.[30] Although the diffusion reaction in this thesis research is believed to have a $t^{0.5}$ dependence for layer thickness, the observations and insights of researchers whose efforts indicate nonparabolic layer growth equations are useful to understanding the basic diffusion process.

The microstructural characterization of the surface properties of Nb_3Sn diffusion layers grown by Sn-vapor reaction with single crystal Nb substrates by Diadiuk indicates the existence of a preferred crystallographic orientation in the surface region of the diffusion layers corresponding to particular orientations of the Nb substrates.[29] Specific A15 orientations at the Nb_3Sn surface were inferred from X-ray and reflection electron diffractometry (RED) data.

The microstructure of Diadiuk's Nb_3Sn layers grown on non-(111) Nb substrate directions is similar to that observed by Strozier, et al.,[60] Jacobson, et al.,[61] and Kniesel, et al.,[34] in that it is comprised of fairly uniform columnar grains of approximately 1 μm size.[29] However, layers grown on the Nb(111) substrate direction differ substantially. These layers exhibit extremely rough morphology, have grains which are loosely packed and irregular in size and distribution, and include actual microcracks and pores in layers grown on curved substrates.[29] Superconducting tunnel junction measurements indicate a degradation of superconducting properties in the layers grown on the Nb(111) substrate; additionally, Auger analysis shows high levels of oxygen and carbon within the bulk of these layers relative to layers grown on non-(111) bcc directions. The carbon impurities remained in the absorbed state for the Nb(111) substrate orientation at least 10,000 Å into the bulk while it changed from the absorbed to a bonded state in the non-(111) substrate diffusion layers within 100 Å from the surface. This evidence points to a relationship, based on structural stress, between Nb_3Sn layers grown on Nb grains of specific orientation and the observed quasinormal regions ("bad spots") in superconducting rf cavities.[72]

Preferred orientation effects previously reported (Jackson,[26] Strozier, et al.,[60] Jacobson, et al.,[61]) examined only a limited variety of substrate directions [Nb(100) and Nb(110)].

Togano has more recently reported texturing effects, determined using X-ray pole figure analysis, in Nb_3Sn and V_3Ga diffusion layers fabricated on polycrystalline substrates. The pole figure determinations illustrate crystallographic texturing of the A15 layers corresponding to the bcc substrate directions. The textures found, however, were other than simple fiber textures due to the polycrystalline nature of the substrate.[27,28]

In addition to the work of Diadiuk[29] and Togano, et al.,[27,28] the interaction of the substrate with an A15 overlayer has also been investigated by Dayem, et al.[17,18] The study was not of diffusion-processed material, but substrate-induced quasi-epitaxial growth of Nb_3Ge on Nb_3Ir and Nb_3Rh. "Epitaxial" growth is not used here in its normal meaning of an ordered growth on a single crystal substrate where both substrate and overlayer have compatible crystalline structures and nearly equal lattice parameters.[58] But rather, "expitaxial" growth refers, in this case, to the idea of growing a polycrystalline film of a desired crystal structure on a polycrystalline substrate of similar crystal structure. The study showed that the range of A15 phase homogeneity, with a commensurate enhancement of T_c, was extended by growing Nb_3Ge on polycrystalline Nb_3Ir thereby taking advantage of the compatibility of lattice parameters and identical crystal structures.[17,18] Engineering of a compatible "substrate" may occur naturally as in the case of Nb_3Ge films. Oxygen profiles in the Nb_3Ge films of

Braginski suggest that oxygen may act to expand the lattice into serving as a compatible "substrate" for the remainder of the film.[47,48]

Preferred orientation in polycrystalline materials can be detected by various experimental techniques most of which involve the use of X-ray diffraction. Variations in scanning X-ray diffraction peak intensities as compared to a powder sample, differing natures of Debye rings on X-ray pinhole camera photographs, nonuniformity in Debye-Scherrer patterns, and direct and inverse pole figure analysis are the most commonly utilized X-ray indications of texturing.[77] Reflection electron diffraction (RED) also yields information which, when interpreted with the necessary caution, can point to preferred orientation in surface material. When preferred orientation is observed in diffusion layer materials, lattice registry arguments are often useful in attempts to match the substrate and overlayer structures, and to understand misfits in the corresponding lattices.[27,28,29] Such arguments were used by Diadiuk, et al., to explain the association of particular bcc substrate directions with specific A15 diffusion layer surface orientations.[29,73,78]

Diffraction of X-rays can occur whenever Bragg's Law

$$n \lambda = 2 d \sin \theta \qquad (2.1)$$

is satisfied (where λ is the X-ray wavelength, d is the interplanar

spacing of the crystal and 2 θ is the angle between the diffracted beam and the transmitted beam). In general, an n^{th} order reflection from (hkl) planes of spacing d' may be considered as a first-order reflection from the (nh, nk, nl) planes of spacing d = d'/n.[79] From the experimentalist's point of view, a continuous variation of either λ or θ must be effected to yield information about the crystal structure of the material. The main diffraction methods used in this thesis are the Laue methods (fixed θ, variable λ) and diffractometer methods (fixed λ, variable θ), although information was also gathered from pinhole photographs with monochromatic radiation (fixed λ, fixed θ).

The Laue method gives information about the crystal orientation for single crystals (a pattern of spots geometrically determined by the crystal structure) and crystal structure (size, quality and orientation of the grains making up the aggregate) in polycrystalline materials. If one ultilizes a monochromatic X-ray beam with the Laue method for a material with a non-ideal fiber texture parallel to the incident beam (this is the type of texture present in most of the diffusion layers discussed to this point), it is possible to generate Debye rings of uniform intensity.[80] This is an exception to the general rule that uniform Debye rings are associated with randomly oriented grains.

The X-ray diffractometer is an instrument for studying crystalline materials by measurement of the way in which they

diffract X-rays of a known wavelength. The output of the diffractometer is a strip chart recording of intensities of the diffracted beam measured directly by an electronic counter. Diffractometer scans can be used to determine crystal lattice parameters, for the determination of preferred orientation (when a powder standard is available for comparison) and for the determination of the phases present in a given sample. Preferred orientation determinations can also be made by comparison of peak intensities with intensities from a randomly oriented powder sample on a scanning diffractometer, or by various pole figure techniques on a texture diffractometer, depending on the geometry of the sample. A pole is the intersection of a crystal plane normal with the surface of a reference sphere which encases the crystal. A pole figure is a stereographic projection, with a specified orientation relative to the specimen, that shows the variation of pole density with pole orientation for a selected set of crystal planes.[77] A sufficient amount of material must be present for the X-ray to see a representative distribution of the grain orientations in the aggregate. In the present thesis research the Nb-Nb_3Sn disc samples were of such limited size that attempts at pole figure anslysis proved unfeasible. However, efforts in this laboratory are presently directed at the pole figure analysis of Nb_3Sn diffusion layers fabricated on polycrystalline Nb foils. The current status of this study is presented in Appendix 3.

It must be remembered that X-ray diffraction is a tool for the investigation of the bulk (~10's of μm) as compared to surface layer information yielded by electron diffraction (~10's of Å). This is due to the difference of the electron's mean free path in the material as compared to the longer mean free path of X-rays.

For a description of the general theory, information yielded and limitations of the scanning electron microscope, energy dispersive X-ray analysis (EDX) and reflection electron diffraction (RED) techniques utilized in this research, the reader is directed to two doctoral theses recently completed in this laboratory by V. Diadiuk[29] and J. Gregory,[46] and references to listed therein.

III. EXPERIMENTAL

This chapter describes the experimental procedures followed in the fabrication and subsequent analysis of Nb_3Sn diffusion layers. The objective of this thesis research is to examine the relationship of correlations between structure and properties of the Nb_3Sn layers and their underlying niobium substrate orientations to processing variables such as layer thickness, niobium geometry and diffusion reaction parameters. There is particular interest in information concerning the nature of the registry between the Nb_3Sn and niobium lattices.

The general experimental protocol is to fabricate a Nb_3Sn diffusion layer on a single crystal Nb substrate, measure its T_c inductively, and obtain X-ray diffraction data, including diffractometer scans and back-reflection pinhole photographs. (Direct X-ray pole figure analysis was attempted on several samples, but the geometric constraint of small sample size prevented collection of any relevant data. See Appendix 2.) Scanning electron micrographs and energy-dispersive X-ray measurements are then made to characterize the morphology and bulk chemical composition of the sample. Also, reflection electron diffraction (RED) is done on selected samples. The crystallographic directions of the Nb single crystal substrates is a convenient basis for categorizing of the results of the various investigative techniques.

Figure 3.1 is a flow chart which illustrates the general

FIGURE 3.1 -- Flow Chart of General Experimental Protocol

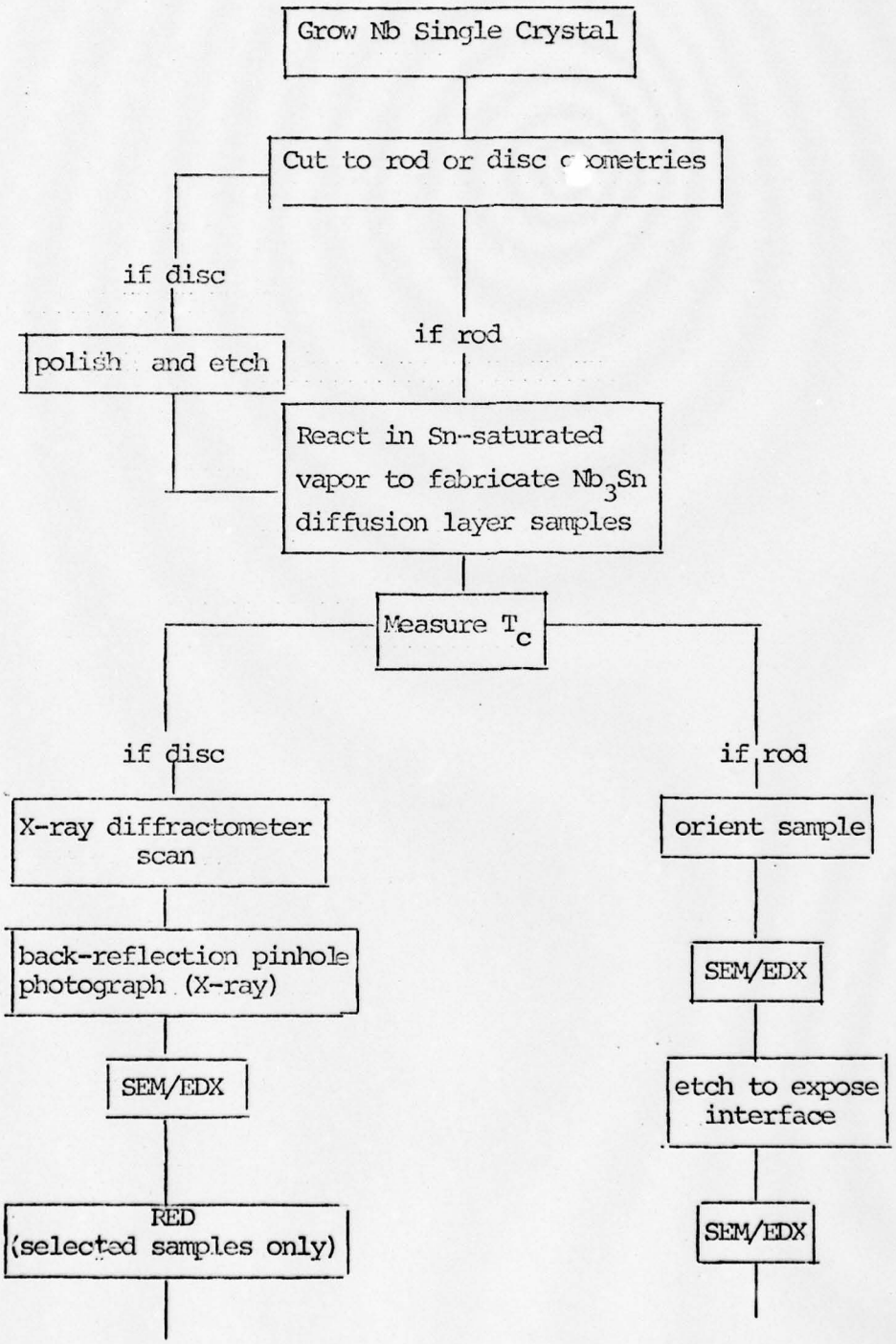

experimental protocol described above More detailed descriptions of specific techniques follow.

Nb_3Sn Sample Fabrication[29]

Single crystal niobium used for sample substrates are grown using an ultra-high vacuum electron beam floating molten zone technique.[81,82] The starting materials for the niobium single crystals are 3.2mm and 4.6mm polycrystalline niobium rods from the Fansteel Corporation and Wah Chang Albany respectively, and both starting stocks are 99.9% pure. Spectroscopic analysis of typical niobium stock received from these companies shows the major impurities to be Ta (~250 ppm), W (<100 ppm), Hf (<100 ppm), Zr (<50 ppm), Mo (<50 ppm), Fe (<50 ppm), O (~50 ppm), and C (~30 ppm). However, the zone refining which takes place during the crystal growth itself has considerable purification effects.[83] Fabricating a single crystal begins with approximately 15 cm of the polycrystalline niobium rod. In the case of the 3.2 mm diameter rod, a 2.5 cm single crystal (110) seed was available to aid the initial growth. In the 4.6 mm diameter rod case, a succession of growth passes finally resulted in a (110) crystal. Initially a polycrystalline rod is outgassed at approximately 1500° C in a vacuum of 5×10^{-5} Pa. Several growth passes are then made (growth speeds are approximately 9.5 cm per hour) with the final growth pass at pressures in the low 10^{-6} Pa range. This technique allows one to grow a single crystal which is relatively free of impurities and has a structurally smooth, stress free surface.[83] The cylindrical axis of the final single crystal

rods (3.2mm and 4.6mm diameters) is oriented along the Nb(110) direction; therefore all major bcc symmetry orientations, (100), (110), (111), and (211), are present at the cylinder's circumference. See Figures 3.2 and 3.3.

The single crystal cylinders are then cut into two substrate geometries: rods and discs. The rods are simply 9-12mm sections cut from the as-grown cylinder. The discs are made such that their planar faces are perpendicular to the major bcc crystallographic directions. Cutting is done with a string saw (.13mm nichrome wire and #600 silicon carbide grit). The disc faces are then mechanically polished utilizing #320 and #600 wet-dry silicon carbide paper, a .3 micron alumina polishing wheel and a .06 micron alumina polishing wheel in succession. Finally, the discs are chemically etched with hydrofluoric acid until no mechanical damage is observable at 40X magnification with an optical microscope.

The actual Sn diffusion processing of the Nb substrates is done in an evacuated quartz ampule by a technique originally developed by the Siemans Laboratory in Germany.[65] In a quartz tube of approximately 2 cm diameter equipped with a tin well, Nb substrates are supported away from the walls of the quartz tube by holders of Nb wire and foil. See Figure 3.4. The supports for the rod substrates are .76mm Nb wires wrapped tightly at the rod ends and coiled in a larger radius away from the rod's end. The disc substrates are wedged between two spot welded .76mm Nb wires bent

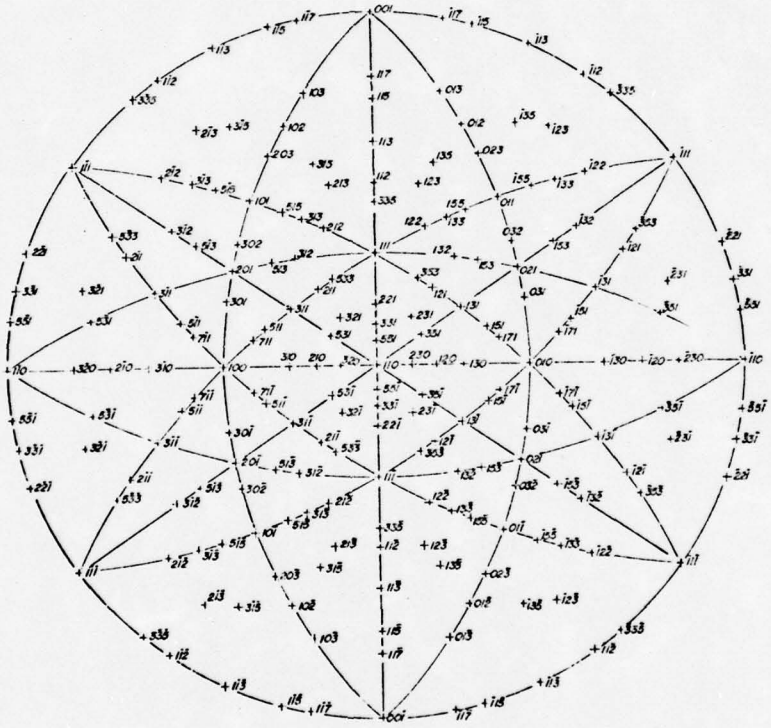

3.2 Standard (110) Plane Stereographic Projection from Ref. 84.

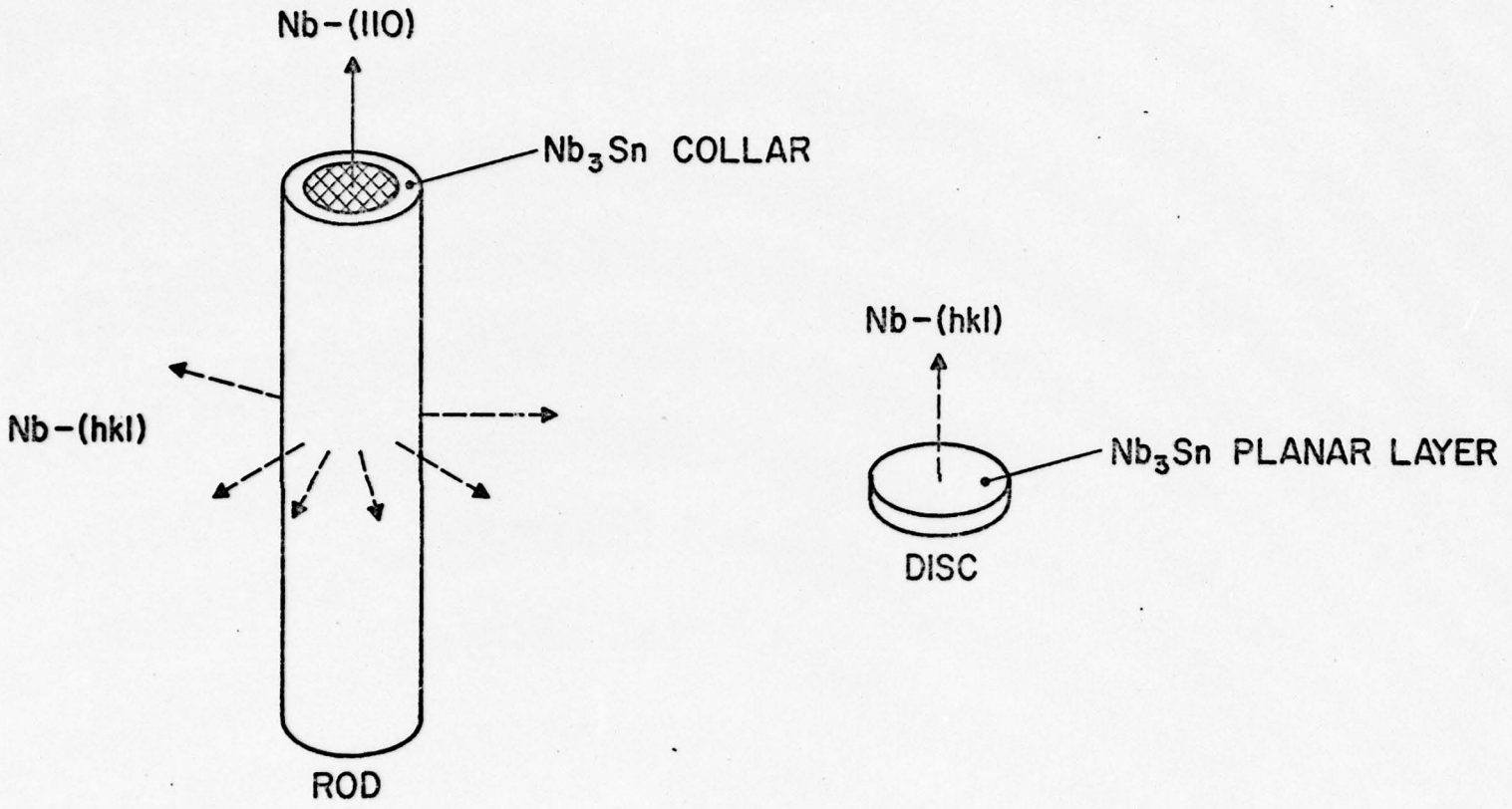

SAMPLES

3.3 Nb_3Sn Diffusion Layer Sample Geometries.

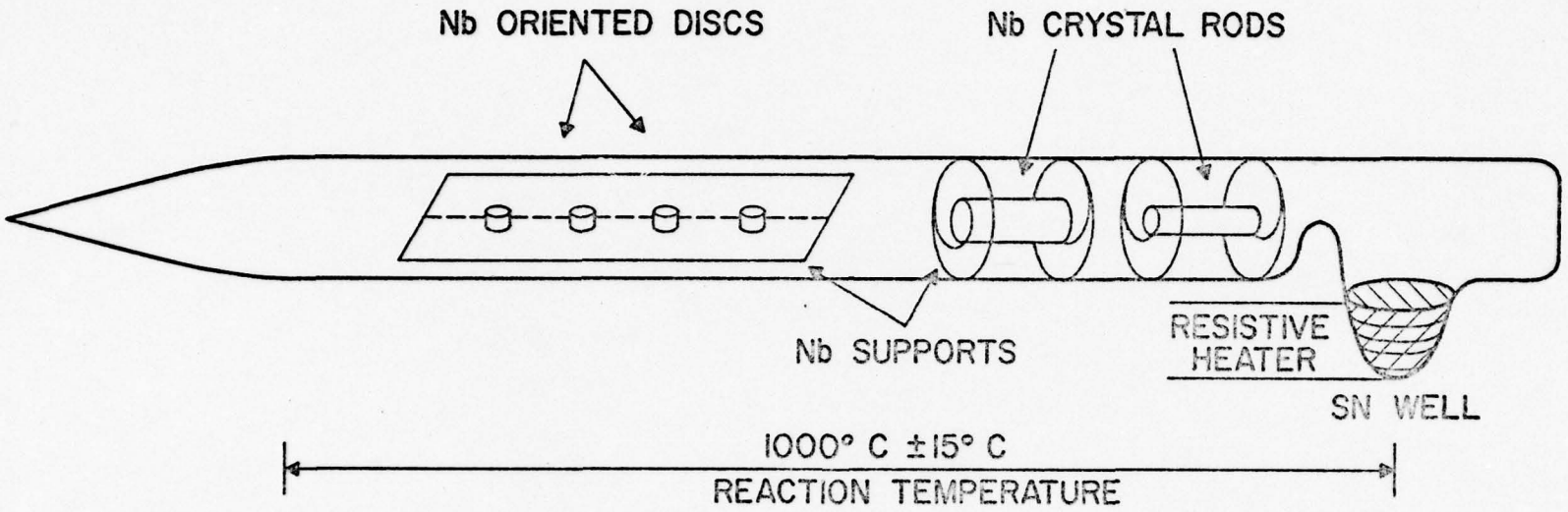

3.4 Configuration of Quartz Ampule and Samples for Reaction.

in a hair-pin shape and subsequently spot welded to a slotted .13mm thick Nb foil. The Nb foil has a slot cut out in order to expose the planar surfaces of the discs to the Sn vapor for reaction.

The quartz tube, with the Nb substrates in position, is mounted to a 200 liter/sec Ultek ion pump via a metallic flange fitted to the end of the quartz tube. Before placing the tube under vacuum, it is necked down between the mounted substrates and the metallic flange to approximately 2mm in diameter using an acetylene-oxygen-hydrogen torch combination. The purpose of the necking is to facilitate sealing of the quartz tube once it is under high vacuum. The ion pump is then started and the quartz tube is baked at 125° C in the 10^{-6} Pa pressure range to drive off residual impurity gases from the tube walls. The necked portion of the quartz tube is now sealed, again utilizing the acetylene-oxygen-hydrogen torch combination. (Note: the necking and sealing procedures are extremely difficult due to the high melting point of quartz.)

The evacuated quartz ampule and samples are then heated to 980-1010° C in a Marshall horizontal tube furnace. The tin well is resistively heated at the same time to produce a tin saturated atmosphere. The resistive heater is made of .25mm platinum-40% rodium wire windings in an alumina cement bowl which fits under the tin well and .5mm platinum-40% rhodium wire leads to a DC voltage source. The resistive heater has 0.5 amps of current applied to

raise the temperature of the tin well approximately 30° C. (This current is optimal for diffusion layer fabrication).[85] The resistive heater, quartz ampule and a thermocouple to monitor the baking temperature are inserted into a 4.1 cm quartz cylinder and slid into the furnace which had been preheated to 1000° C for approximately six hours. The quartz ampule should be centered in a region where the temperature variations over the ampule's length are within acceptable limits according to the phase diagram. (See Figure 3.5.) Determining the specific nature of temperature gradients proved problematic to this author's samples. After the quartz ampule and its ancillary equipment have baked in the furnace for the desired time, they are pulled quickly from the furnace to quench them to room temperature. (Note: When the author cooled one sample set, 9115*, in the furnace, virtually no A15 phase material remained after cooling.) Care must be taken in removing the ampule from the furnace because there is a possibility of sloshing the still molten tin onto the reacted samples. (This was done on one disc of sample set 9141*.) The reacted samples remain in the sealed quartz ampule until analysis begins.

Diffusion calculations can estimate the thicknesses of Nb_3Sn layers for various fabrication temperatures and times. The thickness of the Nb_3Sn layer is estimated from:

---

*See Chapter IV and Table II, the Master Data Table, for the sample numbering system.

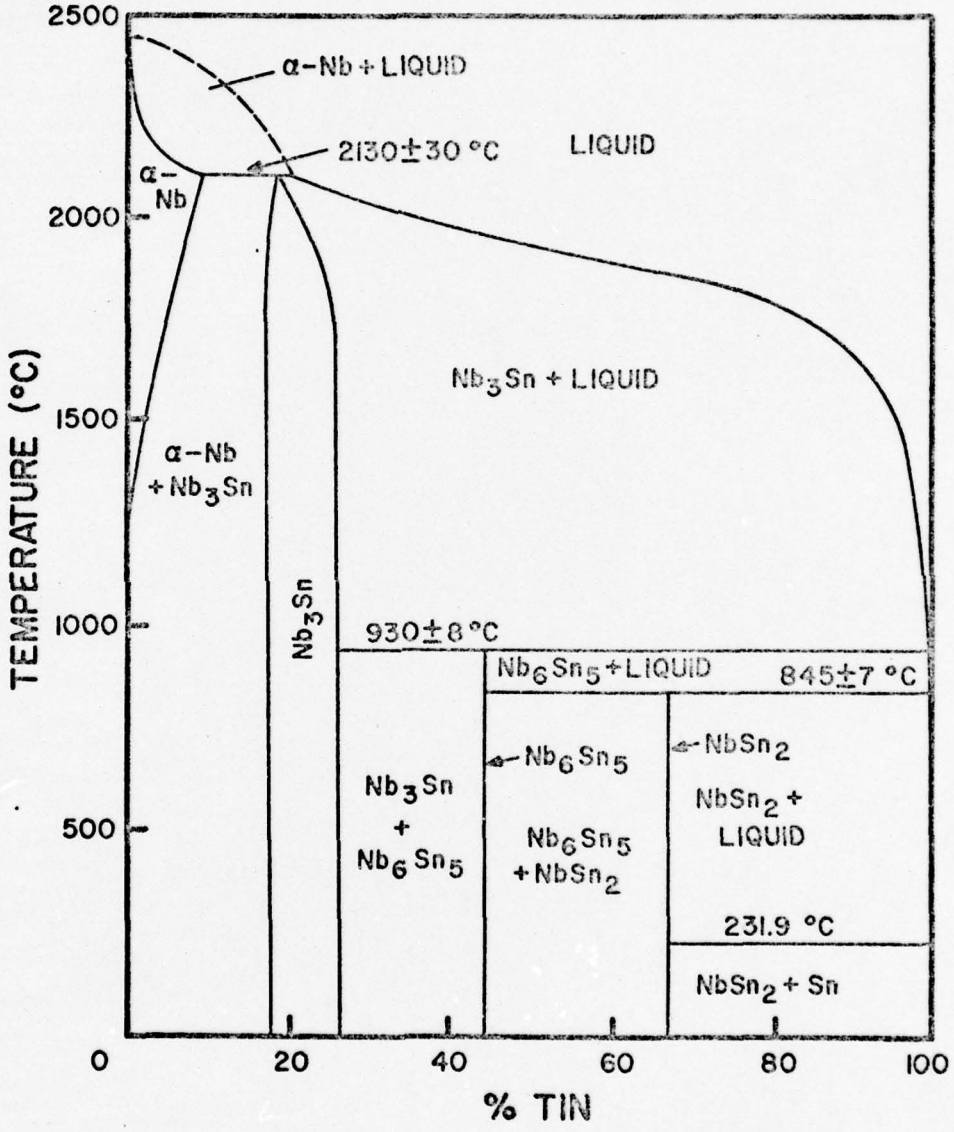

3.5 Nb-Sn Binary Phase Diagram from Ref. 44.

$d = 2\sqrt{Dt}$ where d = diffusion depth (cm),

t = time (sec),

D = diffusion coefficient (cm^2/sec);

and

$D = D_0 \exp(-Q_0/RT)$ where $D_0 = D(T=0)$ and T = temp (° C),

R = 1.987 cal/mole ° C ,

Q_0 = activation energy.

Relevant data: T = 1300 - 1350° C,

$D_0 = .022\ cm^2/sec$,

Q_0 = 55.4 kcal/mole.[86]

Experimental conditions: T = 1000° C

Q_0 = 42.7 kcal/mole (extrapolated),[87]

t_{max} = 20 hrs,

t_{min} = 10 min.

Calculations:

$D = .022 \exp(-42.7\text{x}10^3/1.987\text{x}1.0\text{x}10^3) = 1.067\text{x}10^{-11}\ cm^2$

$d(20\ hrs) = 2\sqrt{1.022\text{x}10^{-11}\text{x}20\text{x}3600} = 1.72\text{x}10^{-3}$ cm

$= 17.2\ \mu m$

and $d(10min) = 2\sqrt{1.022\text{x}10^{-11}\text{x}10\text{x}60} = 1.6\text{x}10^{-4}$ cm

$= 1.6\ \mu m$

The reason for the temperature range listed under relevant data is that this is the temperature range for which D_0 and Q_0 were determined. The experimental conditions call for T>930°C so that

the reaction takes place in that portion of the Nb-Sn binary phase diagram where the only allowable solid solution of niobium and tin is the A15 phase Nb_3Sn.[44] (See Figure 3.5.) The actual thickness of the calculated 17.2 μm Nb_3Sn layer fabricated by Diadiuk was confirmed experimentally to be ~17μm by anodizing across the cross section of a sample and taking advantage of the different color of an anodic film on Nb from that on Nb_3Sn to optically estimate the Nb_3Sn thickness.[29]

The following sample sets (see Table II) comprise the basis for this thesis investigation. Diadiuk's 17.2 μm thick layer sample set (fabricated as described above) is used as the author's sample set of maximum layer thickness. Diadiuk's sample set included four discs of each substrate orientation cut from a 3.2mm diameter Nb single crystal. The author's sample sets, fabricated with layer thicknesses of 12.1 μm, 2.9 μm, 2.9 μm, and 1.6 μm, included one disc of each orientation cut from the 4.6mm diameter Nb single crystal. A 17.2 μm thick layer set (9115) was attempted by the author, but improper quenching (i.e., allowing the quartz ampule to cool slowly in the furnace) prevented the formation of any useful A15 phase material. There are two 2.9 μm sample sets: one set (9152) was made at an undetermined temperature considerably higher than 1000° C (estimated to be ~1150° C). The absence of a sample set of layer thickness ~8 μm is an oversight of the author. It is impractical to make samples thinner than 1 μm by this Sn diffusion process due to

the extremely brief baking period necessary. One disc in the 12.1 μm sample set has an excess of free tin due to sloshing of tin from the well upon removal of the quartz ampule from the furnace. Some of the data is therefore unavailable on this sample.

Sample Analysis

Upon removal from the ampule, the rod shaped samples are examined utilizing a back-reflection Laue photograph (tungsten X-ray tube) of the rod's end through the Nb_3Sn layer and referencing the indexed photograph to a fiducial mark placed on the rod in order to determine specific Nb substrate directions at the Nb_3Sn collar circumference. These X-ray photographs reveal circular rings of fine dots which correspond to reflecting planes of the Nb_3Sn polycrystalline layer on the rod's end. After the ends are subsequently polished (#600 wet-dry silicon carbide paper), etched (HF acid) and rephotographed, one also sees very clearly the geometric pattern of spots corresponding to the Nb(110) single crystal rod substrate. The rings in this second photo are indexed for orientation as described above.

T_c

Sample analysis started with inductive measurements of the superconducting critical transition temperature, T_c. Standard

inductive rigs are used with a 20mV 400 Hz ac signal applied to a primary coil and a phase sensitive detector to receive signals from a secondary coil. (Both rigs utilized were designed and build by I. Puffer). As the sample passed through its transition from the normal to the superconducting state, the change in its magnetic susceptibility is detected in the secondary coil. A germanium cryo-thermometer, kept in thermal contact with the sample and calibrated from 4K to 25K, measures the temperature during the run. The sample is cooled in a liquid helium bath and warmed via a resistively heated copper can encasing the coils and sample holder. The sample and the cryo-thermometer are allowed to reach thermal equilibrium near the transition before going through the transition to prevent any time lag in the thermometer reading as the transition is made. Cooling and heating curves have negligible ($\lesssim$.2K) hysteresis when this procedure is followed. The signals monitored for all sample thicknesses are of the same order of magnitude and were generated with no great difficulties. However, not all samples show the expected 9.2K transition for the Nb. See Chapter IV for a discussion of this behavior.

X-ray Diffraction

The X-ray diffraction studies are carried out in this laboratory on a General Electric XRD5 diffractometer, a Siemans texture diffractometer, and a General Electric/Polaroid back-reflection pinhole camera apparatus.

X-ray diffractometer scans are made only on the disc samples because the small diameter rounded surfaces of the rod samples are not conducive to scanning diffractometer techniques. The samples are scanned from $2\theta = 20°$ to $2\theta = 120°$ with filtered Cu radiation to take advantage of the several uses of diffractometer scans. X-ray diffraction is a bulk investigative technique and one would expect to see (and indeed does) diffraction patterns corresponding to the Nb substrates as well as the Nb_3Sn diffusion layers. By running separate scans of pure Nb substrate discs and scans of glass mounting slides and adhesives, their patterns are identified and can be subtracted from the sample scans to facilitate analysis. The only peaks which cause difficulties in this vein are those caused by the Nb(110) substrate and the Ag conducting paint used as an adhesive, both of which occasionally obscure the A15(210) peak. The presence of any other peaks in the scans other than those belonging to the A15 phase Nb_3Sn, the Nb substrate, or the glass mounting slide and adhesive, would have indicated second phase material in the sample. An anomalous peak does appear in some samples (with no discernable regularity) at $2\theta \approx 37.6°$ ($d \approx 2.39$ Å) which corresponds very closely to the (026) reflection of Nb_6Sn_5. However, no other Nb_6Sn_5 peaks are present in the scans and identification of this single peak as evidence of second phase material is unsupportable.

Comparison of integrated peak intensities of the sample

scans with a scan of single-phase A15 325-Mesh Nb_3Sn powder sample (prepared by Dr. Stuart Cogan) is made to determine the existence of preferred orientation in the diffusion layers. Peak suppression or enhancement provides the key to this determination. (Integrated intensity measurements were made by cutting out each peak from the strip chart recording and weighing the cut outs on a Mettler H31 balance.)

Lattice parameter measurements are also made to determine trends in the lattice parameter as a function of the substrate crystallographic orientation and layer thickness. Because the Bragg Law (Eq. 2.1) shows interplanar spacing, d (and therefore a_0, the lattice parameter) to be a function of sin θ, precision in d depends upon precision in sin θ, a derived quantity, and not upon precision in θ, a measured quantity. It is therefore important to make angular measurements for use in lattice parameter determination as near to $\theta = 90°$ as possible to take advantage of the fact that $\sin\theta$ changes very slowly with θ at these angles.

Back-reflection pinhole photographs are made using Cr, Co and Cu radiation, allowing one to sample various depths (ranging from ~9 μm to ~30 μm) of the specimen. For shorter wavelength (i.e., deeper penetrating) radiation one expects (and does see) the single crystal Nb substrate Laue pattern. For longer wavelengths, the Debye rings of the polycrystalline Nb_3Sn become visible. These rings are indexed to the Nb_3Sn reflecting planes

utilizing the standard lattice parameter value of 5.29 Å.[88] A typical photograph contains four to six continuous rings of fairly uniform but very weak intensity. Most photographs were taken with a Cu X-ray tube at 27 kV, 15 mA and a 20 minute exposure with Type 57 Polaroid film. After etching Diadiuk's 17.2 μm thick layer discs with a solution of $HF:HNO_3:H_2O$ - 1:1:1 for 10 seconds, the photographs again reveal the rings superimposed on the single pattern of the respective Nb substrates.

Sample analysis was attempted on a Siemens texture diffractometer using the Schulz reflection method to determine direct X-ray pole figures.[57] This determination would have combined with diffractometer scans to give a conclusive picture of any preferred orientation, however, the sample geometries (i.e., too small to generate meaningful, detectable X-ray signals) curtailed any definitive pole figure analysis. However, efforts in this laboratory are presently directed at the pole figure analysis of Nb_3Sn diffusion layers fabricated on polycrystalline Nb foils. The current status of this study is presented in Appendix 3.

SEM and EDX

The Mark IIA Cambridge Stereoscan at M.I.T. was used to investigate the morphology and microstructure of the Nb_3Sn samples. Disc-shaped samples are analyzed four at a time, mounted on a rotating sample holder. However, rod-shaped samples have to be

removed from the SEM specimen chamber and manually rotated between desired orientations. Samples are examined initially at a low magnification (500X - 1000X) to inspect general structural features and then at higher magnifications (10,000X - 20,000X) to observe specific details of the microstructure.

Each sample also has an EDX scan taken to determine chemical composition. The detected X-rays originate approximately 1 to 1.5 μm deep in the specimen so that identification of specific elements is an analysis of the sample's bulk composition rather than that of its surface. The EDX output gives information concerning relative concentrations of individual elements. Absolute elemental concentrations can be determined only if a known standard specimen is available for comparison. A portion of a single-phase Nb_3Sn arc-melted button was utilized in this study as the standard and allowed the author to determine the Sn composition of samples to an accuracy of ±1.0 atomic per cent. (See Table II.)

Selective chemical etching of the rod samples was performed in order to expose the Nb-Nb_3Sn interface for observation at various magnification in the SEM. The rod samples were cut in two geometries: along the cylindrical axis, and perpendicular to this axis, in an attempt to get two perspectives on the interface. The cut sections were mechanically polished with #600 wet-dry silicon carbide paper, a .3 micron alumina polishing wheel, and finally a .06 micron alumina polishing wheel. They were then etched

by one of two methods: either by dipping the sample into the etchant for the desired time or by applying drops of the etchant to the sample surface and allowing the surface tension of the drops to hold them in place as they chemically attacked the sample. The drop method normally proved more effective than the dipping method, although neither were readily reproducible.

The dipping etchant protocol was: 30 minutes of HF acid, followed by 1 minute of $HF:HNO_3$ - 1:1, then 2 minutes of HF and finally a 5 minute acetone ultrasonic bath. The $HF:HNO_3$ combination is extremely powerful etchant of Nb_3Sn while HF attacks the Nb alone and is used to remove any oxides left by the nitric acid (nonconductive oxides are detrimental to clear SEM analysis). This protocol gave the revealing electron micrographs shown in Figures 4.19 and 4.20. Other etch protocol were also tried, e.g., combinations of HF, $HF:HNO_3$ (1:1, 2:1), $HF:HNO_3:H_2O$ (1:1:1), and HF. Times varying from 5 to 30 minutes of straight HF and from 5 seconds to 1 minute of the $HF:HNO_3$ combinations could expose the $Nb-Nb_3Sn$ interface as clearly as in the above figures. The problem of the proper etching techniques to examine the interface can possibly be solved by judicious use of new, fresh, uncontaminated acids in a carefully controlled and clean experimental environment.

RED

The reflection electron diffraction experiments were carried out on the Philips transmission electron microscope at M.I.T. Best pattern definition and least background radiation were obtained on Diadiuk's disc samples at beam energies of 60 ke V and on disc samples VD Nb_3Sn-Nb(111), VD Nb_3Sn-Nb(211) [both etched as described in Chapter IV], and 9141-D-111 at beam energies of 80 ke V. Although RED patterns were obtained from the planar surfaces of these disc samples, and from these patterns A15 crystal structure was confirmed in the layer, the faintness of the diffraction rings observed suggested that preferred orientation in the samples could be only very cautiously inferred. The Nb_3Sn diffusion layer rods could not be studied by RED because the electron beam, incident on the sample at glancing angles of ~3°, produces too large a beam spot to focus over the curved surfaces of the rods.[89]

IV. RESULTS AND DISCUSSION

This presentation of experimental results will generally follow a dual format, correlating samples of a given A15 layer thickness and correlating samples fabricated on substrates of the same bcc orientation. "Sample set" refers to a group of rod-shaped substrates and their associated, oriented disc substrates reacted at the same time in the same quartz ampule. Table II is a Master Data Table of all samples comprising this study. The 17.2 μm thick A15 layer samples of V. Diadiuk are designated by VD Nb_3Sn - Nb(h k ℓ); the author's samples are designated by the Julian date of fabrication and substrate geometry (D=disc, R=rod), followed by the (h k ℓ) orientation of the underlying bcc substrate for the disc samples and a 1 or 2 (1=4.6 mm diameter substrate, 2=3.2 mm diameter substrate) for the rod samples. For example, 9192-D-111 refers to a sample fabricated on 11 July 1979 which is a disc-shaped Nb substrate with the bcc-(111) orientation perpendicular to the planar face; 9141-R-2 refers to a sample fabricated on 21 May 1979 that is rod-shaped and 3.2 mm in diameter.

Figures 4.12-4.15 and Figures 4.23-4.27 present data for discs in terms of the four major bcc orientations shown on the standard bcc-(110) stereographic projection of Figure 3.2. This presentation allows one to make a more immediate orientational correlation of the data.

TABLE II

MASTER DATA TABLE

SAMPLE	CALCULATED A15 LAYER THICKNESS (± 0.5 μm)	T_c (°K±0.2°K) ONSET	FINISH	ΔT_c (°K)	EDX % Sn (± 1.0%)	LATTICE PARAMETER (±.0001nm)	COMMENTS
VD Nb_3Sn-Nb(100)	17.2 μm	17.7	16.9	0.8	24.8	0.52849	
VD Nb_3Sn-Nb(110)	17.2 μm	17.5	16.8	0.7	25.2	0.52941	
VD Nb_3Sn-Nb(111)	17.2 μm	18.0	16.2	1.8	24.9	0.52959	
VD Nb_3Sn-Nb(211)	17.2 μm	18.0	17.7	0.3	25.1	0.52879	
9115-R-1	17.2 μm	16.1	12.4	3.7	14.2	a	*
9115-R-2	17.2 μm	18.2	14.0	4.2	14.8	a	*
9115-D-110	17.2 μm	no A15 transition			-		*
9141-R-1	12.1 μm	16.0	14.4	1.6	17.1	a	*
9141-R-2	12.1 μm	17.3	15.7	1.6	18.7	a	*
9141-D-100	12.1 μm	16.8	13.8	3.0	28.4	0.52974	*
9141-D-110	12.1 μm	17.2	17.0	0.2	45.1	b	c
9141-D-111	12.1 μm	16.4	16.0	0.4	25.2	0.53033	
9141-D-211	12.1 μm	16.4	15.6	0.8	23.5	0.52960	
9152-R-1	2.9 μm	15.7	15.2	0.5		a	d
9152-R-2	2.9 μm	16.0	14.4	1.6		a	d *
9152-D-100	2.9 μm	16.3	16.0	0.3	26.0	0.52957	d
9152-D-110	2.9 μm	16.2	15.7	0.5	21.8	0.52920	d
9152-D-111	2.9 μm	16.7	15.7	1.0	23.2	0.52993	d
9152-D-211	2.9 μm	17.2	13.8	3.4	20.9	0.52989	d
9192-R-1	2.9 μm	15.6	14.7	0.9	8.7	a	*
9192-R-2	2.9 μm	14.5	12.7	1.8	-	a	
9192-D-100	2.9 μm	15.9	14.4	1.5	22.0	0.52896	
9192-D-110	2.9 μm	16.8	15.7	1.1	21.6	0.52897	
9192-D-111	2.9 μm	17.3	16.0	1.3	24.2	0.52969	
9192-D-211	2.9 μm	17.8	17.5	0.3	26.9	0.52938	
9197-R-1	1.6 μm	no A15 transition			-	a	*
9197-R-2	1.6 μm	no A15 transition			-	a	*
9197-D-100	1.6 μm	17.7	14.2	3.5	12.2	0.52732	e *
9197-D-110	1.6 μm	17.8	10.0	7.8	11.1	0.52647	e *
9197-D-111	1.6 μm	17.0	16.0	1.0	10.7	0.52870	e *
9197-D-211	1.6 μm	17.8	16.7	1.1	9.4	0.52725	e *

NOTES ON TABLE II -- MASTER DATA TABLE

a - lattice parameter measurements were not made on rod shaped samples.

b - lattice parameter measurements were not made on this disc shaped sample.

c - an excess of free tin on the surface caused by accidental sloshing of molten tin during fabrication gave an unusually high EDX tin composition and obscured a_o measurements.

d - these samples were fabricated at an unknown temperature above 1000°C (estimated to be approx. 1150°C) due to a faulty monitor thermocouple.

e - low EDX tin compositions can be attributed to the 1 to 1.5 μm penetration depth of the EDX measurement and the thin nature of the diffusion layer.

* - indicates sample with an observed 9.2K Nb transition on the superconducting transition temperature curve.

T_c Measurements

Inductive T_c measurements of the superconducting transition temperatures were made as described in Chapter 3. The values presented in Table II (Master Data Table) are the transition onset (T corresponding to 1% of transition magnitude), transition finish (T corresponding to 99% of transition magnitude), and transition width ($\Delta T_c = T_{c\ ONSET} - T_{c\ FINISH}$) in degrees Kelvin. However, in cases of thick Nb_3Sn layers on discs the Nb transition was generally not observed. Perhaps when this geometry of A15 layer is sufficiently thick, it screens the transition of the lower transition temperature niobium interior from the detecting coil. Multiple transitions were observed both for the A15 layers and for the niobium crystal in some cases, as might be expected for a sample configuration consisting of both elemental Nb and Nb_3Sn. (See Figure 3.3.) The sample rods and discs with thinner layers generally exhibited this behavior. The 9.2K transition of the Nb provided a check on the accuracy of the Nb_3Sn transition (±0.2K). The magnitude (vertical curve displacement between the onset and finish temperatures) and shape (slope of the curve) of the transition are generally thought to depend on the volume of the sample with a given T_c and on the uniformity of the sample composition, respectively.[74] Since the magnitude of the transitions in these samples are all of the same general size, suggesting that the variations in diffusion layer volume fall within the same order of magnitude (which they do), it

must be that the supression of the Nb transition signal is sensitive to very small differences in A15 thickness. The 1.6 μm thick A15 layers appear to be the threshold of thickness above which the diffusion layer discs do not exhibit a Nb transition. The slopes of the transition curves are all relatively smooth which means there were no significant volumes of second phase material other than A15.

Some very interesting trends exist on T_c (both onset and finish) as a function of A15 layer thickness as illustrated in Figures 4.1 and 4.2. For a given (h k ℓ) of substrate the T_cs appear to fall into "thickness regimes". Variations in T_c for each substrate seem to occur as the layer thickens from one regime to another. These thickness regimes extend approximately as follows: 1 to 3 μm, 3 to 9 μm, 9 to 15 μm and 15 to 17 μm; Values of T_c finish for all thicknesses tend to show much wider variations than do the T_c onsets. Since T_c finish is probably associated with the lowest quality A15 phase material, the large variations suggest that in situ annealing during fabrication may be significant. Certainly, the short fabrication time of the 1.6 μm layers may mean the incomplete atomic ordering and the unusually wide variation in T_c finish.

There is, within the thickness regimes, an apparent hierarchy of T_c value according to the substrate (h k ℓ). For the

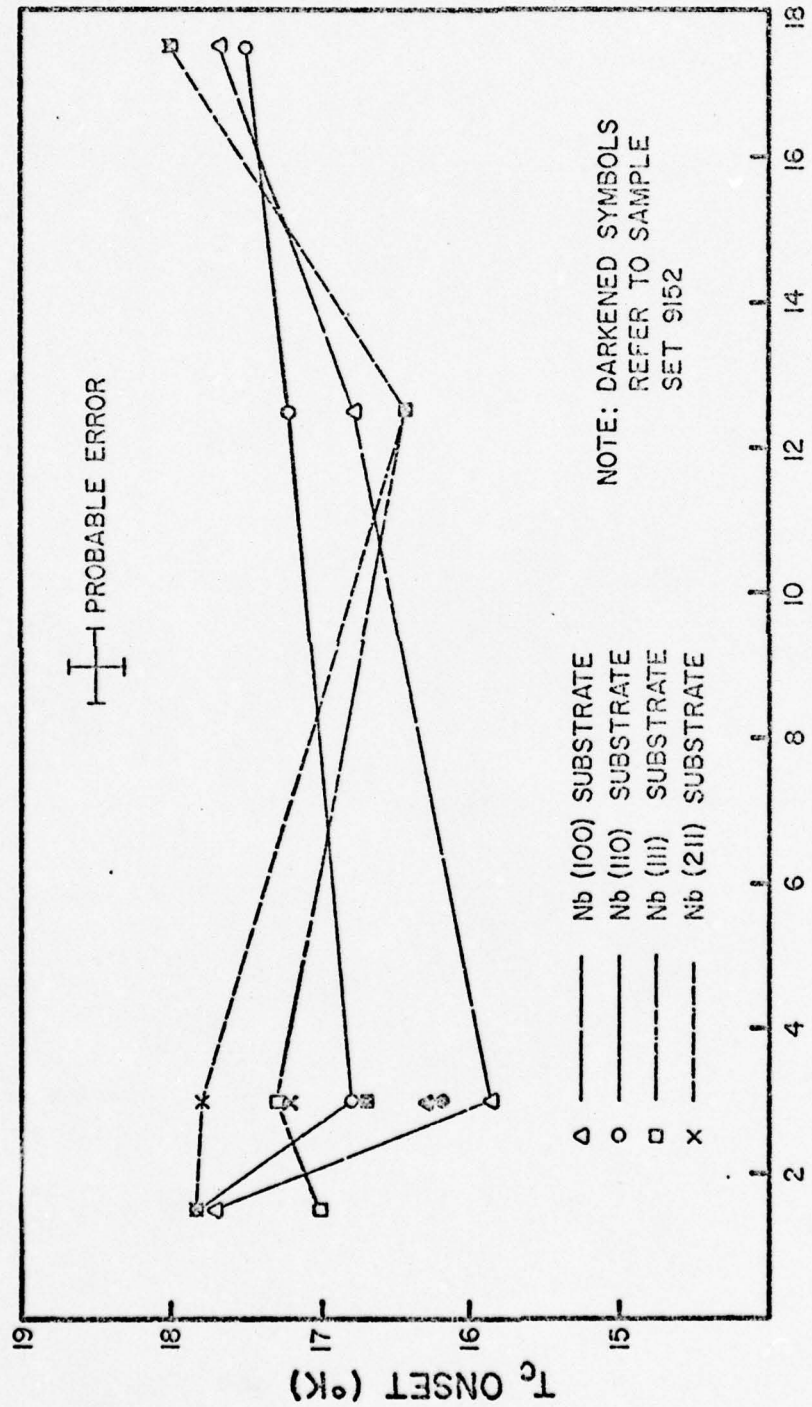

4.1 T_c Onset vs. A15 Layer Thickness as a Function of Nb Disc Substrate Orientation

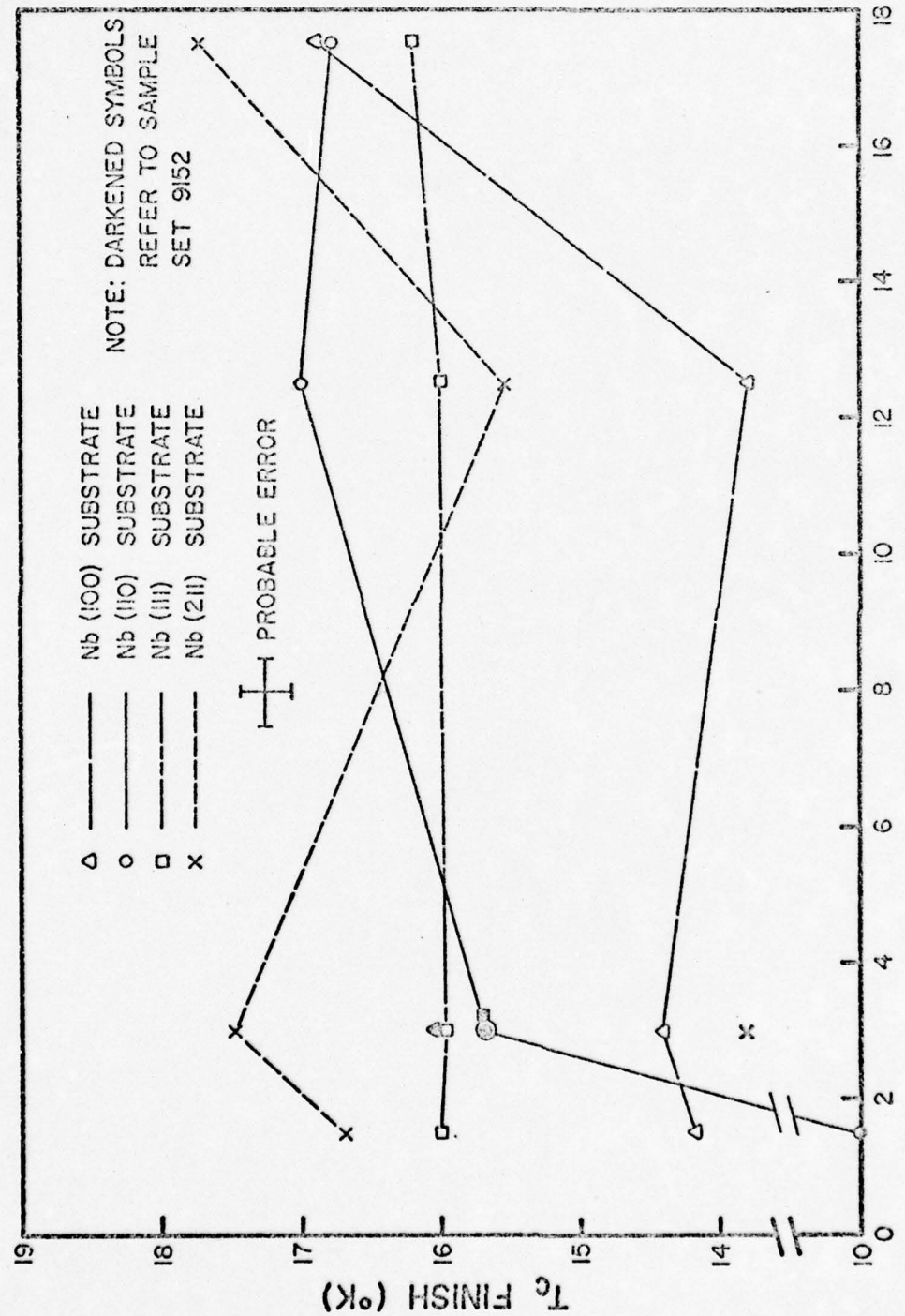

4.2 T_c Finish vs. A15 Layer Thickness as a Function of Nb Disc Substrate Orientation

1 to 9 μm and 15 to 17 μm thicknesses, layers fabricated on Nb(211) substrates have the highest T_c onset and T_c finish values; in the middle range, 9 to 15 μm, A15 layers on the Nb(110) have the highest T_c values. Of particular note is the T_c insensitivity of the A15 layer on the Nb(111) substrate to layer thickness: T_c onset is ~17K and T_c finish is ~16 K for all thicknesses. The consistency of these values may be indicative of relative homogeneity of the A15 material across the layer's thickness as compared to material on other Nb(h k ℓ) directions.

The plots of transition width (ΔT_c) versus layer thickness in Figure 4.3 for each Nb(h k ℓ) substrate bear this out: T_c for layers on Nb(111) substrates is consistently ~1K. Interestingly, ΔT_c's of layers on Nb(211) substrates are of this same size even though the T_c onset and T_c finish values are variable for this substrate orientation. At the other extreme, variations of ΔT_c with thickness of layers on Nb(100) are unusually high. This sensitivity of ΔT_c to layer thickness in this case may relate to the two other observations: for the 2.9 μm Nb_3Sn layers, the increased fabrication temperature (>1000°C) of sample set 9152 as compared to 9192 resulted in depressed T_c onsets and finishes for all Nb(h k ℓ) substrates, except the Nb(100), where T_c increased; in the 1 to 9 μm thickness regime, Nb_3Sn on the Nb(100) substrate orientation has the lowest value of T_c onset of any Nb(h k ℓ) substrate.

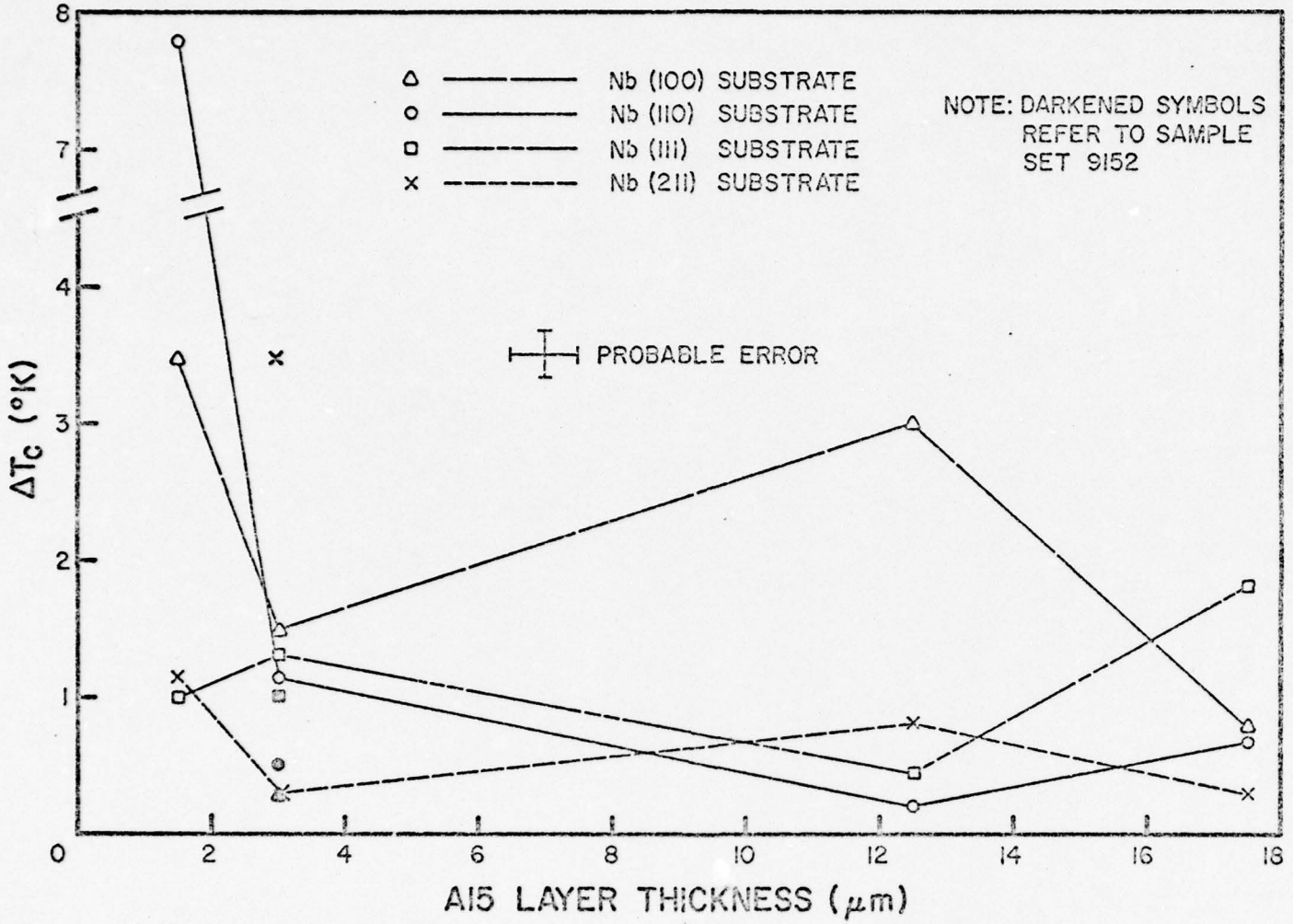

4.3 ΔT_c vs. A15 Layer Thickness as a Function of Nb Disc Substrate Orientation.

Lattice Registry

At this point, before embarking on presenting results pertaining to structure of the A15 layers, it will be beneficial to subsequent remarks to interrupt the discussion of experimental results in order to present some ideas concerning lattice registry between the Nb bcc lattice and the Nb_3Sn A15 lattice. Examination of Diadiuk's 17.2 μm diffusion layer surfaces, which are also the initial growth surfaces of these layers, with RED indicated preferred orientation effects in the Nb_3Sn corresponding to specific underlying bcc substrate orientations. (See Table III -- This RED determination will be discussed later in this chapter, along with the author's RED results). In order to account for these experimental results, geometric arguments for lattice registry were employed by Diadiuk to suggest possible specific bcc-A15 lattice associations.[29]

The calculations of Figure 4.4 show how one might use the interatomic spacing of the various planes to analyze possible matchups of the bcc and A15 lattices. Diadiuk's inferred matchups from her RED results were: bcc-(100)||A15-(110), bcc-(110)||A15-(100), bcc-(111)||A15-(111), bcc-(211)||A15-(110). The precision of these lattice fits are expressed on Figure 4.4 as the percentage of the A15 distance by which the registry is non-ideal: positive percentages involve lattice contractions to match to the Nb lattice and negative percentages refer to the need for A15 lattice expansions to match to the underlying Nb.

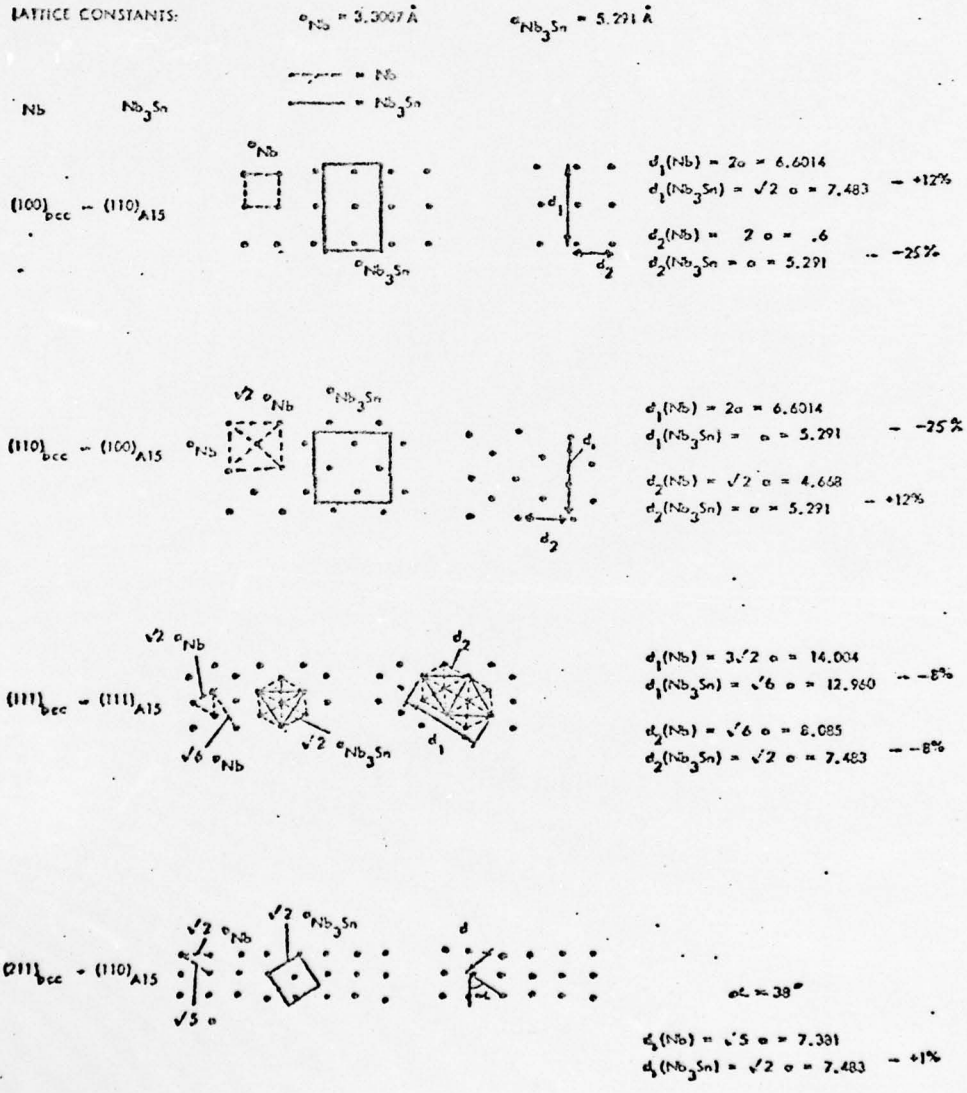

4.4 Geometric Considerations in the Lattice Registry Between the Nb bcc and Nb_3Sn A15 Lattices

Subsequent consideration of Diadiuk's registry associations and the availability of the author's RED and X-ray results (discussed later in this chapter) have allowed testing of the viability of these lattice registry associations both by geometrical simulation of the lattice in 2 dimensions and by monitoring of preferred orientation effects as layer thickness is varied. Diadiuk's bcc-(110)||A15-(100) and bcc-(111)||A15-(111) registry associations have been confirmed by the simulation; however, simulation of the proposed lattice registry associations for bcc-(100) and bcc-(211) to the A15 were unsuccessful. An attempt to find a registry association by a similar simulation for a bcc-(h k ℓ)||A15-(210) was also unsuccessful. This attempt was motivated by the unusually high X-ray intensities of the A15 (210) peak noted in several diffractometer scans (e.g., see Figure 4.26).

Further consideration of lattice registry associations and preferred orientation effects in the Nb_3Sn layers will be made in the course of discussing the natures of the microstructure, surface structure, and bulk structure of these layers.

Lattice Parameter and Composition

The lattice parameter of the A15 phase Nb_3Sn was determined by measuring the d-spacing of several peaks in the X-ray diffractometer scans. Appendix 1 lists the specific peaks used to calculate the lattice parameter of each disc sample. As many high angle peaks as possible (those with sufficient intensity to allow positive h k ℓ identification) were used in order to minimize errors between the observed value θ and the value used in the numerical calculations, $\sin\theta$. See Table II (Master Data Table) for a tabulation of the lattice parameters.

A plot of lattice parameter vs. A15 layer thickness (see Figure 4.5) reveals that for all layer thicknesses, a_o (lattice parameter) of Nb_3Sn on a Nb(111) substrate samples is greater than a_o for Nb_3Sn on non-Nb(111) substrates. A possible basis for this behavior may be the comparatively high and pervasive level of impurities for A15 on Nb(111) observed in Auger profiles of the 17.2 μm by Diadiuk.[24] These impurities may contribute to the lattice expansion and thereby the stability of the A15 structure which grows on the Nb(111) substrate.

The numerical values of a_o for all substrate orientations appear to be similarly behaved to one another for all thicknesses. The behavior defines two thickness regimes: in the thinner, 1.6 μm layers, all exhibit a reduction in a_o, but it is particularly marked in the case of the layers on non-Nb(111) substrates. The

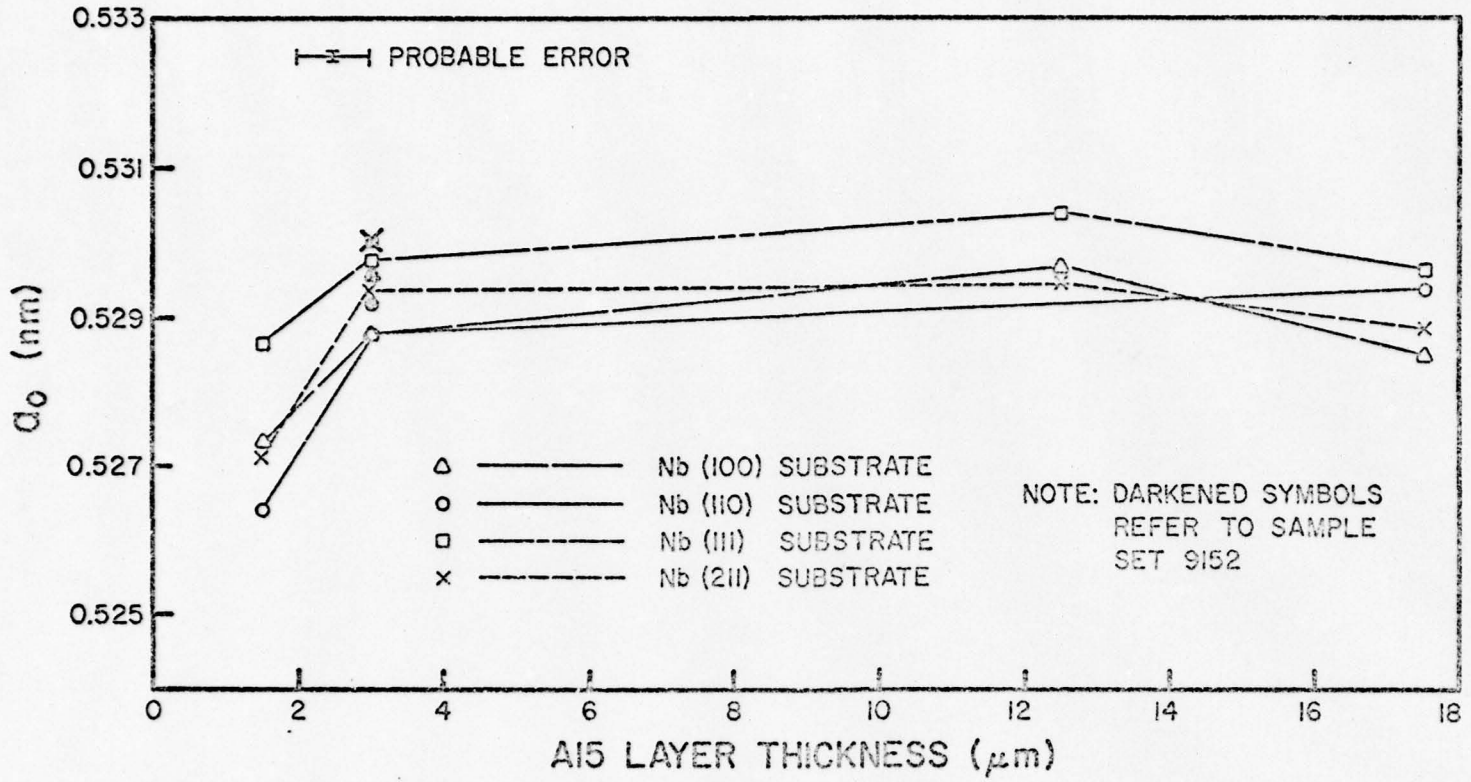

4.5 Lattice Parameter vs. A15 Layer Thickness as a Function of Nb Disc Substrate Orientation.

reduction in a_o may come about because for such a thin layer, lattice registry influences on layer structure and morphology at the Nb_3Sn growth surfaces[46] play a relatively larger role in determining the resultant average value of a_o determined by X-ray analysis of the layer than is true for thicker layers. That the reduction is more severe for the non-Nb(111) substrate sample layers seems consistent with the fact that the Nb_3Sn lattice, during initial layer formation, in these cases, must contract to fit the bcc lattice thus adding to the total reduction.

Of interest is the observation that the lattice parameters of the 2.9 μm thick layer samples fabricated at a temperature greater than 1000°C (sample set 9152) are consistently greater for a given Nb(h k ℓ) substrate than their counterparts in the 9192 sample set (also 2.9 μm thick, but reacted at 1000°C). Since larger grain size also results from fabrication at higher temperatures (see Microstructure Section), perhaps there is also a better developed lattice parameter. Thus, as the X-ray averages the lattice parameter over the layer thickness, the relative impact of lattice registry influences at the growth surfaces are mediated.

Figures 4.6 and 4.7 are plots of T_c onset and T_c finish respectively vs. lattice parameter for each Nb(h k ℓ) substrate orientation. The T_c onset for layers grown on the Nb(111) and Nb(211) reaches a maximum over the range of measured lattice parameters, while they dip to a minimum for Nb_3Sn layer on Nb(100) and Nb(110)

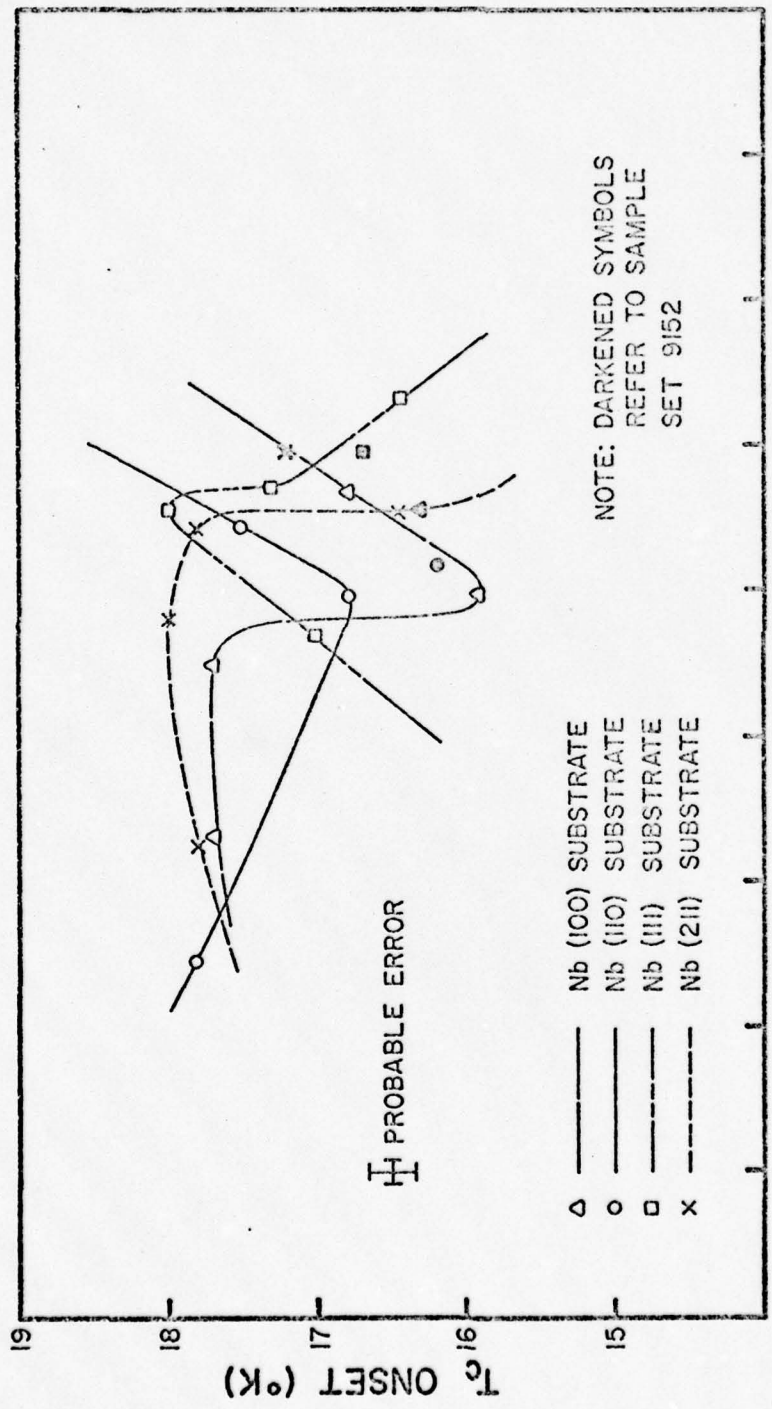

4.6 T_c Onset vs. Lattice Parameter as a Function of Nb Disc Substrate Orientation.

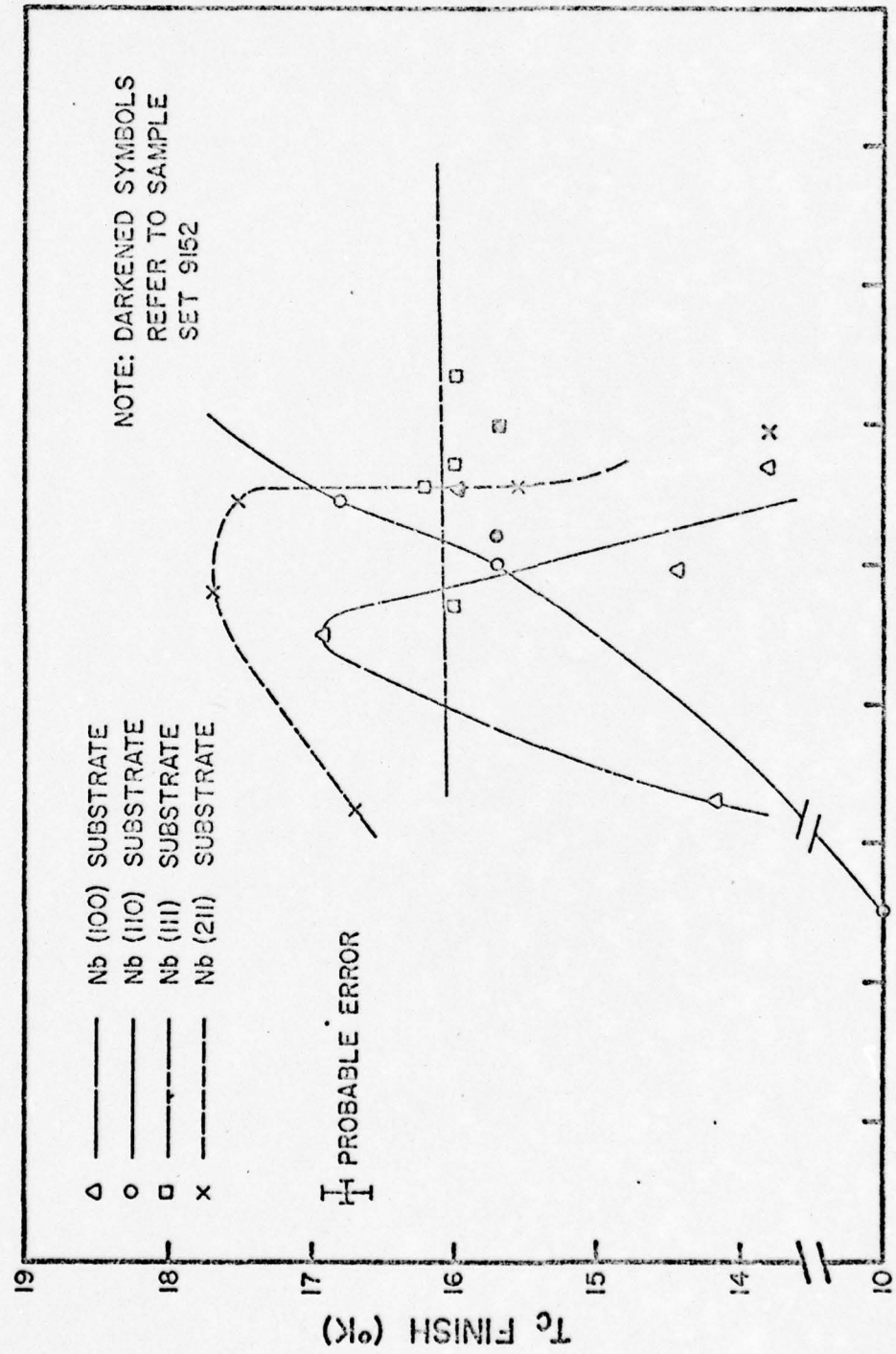

4.7 T_c Finish vs. Lattice Parameter as a Function of Nb Disc Substrate Orientation.

substrates. The Nb (211) substrate layer reaches a maximum T_c onset near an a_o of .5285 nm and drops precipitously beyond .5293 nm. Peaking behavior occurs in T_c finish of these Nb(211) substrate layers corresponding to an a_o of ~.5288 nm. However, then T_c finish drops off sharply for larger a_o values. T_c onset is reached near an a_o of .5296 nm for the Nb(111) substrate layer in keeping with the possibility of the quality of the A15 layer depending on impurity-induced lattice expansion in these layers. The behavior of T_c finish for layers fabricated on the Nb(111) substrates is relatively insensitive to variations in a_o just as it was insensitive to layer thickness. Thus, whatever attribute of the Nb_3Sn layer it is which determines T_c finish must already be present in the thinnest layers studied by the author.

The reason for the minimizing of T_c onset for Nb(100) and Nb(110) substrate layers near the standard .5291 nm values for the Nb_3Sn lattice parameter[88] is not understood. A15 layers fabricated on the Nb(100) exhibit a peak in T_c finish near a_o ~.5285 nm, while for layers on Nb(110) T_c finish appears to be steadily increasing with a_o over the range of observed a_o. It may be significant that, with the exception of the unexplained T_c onset minima for layers on the Nb(100) and Nb(110), none of the behavioral features (e.g., inflections, maxima, etc.) of T_c onset or T_c finish occur close to the standard Nb_3Sn lattice parameter value of .5291 nm.

Figure 4.8 illustrates the variation in lattice parameter with the measured tin composition of the disc layers as a function of Nb substrate orientation. For the Nb(110) and Nb(211) layers the lattice parameter peaks near tin compositions of 25% and 23.5% respectively, while the Nb(100) and Nb(111) substrate orientations have lattice parameters which continuously increase with increasing tin composition over the range of measured a_o's. (However, the scatter in the experimental data could allow one to plot the Nb_3Sn on Nb(211) curve behavior shaped as 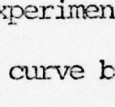

, with a local minimum at 25% tin, and the Nb(111) layer on Nb_3Sn curve behavior sharply peaked, 

, with a maximum at 25% tin. The peak values of lattice parameter for the Nb(110) and Nb(211) layers, besides being different from one another, also do not correspond to their respective a_o values of maximum T_c onset for the same Nb(h k ℓ) substrate. The behaviors of a_o vs. % Sn shown in Figure 4.8 collectively suggest that the possibility of the existence of orientational effects in Nb_3Sn bulk material should generally preclude attempts made by researchers to use lattice parameter as a predictor of T_c.

The behaviors of T_c onset, T_c finish, and ΔT_c with tin composition of the layers for each Nb substrate orientation respectively, are presented in Figures 4.9, 4.10, and 4.11. It should be recalled here that there are no tin losses from the system during fabrication because the ampule is sealed. T_c onset reaches

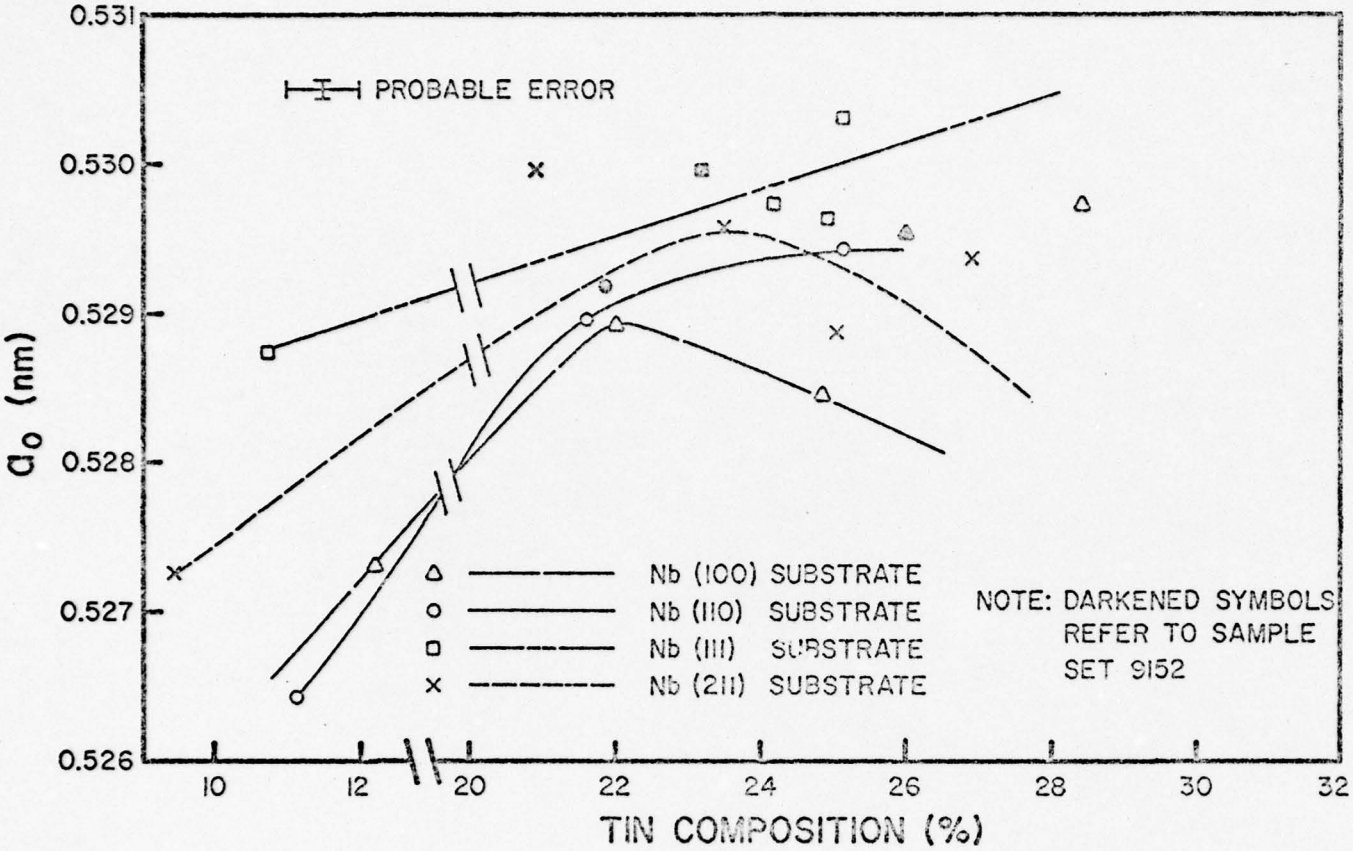

4.8 Lattice Parameter vs. Tin Composition as a Function of Nb Disc Substrate Orientation.

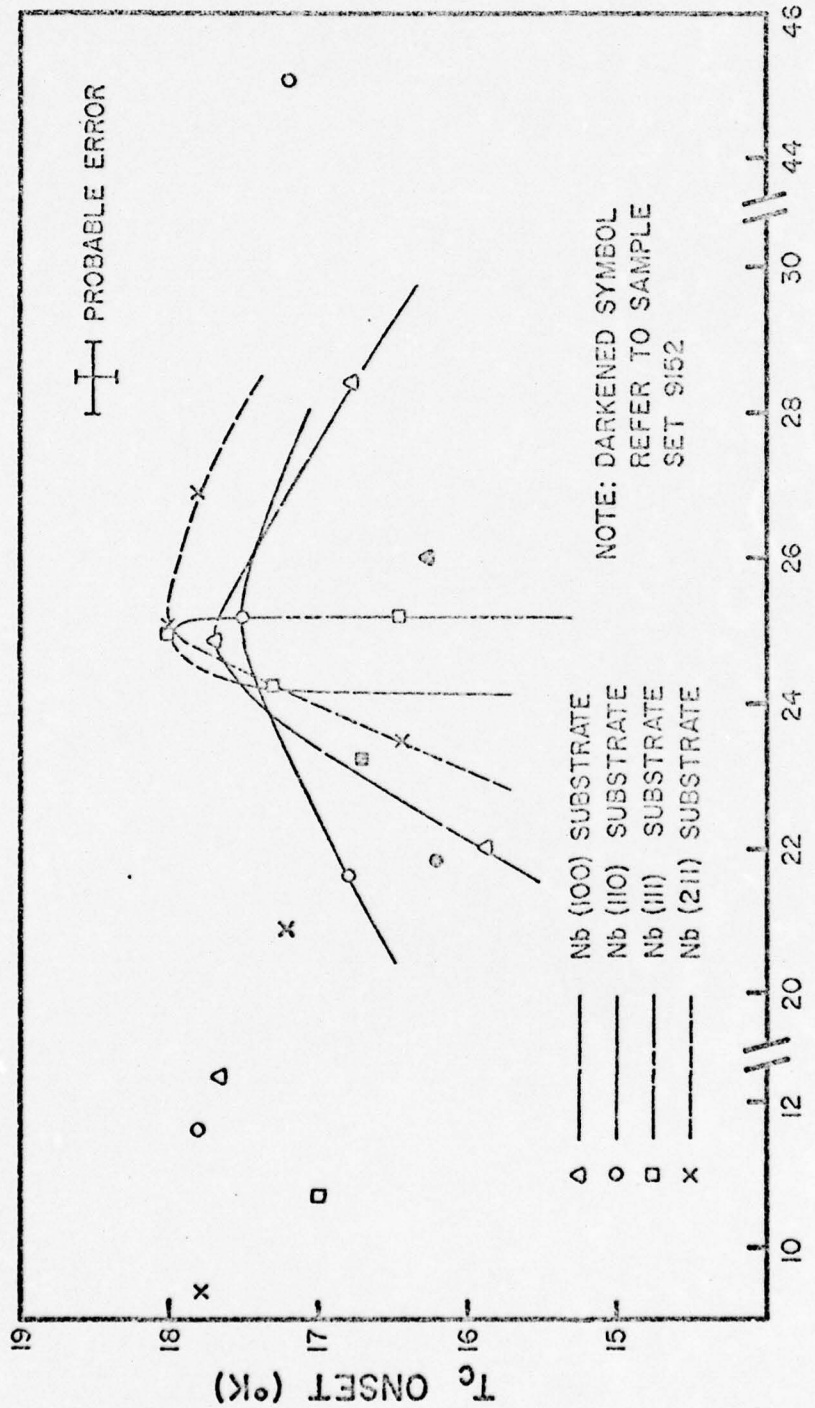

4.9 Tc Onset vs. Tin Composition as a Function of Nb Disc Substrate Orientation.

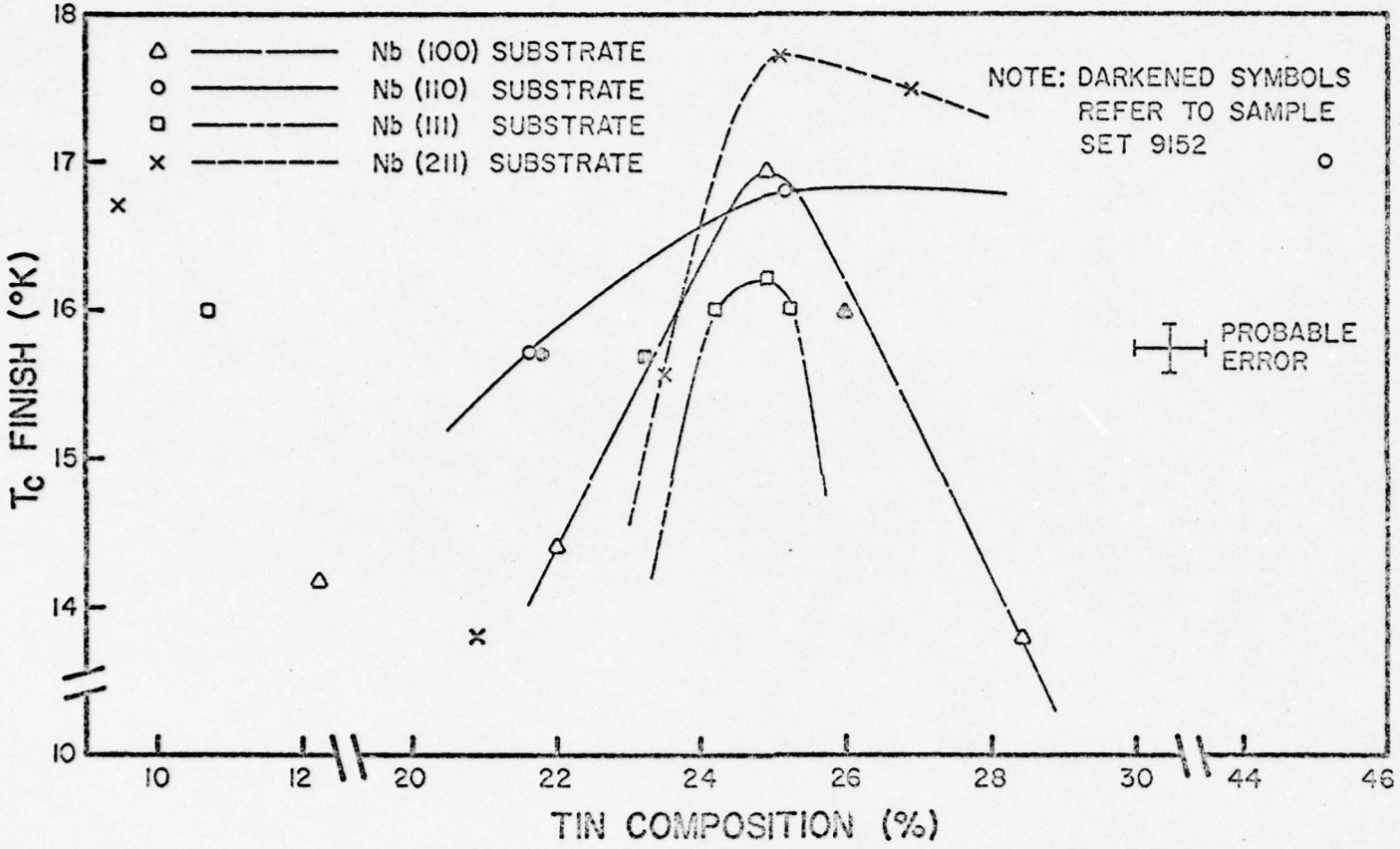

4.10 T_c Finish vs. Tin Composition as a Function of Nb Disc Substrate Orientation.

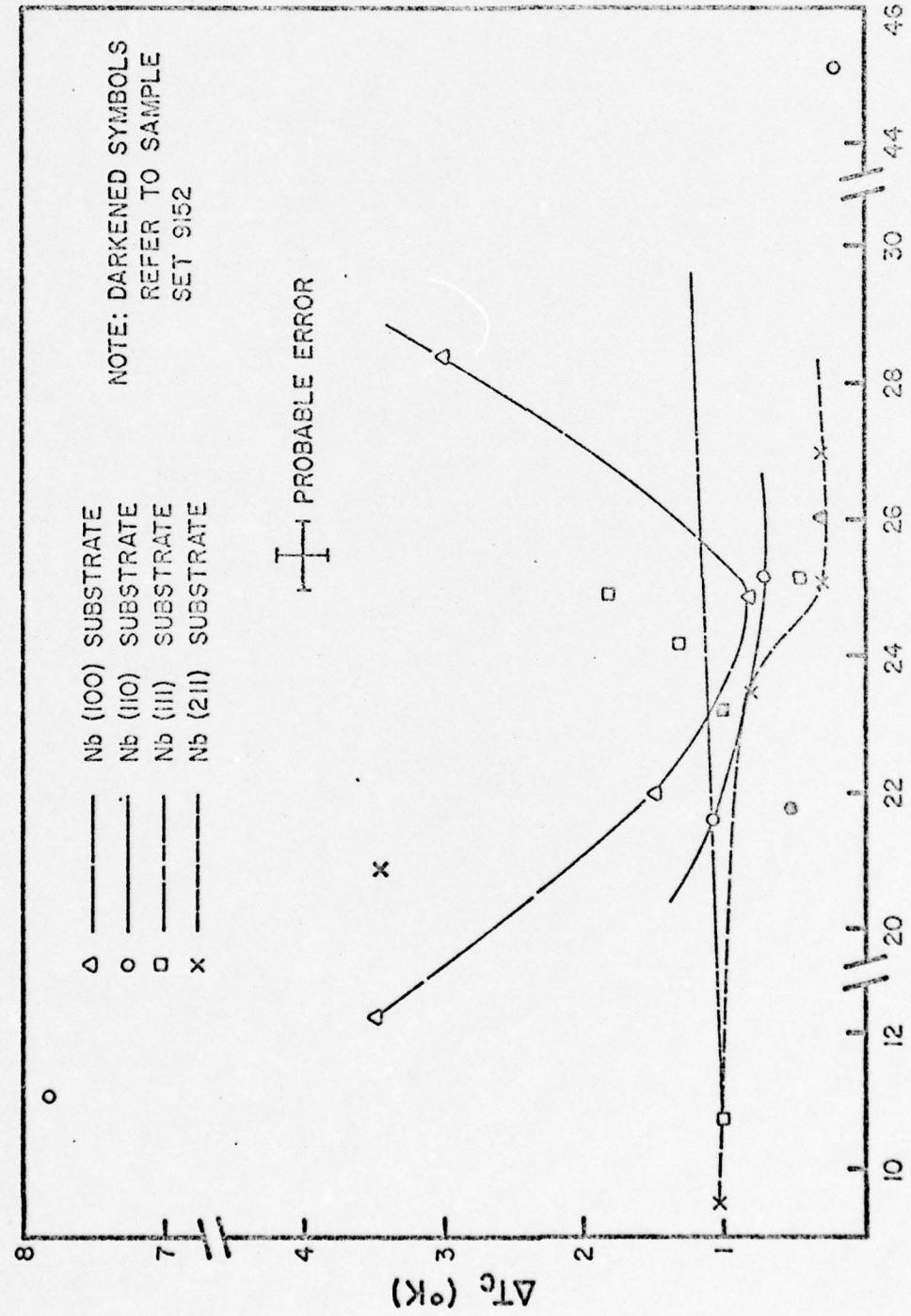

4.11 ΔTc vs. Tin Composition as a Function of Nb Disc Substrate Orientation.

a maximum very close to a tin composition of 25% (i.e. stoichiometic Nb_3Sn) for all Nb_3Sn, whatever its Nb(h k ℓ) substrate orientation. The hierarchy of T_c onsets from maximum to minimum is: Nb_3Sn layer on Nb(111) and Nb(211) substrates both have the same T_c; then layers on Nb(100); and finally layers on Nb(110). An (h k ℓ) hierarchy observed in the narrowness of the T_c onset vs. % Sn peaks: layers on Nb(111) peak very sharply near 25% tin, indicating high sensitivity to the degree of compositional stoichiometry. The peak widens for layers on Nb(211), widens still more for layers on Nb(100), and is the widest for layers grown on Nb(110).

In an attempt to compare the present results with observations by other researchers, the author examined Jacobson's results[61] for electron beam coevaporated Nb_3Sn layers deposited at a rate of 32 Å/sec on 750°C substrates, Jacobson's "low-rate, high temperature" designation. Jacobson reports a very flat maximum in T_c (presumably T_c onset) corresponding to approximately 27% tin and an increasing lattice parameter up to approximately 26.5% tin, where it levels off. The constancy of a_o and the accompanying slow decrease in T_c beyond approximately the same value of tin composition is attributed to the phase boundary between single phase A15 and the two phase region (A15 + Nb_6Sn_5). Following this logic a step further leads this author to infer that Sn composition values corresponding to T_c onset maxima for layers on particular Nb(h k ℓ) substrates may be due to textural modifications of the standard Nb_3Sn phase diagram (Figure 3.5). Phase diagram

determinations are usually made on bulk polycrystalline material without regard to orientational effects and then utilized without consideration of this fact of origin. On the other hand, the diffusion layers of this thesis study are not necessarily fabricated under the conditions of equilibrium pertaining to the standard phase diagram.[44]

The plot of T_c finish vs. tin composition, as T_c onset did above, shows peaked behavior that has different T_c finish maxima for each Nb substrate orientation: although the curve for the Nb_3Sn layer on Nb(110) does not bend completely over, the curve for layers on the other Nb(h k ℓ) substrates all peak near 25% tin. The same hierarchy of Nb(h k ℓ) designations also occurs for peak narrowness: layers on Nb(111) exhibit the peak that is most narrow, then layers on Nb(211), on Nb(100), and on Nb(110) respectively in increasing width. The peaking of T_c finish with % Sn, although consistent with the layer material being A15 in nature (the higher the value of T_c finish, the higher the quality of the "worst" A15 material) is also consistent with the existence of lower T_c phase material, which at stoichiometric composition, is minimized.

The fabrication of a second set of 2.9 μm thick Nb_3Sn layers (9152) on the four Nb(h k ℓ) major bcc symmetry directions at a temperature greater than the 1000°C used for the other 2.9 μm sample set (9192), gave T_c finish vs. % Sn data that fits exactly on the

curves of Figure 4.10. This suggests that the existence of significant amounts of second phase material as discussed above is remote. This leaves the varying behaviors of T_c onset with Nb(h k ℓ) substrate orientation as further evidence of a possible phase diagram sensitivity to layer texture.

The ΔT_c vs. tin composition plots of Figure 4.11 show that for layers on the Nb(211), ΔT_c, i.e., layer homogeneity, passes through an inflection near $\sim$ 23.5% tin, a value of composition which also corresponds to the composition of maximum lattice parameter. The minimum in ΔT_c at 25% tin for Nb_3Sn layers on Nb(100) substrates is indicative of a sensitivity of homogeneity to stoichiometry of composition. Although the behavior of ΔT_c for the layers on Nb(111) substrates is plotted as a straight line (representative of insensitivity of homogeneity to tin composition), it is also possible that the data points could determine a curve which peaks sharply at 25%, as do T_c onset and T_c finish for layers on Nb(111). This peak would lead one to suggest that, while layers of Nb_3Sn on Nb(111) substrates are relatively insensitive to variations of layer thickness and lattice parameter, they are very sensitive to compositional stoichiometry.

Microstructure

Diadiuk observed a very definite dependence of diffusion layer microstructure on the orientation of the underlying Nb substrate. Figure 4.12 shows scanning electron micrographs of Diadiuk's 17.2 μm disc samples.[29] The layers grown on the non-Nb(111) substrate though differing from one another, are generally similar: exhibiting a rough microstructure comprised of a fairly uniform distribution of columnar grains of approximately 1 μm size. The A15 layer on the Nb(111) substrate, on the other hand, shows a much rougher and more fragmented microstructure with a nonuniform distribution of grains that varies widely in size and shape. Of the non-Nb(111) layers, diffusion layers the Nb(100) substrate have the most uniform, smooth microstructure, followed by layers on the Nb(211), and finally, by layers on the Nb(110).

Scanning electron micrographs of the author's disc samples are displayed in the same format at Figure 4.12 as follows: sample set 9152 (2.9 μm) in Figure 4.13; sample set 9192 (2.9 μm) in Figure 4.14; sample set 9197 (1.6 μm) in Figure 4.15. Figures 4.16-4.18 depict rod-shaped sample surfaces and Figures 4.19-4.22 expose the Nb-Nb_3Sn interface. Figures 4.16-4.22 will be discussed in more detail in this section. Note that there are no scanning electron micrographs of the discs of sample set 9141 (12.1 μm) because the poor picture quality (due to surface charging) added no substantive information to the following comments.

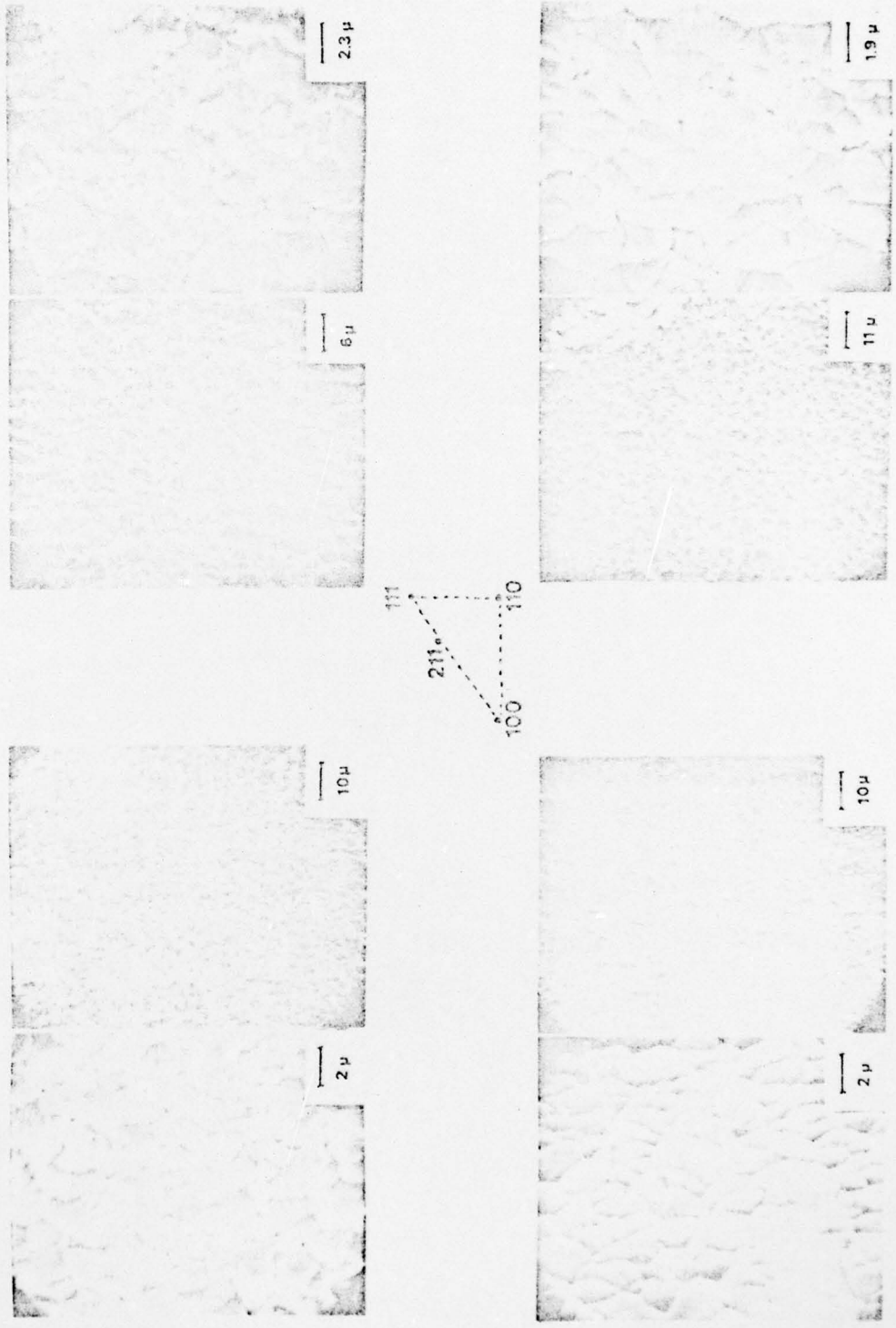

4.12 SEM's of Nb_3Sn Diffusion Layer Disc Samples as a Function of Nb Disc Substrate Orientation - VD Discs.

4.13 SEM's of Nb_3Sn Diffusion Layer Disc Samples as a Function of Nb Disc Substrate Orientation - Sample Set 9152.

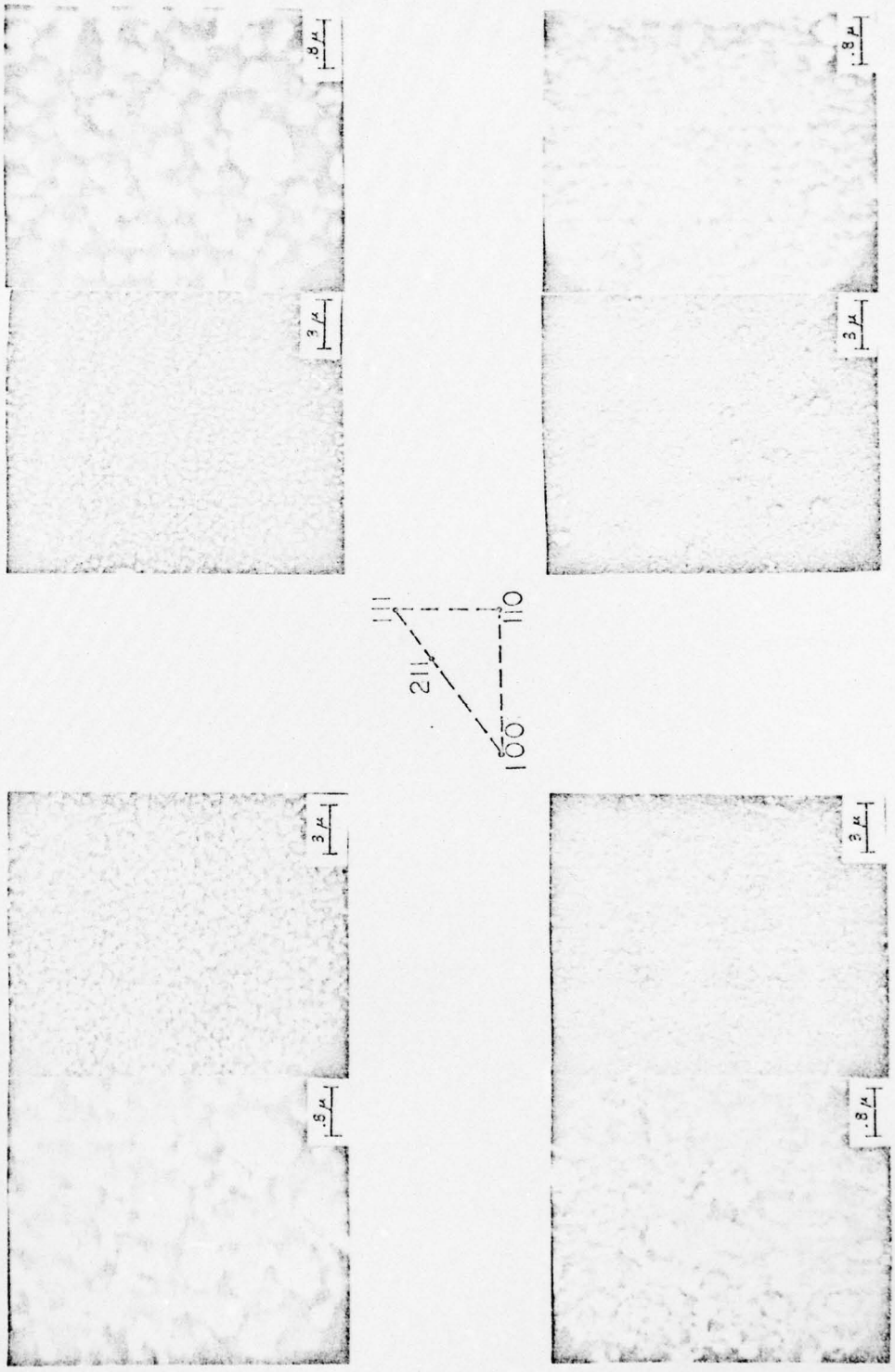

4.14 SEM's of Nb_3Sn Diffusion Layer Disc Samples as a Function of Nb Disc Substrate Orientation - Sample Set 9192.

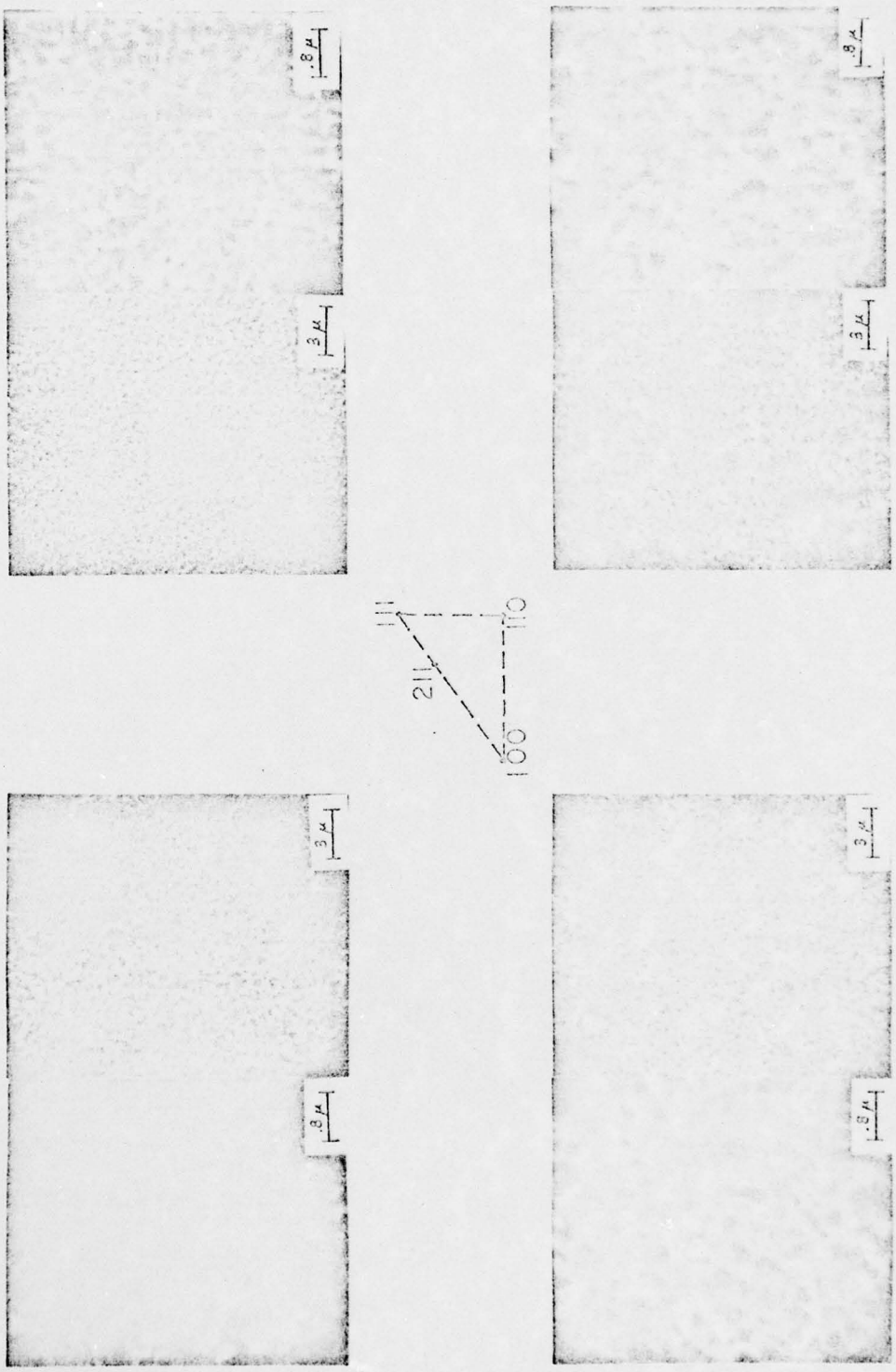

4.15 SEM's of Nb_3Sn Diffusion Layer Disc Samples as a Function of Nb Disc Substrate Orientation - Sample Set 9197.

Additionally, a low magnification photo of sample 9152-D-110 was overlooked.

Examination of the diffusion layer discs of the 2.9 μm thick sample set 9192 in Figure 4.14 confirms the observations of Diadiuk for the 17.2 μm layer on discs of niobium orientation (100), (111) and (110). The microstructure of the two non-Nb(111) layers is rough but the grains are packed with fair uniformity. Interestingly, for Diadiuk's 17.2 μm thick Nb_3Sn diffusion layers, that on Nb(100) was of higher microstructural perfection than the one on Nb(110). For the author's much thinner 2.9 μm thick Nb_3Sn the order of quality is reversed. The reversal echos the behaviors of T_c onset and T_c finish with layer thickness, Figures 4.1 and 4.2. The Nb(211) substrate layer is the poorest in microstructural quality of the layers on non-Nb(111) orientations, and looks similar to the Nb(111) layer, where grains are loosely packed and vary widely in size. No microcracks were observed in the Nb(111) substrate layers. Thus, the 2.9 μm thick layers fabricated under the same conditions as the 17.2 μm layers suggest that the differences observed between the thicker layers as a function of Nb(h k ℓ) moderate with decreasing thickness.

Changes in microstructure between the 2.9 μm thick layer discs (sample set 9192) and the 1.6 μm thick layer discs (sample set 9197) are readily apparent in Figures 4.14 and 4.15 respectively. The 1.6 μm samples have lost the "puffy" character of the grains and

the substantial differences between 17.2 μm thick Nb_3Sn layers on discs of various Nb(h k ℓ) have all but disappeared, with only the Nb(211) substrate layer showing any distinction. The sameness of microstructure in the 1.6 μm layers irrespective of substrate orientation, may find its origin in layer growth kinetics related to the shortness of the time required to react thin-layer diffusion samples, or in a relationship of microstructure, itself, to layer thickness, which is consistent with the above discussion concerning the 2.9 μm thick layers. The time of reaction is believed to be the more likely cause because in the case of thin layers, there is little time for in situ annealing of the already formed Nb_3Sn while the interface advances into the niobium substrate.

Gregory observed such annealing affects in dc sputtered Nb_3Ge films: in situ annealing during film growth maximized the superconducting properties of continuously sputtered additions to the films while simultaneously over-annealing the initially sputtered portion of the films, causing precipitation of phases other than Nb_3Ge and concommitant degradation of the film's overall superconducting properties.[46] Although no second phase materials are observed in the 1.6 μm samples (see Bulk Structure Section) T_c finish is much lower than for thicker layers: possibly this is due to the inadequacy of time available for the thin layer to form a well ordered A15 phase. The similarity of T_c onset values for these thin layers and the 17.2 μm thick layers (see Figure 4.1) suggests that the A15 material present

in the diffusion layers is of higher quality for the thin and thick extremes of layer thicknesses studied than for the middle regime. At these same extremes of thickness, data is also more tightly grouped in value irrespective of Nb(h k ℓ).

The effects of fabrication conditions can be observed in Figures 4.13 (sample set 9152) and 4.14 (sample set 9192). Sample grain size depends on reaction temperature through an exponential dependence of size on the temperature of the Sn vapor in the ampule.[35,90] Larger grains result from higher temperatures as indicated by comparison of the two 2.9 μm sample sets (9152 and 9192): the 9152 disc layers (fabricated only approximately 150°C hotter than 9192), in Figure 4.13, show a larger grain size and more uniformity in the size of individual grains than do the 9192 disc layers, Figure 4.14. Similar trends in grain size enlargement as the result of higher fabrication temperature were noted by Jacobson, et al.[61] The shape of the grains in the author's study remains generally unchanged, but is of a more "puffy" character than are the 17.2 μm layer grains.

Diadiuk observed that 17.2 μm diffusion layers grown into the Nb(111) orientation on the circumference of rod shaped substrates exhibited actual microcracks, see Figure 4.16. However, the author's rod samples do not exhibit this cracking phenomena for any Nb substrate orientation or layer thickness or rod diameter studied.

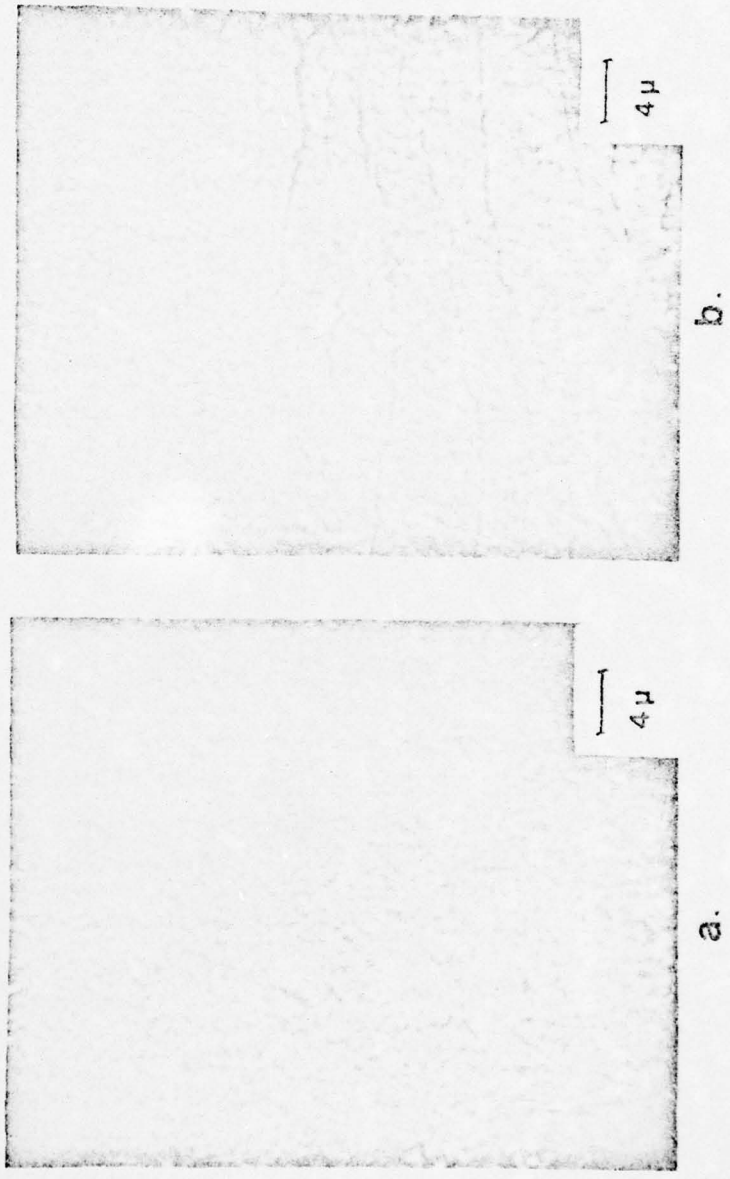

4.16 SEM's of VD Rod Sample Before Temperature-cycling:
(a) non-(111) Nb substrate direction;
(b) Nb(111) substrate direction.

The author's 17.2 μm thick rod samples (9115) however, were fabricated with an improper quench (i.e., too slow); this difference in fabrication process could explain the absence of the cracks in this layer thickness. The thinner layers, however, were fabricated under the same protocol as that of Diadiuk. These observations would seem to indicate that the critical layer thickness for cracking of 3.2 mm rod samples lies in the regime between sample set 9141 (12.1 μm) and 17.2 μm.

Figure 4.17 illustrates the microstructure of 12.1 μm layerson the Nb(111) and Nb(110) orientations around the circumference of the niobium crystal rods (sample set 9141). There appears to be little difference between the layers on the two different orientations around the rod, but the existence of surface crystallites is a major difference between these circumferential microstructures and the "puffy" nature of grains typical of the 12.1 μm layer of Nb_3Sn fabricated simultaneously on oriented discs comprising this sample set. Figure 4.18 illustrates similar microstructure as in Figure 4.17, but for the layer diameter of rod and comparing 12.1 μm thick Nb_3Sn layers on Nb(100) and Nb(111). The Nb(111) orientation layer appears to have fewer crystallites on the bigger diameter than on the smaller.

Figures 4.19 and 4.20 illustrate the exposed Nb-Nb_3Sn interface on rod shaped samples of Diadiuk. The interface represents the final growth surface of the Nb_3 Sn; it shows a uniformly

4.17 SEM's of Sample 9141-R-1: Left, top and bottom - Nb(111) substrate direction; Right, top and bottom - Nb(110) substrate direction.

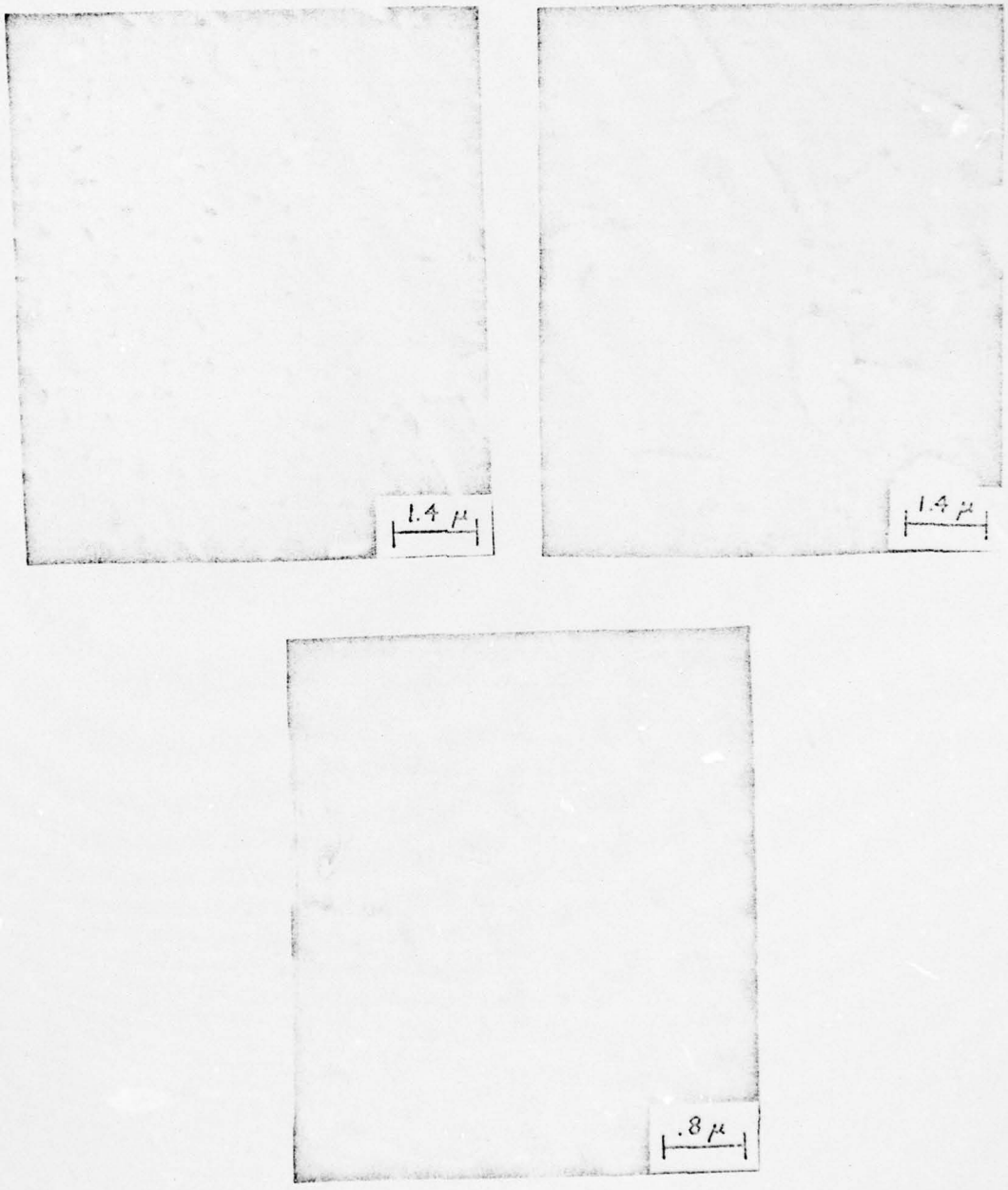

4.18 SEM's of Sample 9141-R-2: Top left and bottom - Nb(111) substrate direction; Top right - Nb(100) substrate direction.

AD-A074 738 ARMY MILITARY PERSONNEL CENTER ALEXANDRIA VA F/G 13/13
STRUCTURAL PROPERTIES OF NB3SN DIFFUSION LAYERS FABRICATED ON S--ETC(U)
SEP 79 J F DEBROUX

UNCLASSIFIED NL

2 OF 2
ADA 074738

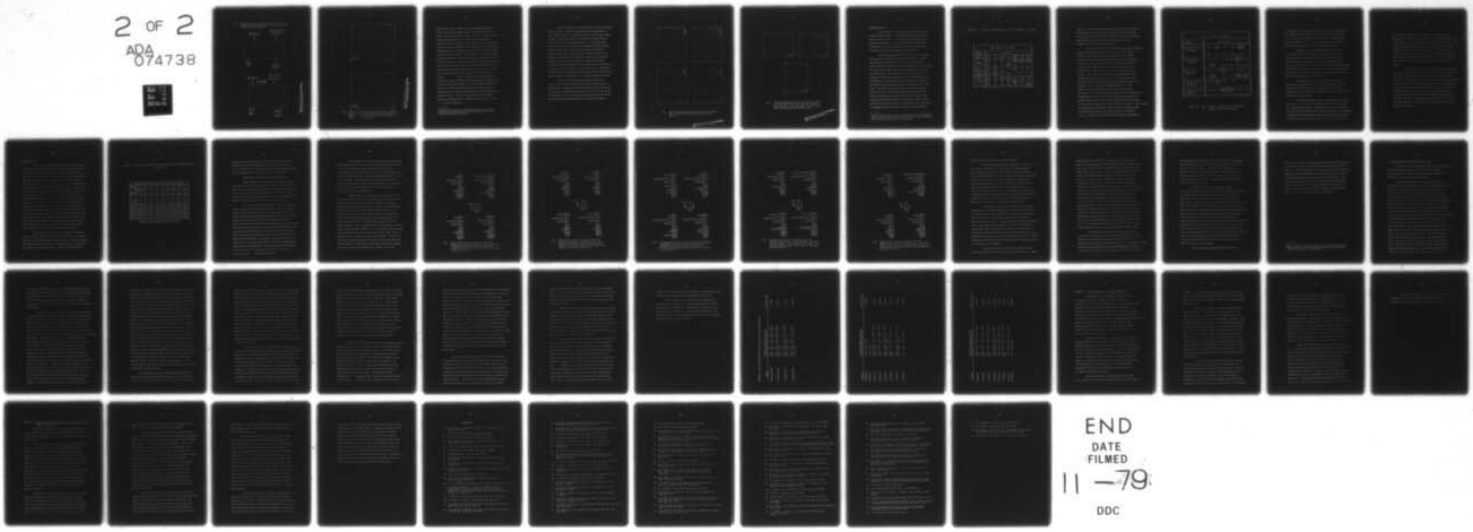

END
DATE FILMED
11-79
DDC

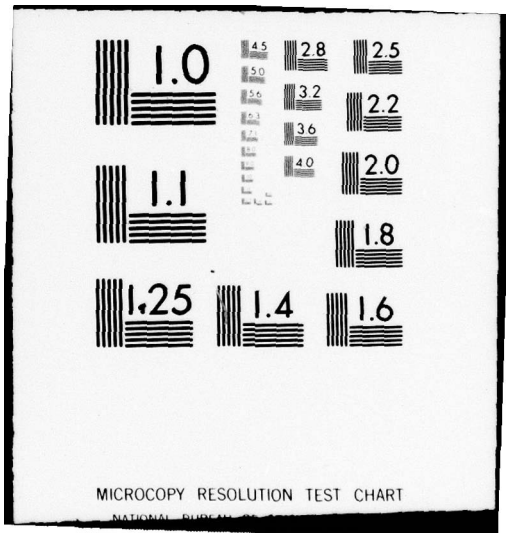
1.0
1.1
1.25
1.4
1.6
1.8
2.0
2.2
2.5
2.8
3.2
3.6
4.0
4.5
5.0
5.6
MICROCOPY RESOLUTION TEST CHART

4.19 SEM's of Nb-Nb_3Sn Interface Exposed by Chemical Etching of Rod-Shaped Sample. Note Nb_3Sn "collar" on the Nb Substrate Core.

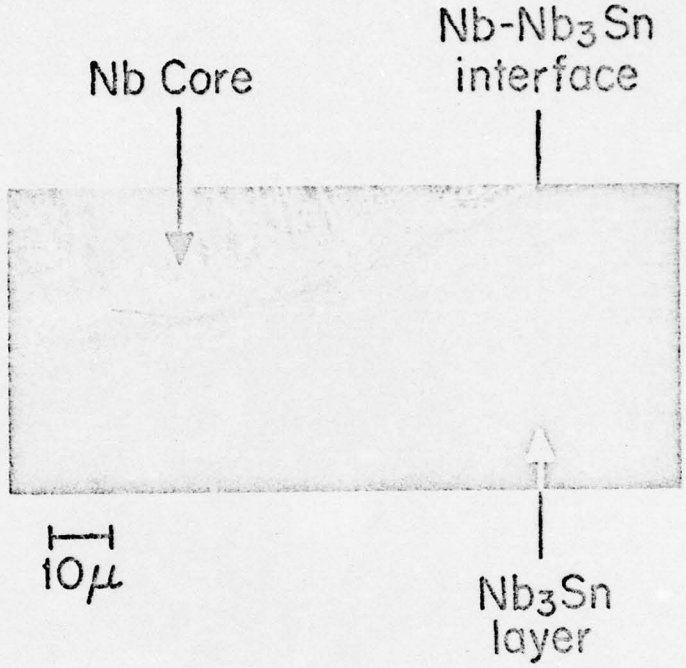

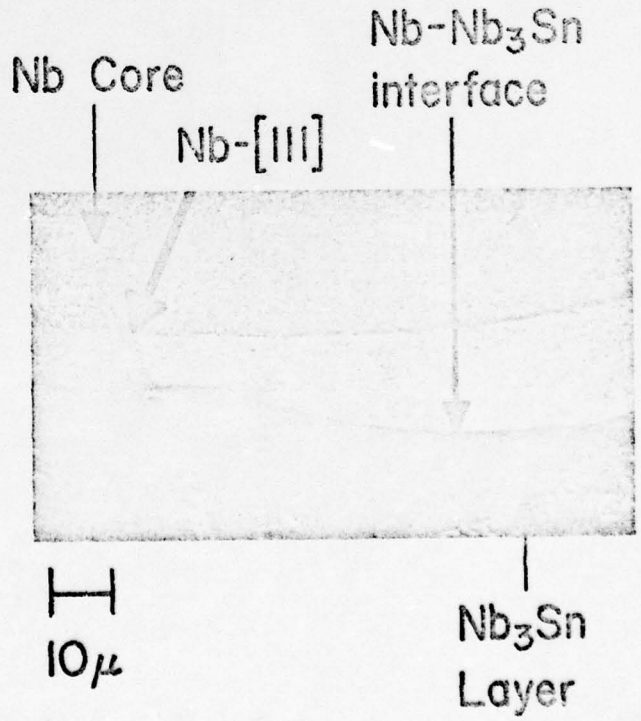

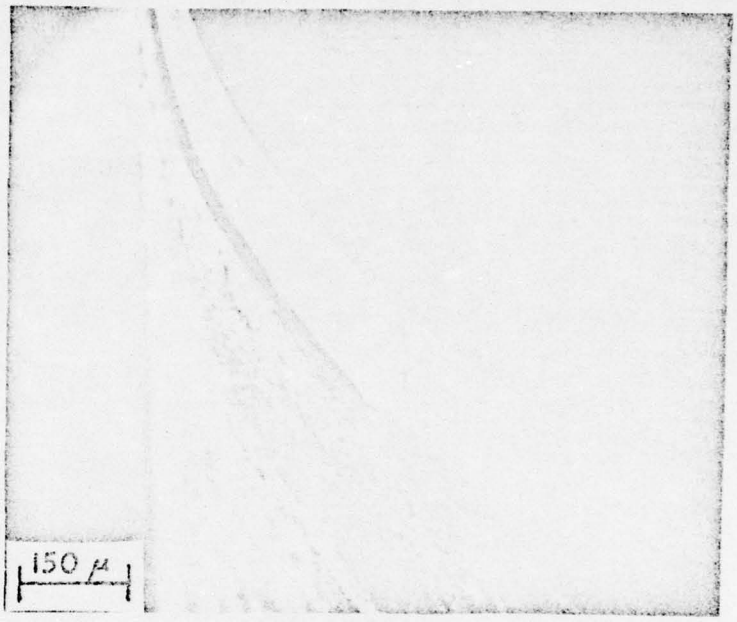

4.20 SEM's of Rod-Shaped Sample after Chemical Etching: Top - Nb-Nb_3Sn interface with non-Nb(111) directions exposed; Bottom - Vertical surface of Nb after Nb_3Sn has been etched out.

advancing A15 layer, leading to a very sharp transition from Nb_3Sn to Nb along the sample radius. No Kirkendall voids were expected to be observed[30] and indeed none were. However, at the Nb(111)-Nb_3Sn portion of the circumferential interface an outstanding feature is noted. (See Figure 4.19.) The Nb_3Sn layer exhibits appearances suggestive of second phase material (Nb_6Sn_5 for example) or oxides, although the overall EDX measurements confirm the Nb:Sn ratio to be 3:1.* The thickness of A15 layer at this Nb(111) orientation is less than elsewhere. Perhaps this thinness can be attributed to preferential etching (the layer is thinner from the surface, not from the interface), such as might result from an etchant attacking regions of differentially high free energies, e.g., arising from strains, impurities, or crystallographic effects. Thus, the etch acts to map out the extent of the strain field associated with the formation of Nb_3Sn on this particular substrate orientation, the concentration profile of impurities associated with this Nb_3Sn, and/or the extent of a particular texture character of the Nb_3Sn. The extent of these is extremely limited: only 35 μm to either side of the Nb(111) direction, corresponding to an angular spread of only ~1° around the sample circumference.

---

*It should be noted that the standard Nb_3Sn specimen used for determining absolute EDX elemental compositions was not run simultaneously with each sample.

Figure 4.20 shows another portion of the exposed interface with non-Nb(111) substrate orientations and the Nb_3Sn layer in view. Also shown is the cylindrical surface of the exposed single crystal Nb core after etching: the "pockets" possibly indicate an inward growth of Nb_3Sn columnar grains. It is particularly interesting to note the similarity in appearance of these pockets to the microstructure of the 1.6 μm disc sample 9197-D-100 shown in Figure 4.15. This similarity, together with the T_c vs. thickness regime behaviors of Figures 4.1 and 4.2 and the microstructual character of thin layers vs. thick ones which has already been discussed, suggests a relationship between the thinnest and thickest layer thicknesses comprising this study. Perhaps the key will lie in considerations of similarity of the initial and final growth surfaces of the Nb_3Sn, i.e., the surface and the interface.

The extreme difficulties of exposing the Nb-Nb_3Sn interface as desired through chemical etching is demonstrated in Figures 4.21: a Nb_3Sn crown rises above the single crystal Nb core as a result of unexpected over etching of the Nb core. The photos of Figure 4.22 show the mechanical damage caused during the string saw cutting and mechanical polishing employed before etching.

4.21 SEM's of Rod-Shaped Samples after Chemical Etching. Note the crown of Nb_3Sn which rises above the Nb core.

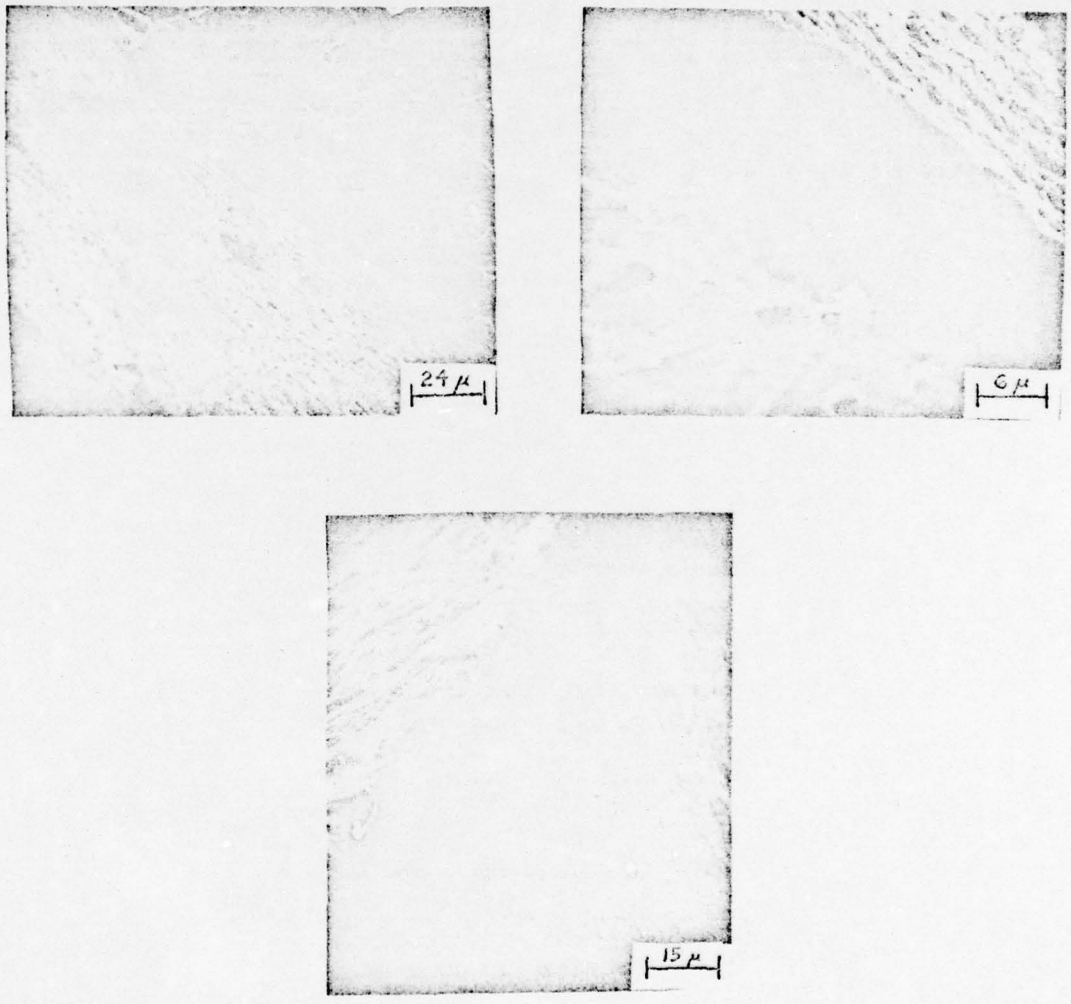

4.22 SEM's of Rod-Shaped Samples after Cutting, Polishing and Etching: Top, left and right - rubbed edges of Nb core after polishing; Bottom - burnt edge of sample after string saw cutting.

Surface Structure

Limited RED analysis of selected Nb_3Sn layers on disc-shaped samples was carri[illegible] out by the author to determine the nature of the A15 layer [illegible]face with respect to structure and preferred orientation. Due to the flat geometry required for RED analysis, it was not possible to carry out studies on the circumference of the Nb_3Sn diffusion layers on rods.

Diadiuk's RED patterns obtained for the 17.2 μm thick Nb_3Sn layers on the Nb discs of Table II exhibited clearly distinguishable rings in the case of Nb_3Sn on Nb(110) and Nb(111) substrates, whereas for the Nb(100) and Nb (211) substrates, the Nb_3Sn layers yielded only arcs or a limited number of spots on circular paths. (The completeness of an RED ring is an indication of the number and size of grains contributing to the diffraction.) All four RED patterns of Diadiuk show regions of increased brightness along the rings or at certain areas of the spots. Table III lists the reflections of layer observed by Diadiuk for each of her Nb disc orientations of Table III.* Every ring present in the patterns was indexed to an A15 plane strongly hinting that the nature of Nb_3Sn layers formed on disc geometry substrates by diffusion is single-phase A15. Indices of the brightest reflection (ring) by eye have been encircled in

*The RCA-X and SF film entries of Table III refer to an RCA Nb_3Sn single crystal and Nb_3Sn polycrystalline film prepared at Stanford which Diadiuk analyzed as part of her study.

TABLE III Nb_3Sn PLANES OBSERVED IN RED PATTERNS - VD DISCS

RED INDEXED REFLECTIONS							
sample	A15 Rings						
bcc (100)-disc	200	320	(330)	400	{431 510}	610	541
bcc (110)-disc	200	211	310	320	(400)	{411 330}	{431 510}
	610	541	614	{554 741}	761		
bcc (111)-disc	200	(222)	330	422	{431 510}	440	541
	534	614	752				
bcc (211)-disc	320	(330)	422	534			
RCA-X	220	321	{411 330}	{433 530}	541	613	615
SF film	200	211	310	320	(400)	422	
	440	610	534	614	615	752	{743 750}

Table III; they correspond to what is believed to be the preferred orientation of the Nb_3Sn layer for each Nb sample, being mindful that one must proceed with caution concerning preferred orientation determinations on the basis of RED patterns because of the dynamic nature of electron diffraction.[91]

The disc samples studied by RED by Diadiuk had been lightly etched with HF before RED analysis in order to remove surface oxides in order to generate clear RED patterns. The A15 layer thickness after this etch is estimated to have been approximately 14 to 16 μm. Thus, the results in Table IV pertain to an etch-exposed surface within a 1 to 3 μm wide region at the initial growth surface of the layer (i.e., 1 to 3 μm inwards from the Nb edge). The author further etched the VD Nb_3Sn-Nb(111) and VD Nb_3Sn-Nb(211) samples (HF: HNO_3 - 1:1 for 1 to 2 seconds, then HF for 5 seconds) to reduce the A15 layer to approximately 8 μm in thickness. (The etch rate is highly speculative.) These samples were then re-examined by RED (thanks to the help of John Parsey - M.I.T. Course III graduate student) for comparison with Diadiuk's observations. The objective of this comparison was to determine whether the "surface" nature revealed by RED at one place in a given layer changed as that layer's thickness increased. Also examined for comparison was the author's sample 9141-D-111 (lightly etched to remove surface oxides), initially of Nb_3Sn layer thickness ~12.1 μm. Hereafter, the two lighyly etched samples are referred to

RED INDEXED REFLECTIONS	
sample	A15 Rings
VD Nb_3Sn-Nb(111) (as-grown)	200 (222) 330 422 {431, 510} 440 541 534 614 752
VD Nb_3Sn-Nb(111) (etched)	110 or 111 211 or 220 {300, 221} or 310 (400) 421 or 332 521 or 440
9141-D-111 (as-grown)	210 or 211 {300, 221} or 220 310 or 311 (400) 421 or 332 {520, 432} or {511, 333}
VD Nb_3Sn-Nb(211) (as-grown)	320 (330) 422 534
VD Nb_3Sn-Nb(211) (etched)	110 or 111 (220 or 211) 411 or 330

TABLE IV Nb_3Sn PLANES OBSERVED IN RED PATTERNS - ETCHED AND AS-GROWN DISCS

as "as-grown" and the heavily etched sample simply called "etched". The objective of the second comparison was to discern whether the "surface" nature of an as-grown layer of a given thickness differs from the "surface" nature of a layer resulting from etching down to that same thickness from an originally thicker layer.

The RED patterns of VD Nb_3Sn-Nb(111) after etching were extremely faint and consequently unusually difficult to accurately index. Uncertainties in the determination of the d values (d=interplanar spacing) for several rings often gave the author more than one choice of h k ℓ for those particular reflections. (See Table IV.) Circled in Table IV are the indices of the brightest rings which, as previously mentioned, correspond to what is believed to be the layer's preferred orientation.

A comparison of the RED patterns of the as-grown and etched samples VD Nb_3Sn-Nb(111) dramatically illustrates that the as-grown surface of nominal 17.2 μm layer thickness is quite different in nature from the internal surface at the estimated 8 μm thickness exposed by etching.

The etched VD Nb_3Sn-Nb(111) and the as-grown 9141-D-111 surfaces of the same (~10 μm) thickness have many of the possible h k ℓ reflections in common. (9141-D-111, like the above samples, also exhibited only extremely faint diffraction rings). This leads one to suggest that the structural/orientational nature of the as-grown surface of a given thickness of diffusion layer on Nb(111) is not

related to the surface being as-grown, (i.e., being the initial growth region of the layer), but rather, it is determined by the layer's net thickness. Further, the similarity of possible reflections in the etched VD Nb_3Sn-Nb(111), thought to be ~8 μm thick, and the as grown 9141-D-111, nominally 12.1 μm thick, despite the uncertainty in the layer thickness values, points toward the possibility that the surface nature revealed by the RED's for this region of layer thickness may extend over some considerable distance within the bulk of the layer.

The comparison of the as-grown VD Nb_3Sn-Nb(211), approximately 17 μm thick, and the etched VD Nb_3Sn-Nb(211), approximately 8 μm thick suggests that if the A15-(111) reflection of Table IV is valid, intermediately thick layers of Nb_3Sn on Nb(211) may be of lower quality than those of the extremes of thickness so far investigated. It should be noted at this point that, indeed, for layer thickness of order 8-15 μm, T_c both onset and finish, minimizes at ~12 μm. The best material present in the layer on Nb(211), according to the behavior of T_c onset, is the worst A15 material of all the layers on any of the Nb(h k ℓ) substrates over this thickness range (see Figures 4.1 and 4.2).

Bulk Structure

The results of X-ray scanning diffractometer data taken on Nb_3Sn layers on discs, sample set VD Nb_3Sn-Nb(h k ℓ), are presented as comparisons of relative intensities. Peak intensities for the layer on each Nb(h k ℓ) substrate are normalized to the A15(211) peak for that layer and these layer intensities are listed in Table V. Also listed in this table are the relative intensities of the pattern of a Nb_3Sn powder standard (provided by Stuart Cogan). The A15(211) peak is one of the three major A15 reflections and was chosen as the normalization peak because it is believed to be less sensitive to preferred orientation effects than the A15(200) peak and more useful in detecting deviations from the powder sample relative intensities than the stronger A15(210) peak. In particular, the Nb_3Sn layers on the Nb(110) discs exhibit very enhanced A15(200) and (400) peaks and moderately enhanced (210). The layers on the Nb(100) and Nb(211) discs appear similar to one another, exhibiting modest enhancements of the (321), (400), (420) and (400) A15 peaks. The Nb_3Sn layer on the Nb(111) disc has a modest enhancement of the A15(321), (400), (420) and (440) peaks and a smaller enhancement of A15(222).

From these observations, one infers that the underlying oriented niobium substrate exerts a definite influence on the growth orientation of an overlying Nb_3Sn diffusion layer. However, unraveling the specific nature of the lattice relationships between the bcc and A15 lattices is not straightforward. The RED results (Table III)

TABLE V RELATIVE INTEGRATED INTENSITIES OF X-RAY REFLECTIONS - VD DISCS

RELATIVE INTEGRATED INTENSITIES OF X-RAY REFLECTIONS*									
A15 Reflection / Sample	200	210	211	222	320	321	400	420	440
powder standard	.51	1.43	1	.061	.25	.54	.18	.14	.15
(100)-disc	.52	1.36	1	.110	.41	.86	.40	.31	.38
(110)-disc	1.75	1.77	1	.087	.33	.52	1.10	.25	.17
(111)-disc	.38	1.15	1	.084	.37	.74	.30	.35	.49
(211)-disc	.38	.75	1	.046	.27	.71	.33	.24	.28

*[normalized to the A15 (211) reflection]

of Diadiuk on these 17.2 μm thick diffusion layer discs indicate probable A15 preferred orientations at the surface of this layer for each Nb(h k ℓ); the results of Table V pertain to preferred orientation character within the interior, or bulk, of the layer.

These results lead one to several suppositions:

First, that the bulk preferred orientation of a layer might differ from the as-grown surface preferred orientation. This possibility is substantiated by the X-ray and RED results on Diadiuk's 17.2 μm layers, sample set VD Nb_3Sn-Nb(h k ℓ). However, without similar data for other as-grown layer thicknesses, the substantiation might be unique to the particular thickness value of 17.2 μm.

A second supposition might be that surface orientation, or texture, evolves as the growing layer thickens. Evidence for this supposition exists in the RED patterns of the as-grown and etched samples VD Nb_3Sn-Nb(111) and VD Nb_3Sn-Nb(211). No X-ray investigation was done on these two samples to see if the nature of the bulk orientation changed with etching down of the layers. Such an investigation would only indirectly answer this question anyway because, since X-ray-implied preferred orientation effects derive from averaging over the entire layer thickness, X-ray data on the as-grown 17.2 μm thick layers would include contributions from precisely that layer region from 17.2 μm down to ~8 μm which is etched away and thus non-contributing in the etched case. Only if the nature of this etched away material deviates greatly from that of the remaining layer could one expect to see manifestations in X-ray data.

The RED results in Table IV show for the etched VD Nb_3Sn-Nb(111) comparison to the as-grown 9141-D--111 that surface orientation is not inherent to surface nature (as-grown or etched) of the examined material, but rather seems to be a function of the net thickness of the diffusion layer. Thus, a third supposition might be that bulk orientation is determined by the net thickness of the layer. In order to determine the validity of this supposition, X-ray studies of the author's discs with layers of 12.1 μm, 2.9 μm, and 1.6 μm layer thicknesses were also performed.

Diffractometer scans of the disc-shaped samples have a high signal to noise ratio due to the smallness of the sample making exact integrated intensity measurements unfeasible. Intensity measurements of Diadiuk's disc samples were made by the simultaneous scan of four discs with the same layer thickness and Nb(h k ℓ) orientations (these four discs were fabricated at the same time); intensity measurements of the author's disc samples were made on a single sample of each Nb(h k ℓ) substrate orientation from a larger single crystal (4.6 mm). Presentation of the X-ray results, including Table V, are displayed in Figures 4.23-4.27 as relative intensity plots of the A15(200), (210), (211), (222), (320), (321), (400), (420), and (440) peaks as compared to the Nb_3Sn powder standard. It should be noted that the plots in Figure 4.23 differ from previously published intensity plots by Diadiuk because this author believes that Diadiuk incorrectly attributed the A15(210) peak present in her X-ray

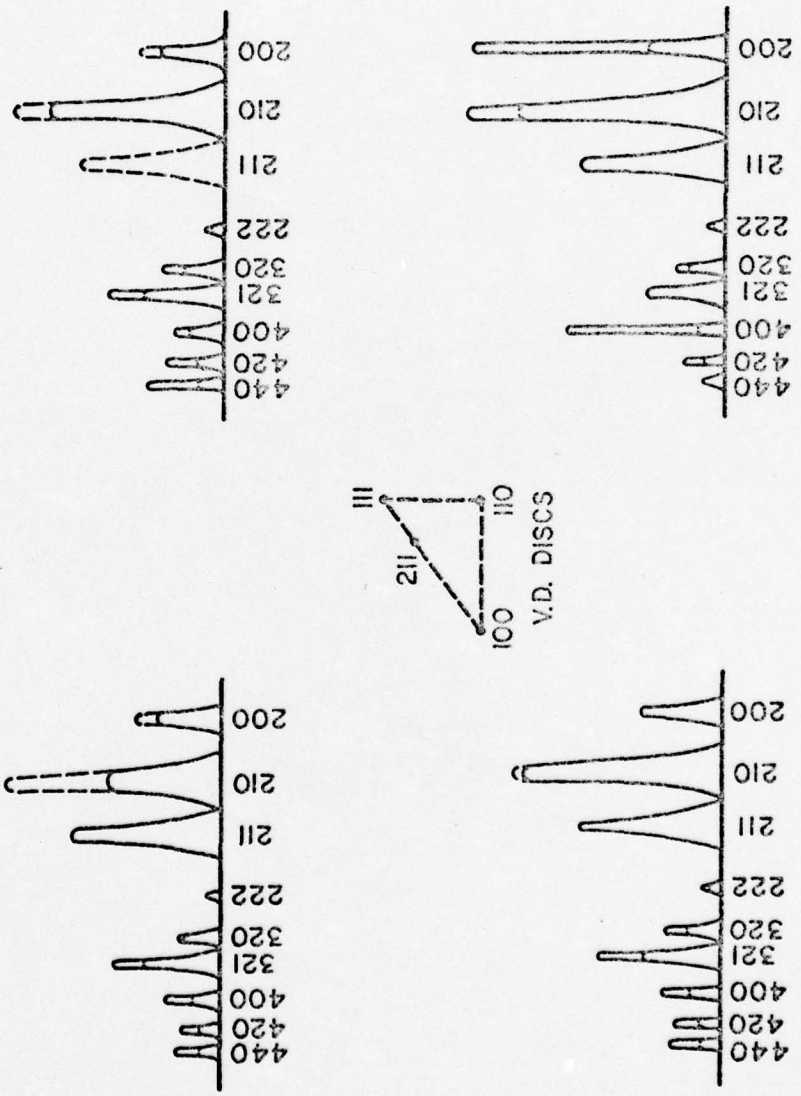

4.23 Diffractometer data as a function of Nb disc substrate orientation - VD discs - All sample data is normalized to the A15(211) peak height of a randomly oriented powder sample which is represented by the dotted line.

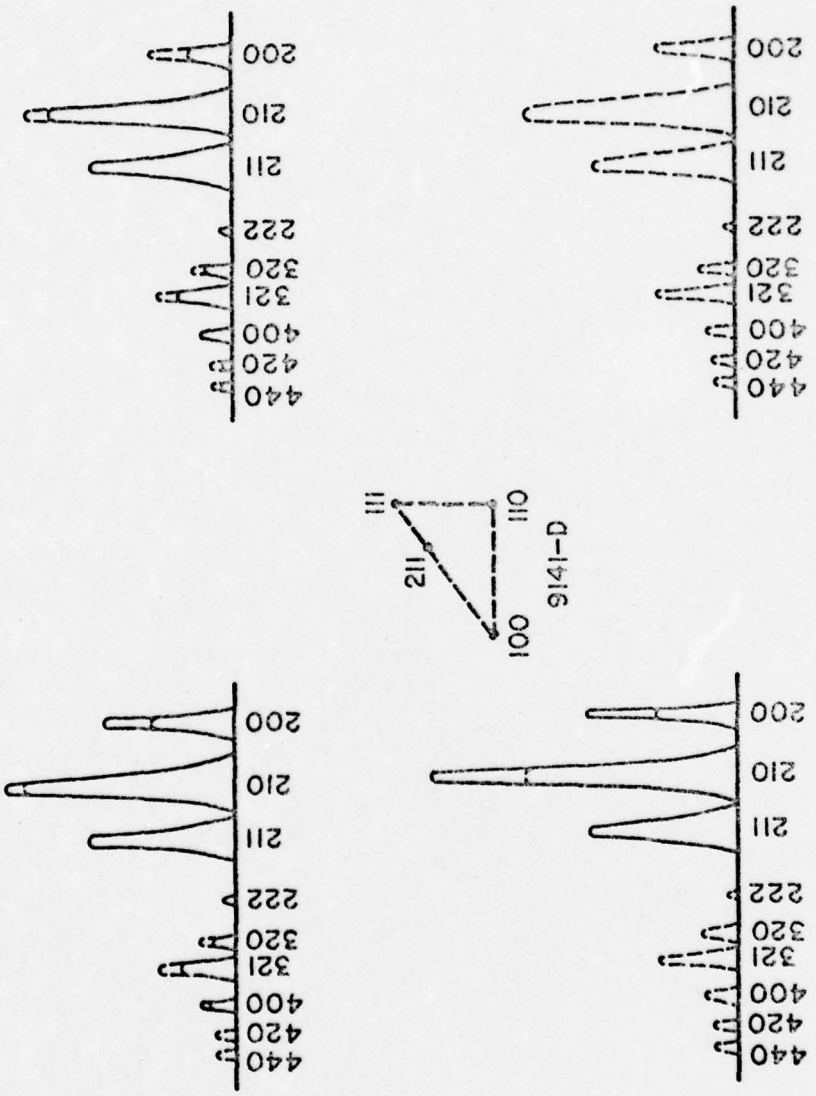

4.24 Diffractometer data as a function of Nb disc substrate orientation - Sample Set 9141 - All sample data is normalized to the A15(211) peak height of a randomly oriented powder sample which is represented by the dotted line.

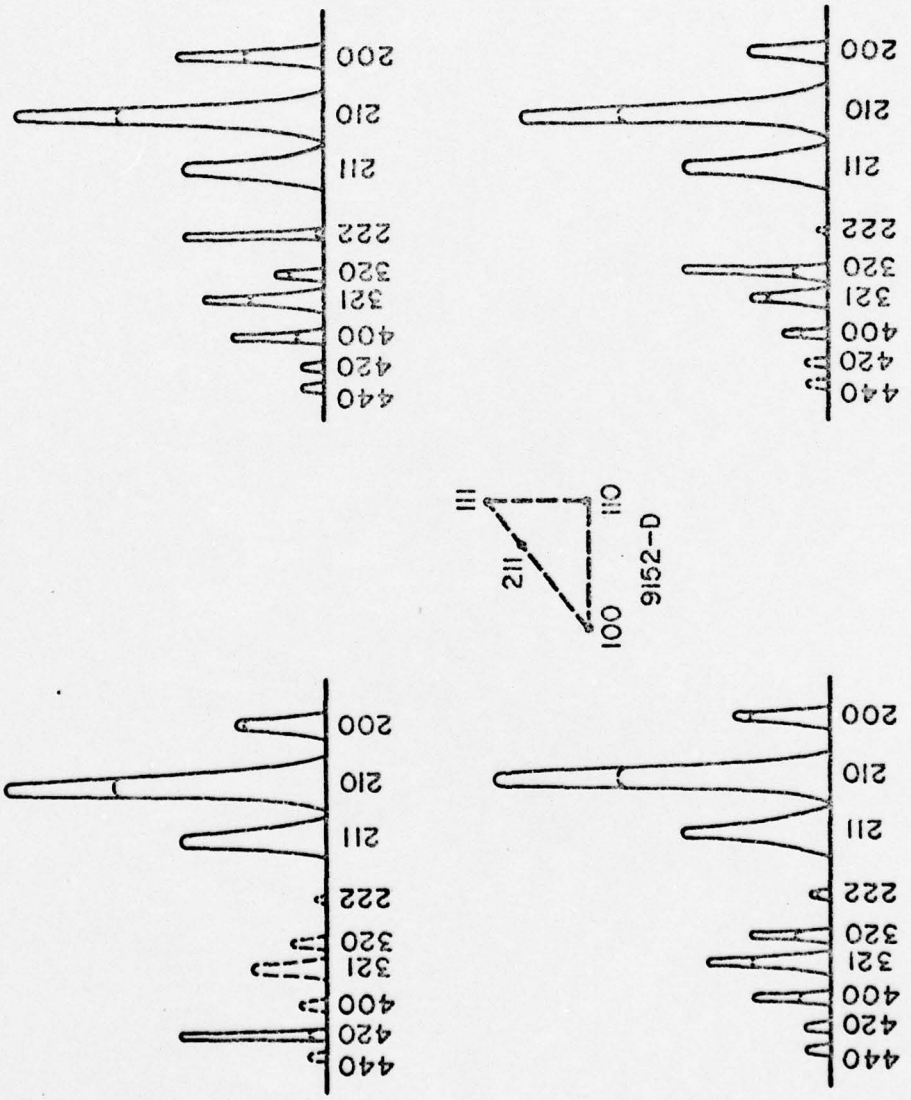

4.25 Diffractometer data as a function of Nb disc substrate orientation - Sample Set 9152 - All sample data is normalized to the A15 (211) peak height of a randomly oriented powder sample which is represented by the dotted line.

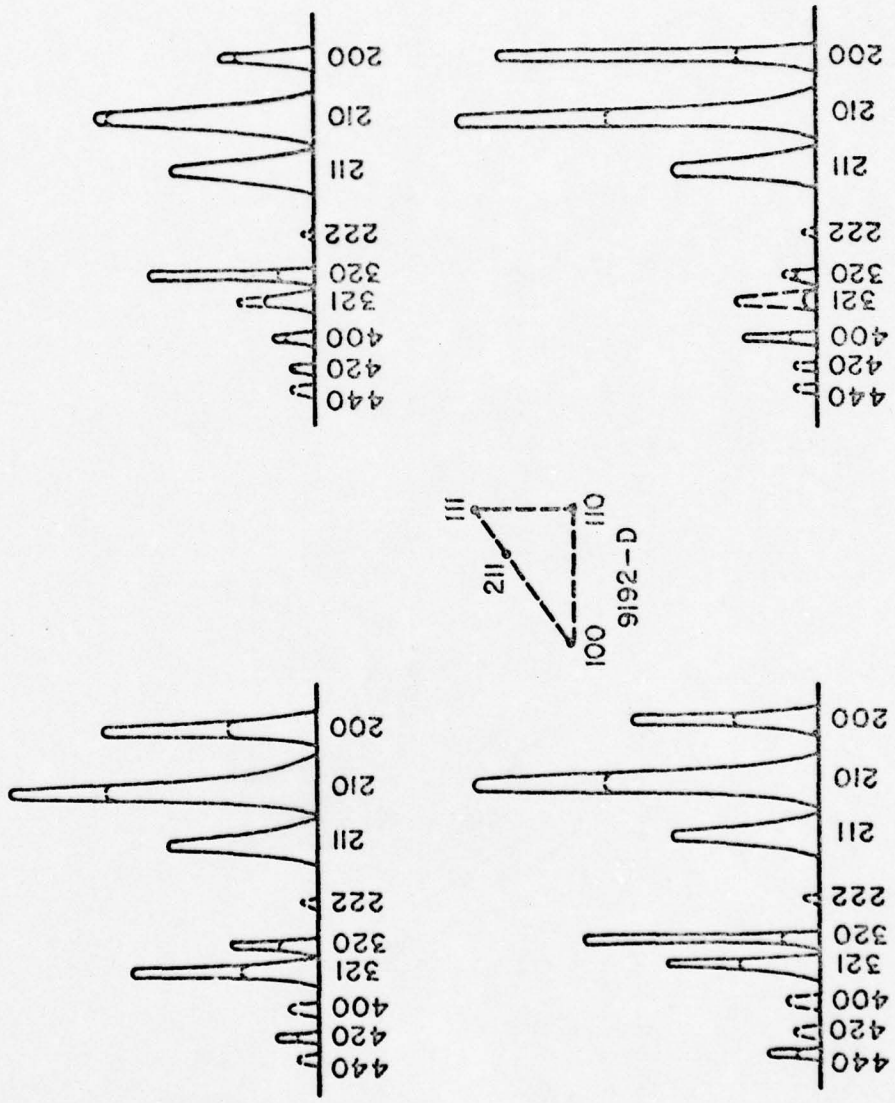

4.26 Diffractometer data as a function of Nb disc substrate orientation - Sample Set 9192 - All sample data is normalized to the A15(211) peak height of a randomly oriented powder sample which is represented by the dotted line.

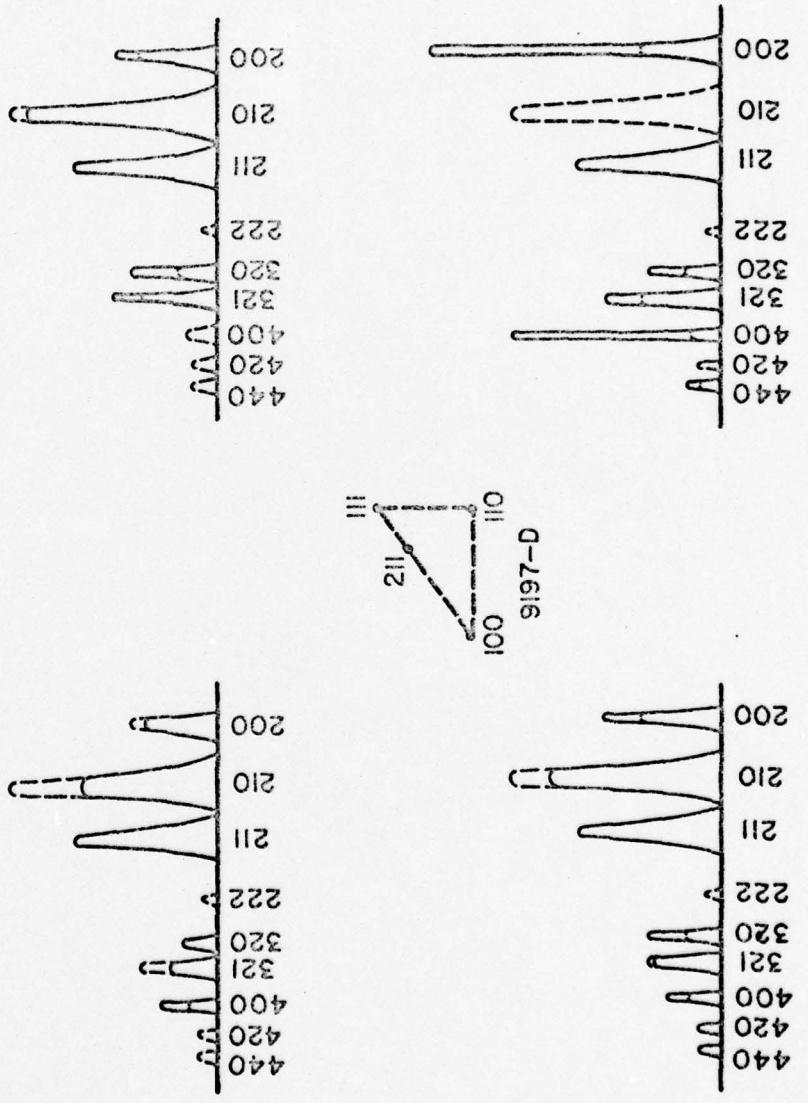

4.27 Diffractometer data as a function of Nb disc substrate orientation - Sample Set 9196 - All sample data is normalized to the A15(211) peak height of a randomly oriented powder sample which is represented by the dotted line.

patterns to the Ag paint used as a sample adhesive.

The RED measurements listed in Table III for the 17.2 μm A15 layers led to geometric lattice registry associations which X-ray observations of the bulk substantiate in the layer interior only for Nb-(110)||A15-(100). This particular A15 orientation appears to be the natural growth orientation of Nb_3Sn as indicated by investigations of Jacobson, et al.[61] and Diadiuk's examination of the Nb_3Sn polycrystalline film listed on Table III which was fabricated at Stanford by the same research group. The premise of a Nb_3Sn natural growth perferred orientation appears to be reinforced by the strong (200) and (400) A15 X-ray reflections observed by Neugebauer in thin films of Nb_3Sn grown by codeposition.[92]

The remaining three 17.2 μm thick bcc (h k ℓ) substrate orientations of Diadiuk have Nb_3Sn layers which do not show evidence in the bulk of the preferred orientation suggested at the surface by RED. Drawing on the X-ray information from his thinner Nb_3Sn layers, the author is led to proposing that net preferred orientation evolves and changes as layer thickness is varied. The texture in the diffusion layers appears to be an evolution of admixtures of A15 orientations which is sensitive to the underlying bcc (h k ℓ). More importantly, this admixture probably results from a competition between the bcc-A15 lattice registries and the natural preferred growth orientation of the Nb_3Sn (i.e., A15-(100)).

Evolution of bulk orientations in the diffusion layer disc samples from the surface layer is a compelling concept: at the

Nb(110) substrate orientation, lattice registry arguments (see Figure 4.4) make growth along the Nb_3Sn(100) the most conducive growth orientation. Because this orientation is also the natural preferred growth orientation of Nb_3Sn, it is likely that this orientation of growth would easily continue throughout the bulk to the Nb-Nb_3Sn interface. For Nb_3Sn layers at Nb(100) and Nb(211) substrate orientations, layer structure may start out with the Nb_3Sn(110) orientation as suggested in Figure 4.4 and the RED data of Table III, and then evolve into a Nb_3Sn-(110)/(100) admixture due to competition of the Nb_3Sn natural growth orientation and the efforts of the forming layer to both follow the template of the initial layers and to confront the continual presence of the bcc lattice at the advancing interface. In the case of Nb_3Sn at the Nb(111) orientation, the lattice paramenter of the Nb(111) diffusion layers of a given sample are consistently greater than those of layers at non-Nb(111) orientations, possibly indicating a continuation of the influence of the surface Nb(111)-Nb_3Sn(111) lattice registry association into the bulk. The X-ray results for the layers at Nb(111) indicate that an admixture probably exists, made up of Nb_3Sn-(111) and Nb_3Sn-(100).

The viability of the proposed orientational growth competition model may be tested by a closer examination of specific features in the diffratometer scans of Figures 4.23-4.27. The intensity plot of sample set 9197 (Figure 4.27 -- 1.6 μm thick A15 layer) might be expected to show little preferred orientation in layers at non-Nb(110) orientations due to the combined effects of the proposed

growth competion being in its initial stages at this small thickness and the fact that the X-rays are sampling a much deeper volume than just the A15 layer (thereby reducing signal sensitivity to intensity variations arising from the A15). The Nb_3Sn layer at the Nb(110) orientation would be expected to exhibit its A15(100) predilection because there is no evolution occurring. Both expectation are fulfilled in the data.

One might expect that due to in situ annealing, preferred orientation effects [admixtures of the initial growth orientation plus A15(100)] will become more evident as the growing layer gets thicker. This is seen in the 2.9 μm sample set, 9192, of Figure 4.26, as compared to the 1.6 μm set, 9197, of Figure 4.27. These effects might then be moderated as the layers get still thicker by over-annealing, although the orientational competition continues at the advancing interface. This competition plus evolution of annealing effects may be associated with the thickness regime behaviors previously noted for T_c and a_o, and may well be the basis for the marked similarity of the X-ray peak intensities for the 1.6 μm layers and the 17.2 μm thick layers. These two extremes of thickness bracket the range of thicknesses studied so far; similarity of behavior for these two thicknesses has already been noted for T_c onset values and with respect to similarity of microstructure for the thin layer and at the interface region of the thick layer.

The above mentioned in situ annealing also may be a

reason for the observed moderation of peak enhancement in the X-ray scans of the 2.9 μm sample set (9192 and 9152) with increased fabrication temperature. The 9152 sample set was reacted at the higher temperature, allowing more atomic mobility during fabrication and thus, possibly a resultant predilection to randomize preferred orientation.* The enhancement of the A15(222) peak in sample 9152-D-111 may echo the existence of sensitivities in the phase diagram as previously conjectured. The existence and retention of highly enhanced A15(210) peaks in sample sets 9152 and 9192 is as yet unclear.

*There is evidence from annealing of foils of Nb in this laboratory that annealing at ~1000°C virtually destroys the strong initial texture of the foils. (See Appendix 3.)

V. CONCLUSIONS AND SUGGESTIONS FOR FURTHER WORK

This study of the structural properties of Nb_3Sn diffusion layers fabricated on oriented Nb substrates has revealed that systematic behaviors result from the nature of the interactions between the substrates and the A15 overlayers.

Analysis of layers fabricated to various thicknesses allowed for the identification of layer thickness regimes over which the structural properties of the Nb_3Sn appear to evolve. These regimes can be designated approximately as 1 to 3 μm, 3 to 9 μm, 9 to 15 μm, and 15 to 17 μm with certain unique features observed specifically for the 1.6 μm thick layers. The T_c onset (an indicator of the "best" A15 material on the sample) appears to be the highest for the 1.6 μm and 17.2 μm layers, while T_c finish (an indicator of the "worst" A15 material that still superconducts) is low for the 1.6 μm samples and shows wide variations throughout the thicker regimes. It must be noted however, that there is a hierarchy of T_c values within the thickness regimes which depends on the particular (h k ℓ) of the Nb substrate. In the thinnest and thickest regimes, the Nb_3Sn layers on the Nb(211) substrates have the highest T_c onset values observed for any orientation of substrate, while layers grown on Nb(110) have the highest T_c onset values in the middle thickness regime. Lattice parameter measurements also fall into particular (h k ℓ) hierarchies within the thickness regimes, with the Nb(111) substrate layer always having an a_o greater than that of the same thickness non-Nb(111) layers. The thinnest layer (1.6 μm) is

particularly interesting in that it shows strong deviations from the other regimes for certain properties (depressed T_c finish and smaller a_o's) while showing marked similarity to the thickest regime layers (17.2 μm) in T_c onset and bulk preferred orientation. Structure investigations sought to illuminate the basis of these observed thickness sensitivities.

Orientational response of the A15 overlayer to its substrate is clear in the disc samples of Diadiuk.[29] Studies of these samples by her and in this thesis show that the as-grown surface orientation of each Nb(h k ℓ) diffusion layer of Nb_3Sn of given thickness differs from its associated Nb(h k ℓ) bulk orientation, as determined by RED and X-ray measurements, respectively. This comparison was made for all four of the 17.2 μm layer-Nb(h k ℓ) orientations and for the 12.1μm Nb(211) orientation. The question of whether the RED-determined surface orientations are related to something inherent to the as-grown nature of the surface or to dependence of surface orientation on layer thickness motivated a comparative RED examination of surfaces of as-grown and etched down diffusion layers. The internal surfaces exposed at 8 μm by etching down the 17.2 μm Nb_3Sn layers on Nb(111) and Nb(211) exhibited structures different from those of the original as-grown 17.2 μm layers. In the case of Nb(111) substrates, this was quite pronounced, and the etched down structure was similar to the structure of the as-grown layer of comparable thickness, 12.1 μm, on the same Nb(111) orientation (which was the only comparison made). Thus, surface orientation is believed to be determined by layer thickness. This is also true for bulk orientation of the A15 on a

given Nb(h k ℓ) substrate. Bulk structure determinations of preferred orientations in layers of different thicknesses show the nature of the layers to be determined by the thickness of the layer contributing to the X-ray diffraction. The dependences of surface and bulk orientations on net layer thickness suggest that the structural nature of the layer evolves inwards radially from the niobium crystal surface in accordance with a qualitative model based on the competition of the growth region orientation at the advancing interface (determined by lattice registry of the bcc and A15 lattices) and the drive of the Nb_3Sn layer to form in its natural growth direction [i.e., $Nb_3Sn(100)$], moderated by *in situ* annealing of the already formed Nb_3Sn as the growth advances. For very thin layers microstructural observations of the 1.6 μm layer show that the grain structure of the layers may not have time to fully develop because of the short diffusion reaction time; at thicker values the microstructure shows the influence of particular Nb(h k ℓ) orientations. The hierarchy of microstructural perfection for the 17.2 μm VD diffusion layers [in order of decreasing perfection-Nb_3Sn on Nb(100), Nb(211), Nb(110), Nb(111)] seems to be reversed for the 2.9 μm thick A15 layers [in order of decreasing perfection-Nb_3Sn on Nb(110), Nb(100), Nb(211), Nb(111)]. This reversal may be linked to the effects of the shorter *in situ* annealing which occurs with thinner layers.

An interesting feature of the thickness regime behaviors and A15 orientational dependences on substrate is the suggestion of individual "personality profiles" for the various Nb(h k ℓ) substrate

diffusion layers. For example, the Nb_3Sn on Nb(111), whose structural properties were so undesirable in Diadiuk's investigation,[29] exhibit a remarkable insensitivity to layer thickness and lattice parameter in the T_c values but an equally strong sensitivity to proper composition. On the other hand, the seemingly well-behaved Nb_3Sn on Nb(100), the most structurally perfect of the 17.2 μm diffusion layer sample discs, exhibits large fluctuations of T_c and lattice parameter but is somewhat less sensitive to layer tin composition. The Nb_3Sn layer grown on the Nb(211) substrate displays the highest T_c onset values seen at any Nb(h k ℓ) in the thick and thin regimes, but the worst values in the middle thickness regime where layers on the Nb(110) are the best in value. Thus, even with the countervailing effects of the growth competition model and in situ annealing, the particular (h k ℓ) of the Nb substrate is an overriding influence on the final properties of the diffusion layers.

The substrate (h k ℓ) (and thus A15 orientation) variations of A15 T_c values and a_o with tin composition lead to speculation on the possibility of orientational effects on the Nb-Sn phase diagram and constituent ordering. The maximizing behavior of T_c at differing tin compositions for Nb_3Sn layers on different Nb(h k ℓ) substrates may be an indicator that the layers are governed differently by the boundary of the single phase A15 region of the phase diagram, or even that the phase field is different for layers of different preferred orientation. [The peaking of T_c finish, in particular, with 25% Sn is consistent with the existence of lower T_c A15 phase material which

is minimized at stoichiometric composition.] The behavior of lattice parameter with composition as a material approaches the phase boundary between a single phase region and a two phase region is normally a gradual increase and subsequent leveling off as the two phase region is entered The peaking of lattice parameter with per cent Sn observed in this study is indicative of the fact that, at the fabrication temperature (1000°C), Nb_3Sn is the only allowable Nb-Sn solid solution, and this a_o behavior may be attributed to a combination of in situ annealing and possible phase field effects. Thus, it appears that the variations of T_c onset and a_o with per cent Sn and layer thickness on a particular Nb(h k ℓ) substrate could be due to textural modifications of the standard Nb-Sn phase diagram in conjunction with the ordering effects of in situ annealing.

This study of the Nb_3Sn diffusion layers fabricated on single crystal Nb substrates has examined the nature of several properties and their relationship to the layer's structure. Preferred orientation in these layers is confirmed and attributed to the influence of the underlying Nb substrate. The texture of the diffusion layer bulk material appears to be determined by layer thickness. The mechanism for layer texture is proposed as a qualitative model of competition between lattice registry required for growth and the natural growth direction, A15(100). This competition occurs simultaneously with in situ annealing. Within the observed thickness regimes, there is a hierarchy of given property values arising from

the A15 preferred orientation deriving from the underlying Nb substrate orientations. These hierarchies change with thickness and in the case of 2.9 μm, with fabrication temperature, suggesting that layers fabricated on Nb(h k ℓ) substrates which show desirable structural and superconducting behavior (i.e., layers on non-Nb(111) substrates) have especially sympathetic values of T_c and a_o to layer thickness and per cent Sn. Whereas Nb_3Sn layers fabricated on Nb(111) substrates have poorer local structural and superconducting properties,[29] they show in their bulk properties a relative insensitivity of T_c values to layer thickness or lattice parameter. The behaviors of lattice parameter and T_c onset with layer tin composition, however, show that layers on Nb(111) are the most sensitive to composition of any Nb(h k ℓ) studied. Thus, it appears that there are trade-offs in the fabrication of Nb_3Sn diffusion layers on oriented Nb substrates between the ease and sensitivity of fabrication, the thickness of the diffusion layer, and the quality (superconducting and structural properties) of the final layer.

Further studies with Nb_3Sn diffusion layers fabricated on single crystal Nb substrates should be carried out to examine a more systematic variation of layer thickness over both a wider range of thickness values and in the range 3 to 12 μm. The specific nature of the thickness regimes could then be confirmed with X-ray diffraction, RED, SEM, EDX, and T_c measurements at each thickness for each Nb substrate orientation. Also, anaylsis of systematically etched layer thicknesses should better distinguish the character of "internal

surface" properties associated with thickness from those associated with the inherent nature of an as-grown surface. Also, comparative PED analysis for layer surfaces at both extremes of thickness are needed to help understand the similarities of the 1.6 μm and 17.2 μm layers in this thesis study.

Preferred orientation effects observed in this investigation can be studied further by fabricating Nb_3Sn diffusion layers on polycrystalline Nb foils (see Appendix 3). Systematic thickness variations suggested above and use of the investigative techniques listed could be applied to see if the observations of trends (e.g., thickness regime variations of a_o and T_c - sensitivity to composition) and model predictions for Nb_3Sn layers on single crystal substrates apply equally to layers on polycrystalline substrates.

The nature of the Nb-Nb_3Sn interface should be investigated much more thoroughly; this requires perfecting etching techniques to expose the interface. Photo-resist etching may be a possible approach to the problem. A resemblance was noted between the microstructure observed in the scanning electron micrographs of the surface of the 1.6 μm layer (Figure 4.15) and the high magnification electron micrographs of the etch pockets of the advancing Nb_3Sn on the surface of the exposed Nb core of Figure 4.20. Possibly their similarity arises from the fact that each of these regions of layer has two boundaries, one of which faces Nb_3Sn. Although the surface layer faces a vacuum on its other side and the advancing growth region, a bcc Nb crystal core, they both encounter an abrupt

change of free energy across these boundaries. The existence of these free energy steps may be a key to the similarities observed.

The possibility of the existence of and feasibility of determining the specifics for orientational effects on a phase diagram should be considered. And finally, an investigation into the observed screening of the Nb superconducting transition in the author's inductive T_c measurements should be undertaken to determine the nature of this anomalous behavior.

APPENDIX 1 A15 X-Ray Reflections Used to Calculate Lattice Parameters

Sample	A15 X-Ray Reflections Used to Calculate Lattice Parameters	Average a_o (nm)
VD Nb_3Sn-Nb(100)	(200), (210), (211), (320), (321), (400), (420), (421), (520), (440)	0.52849
VD Nb_3Sn-Nb(110)	(200), (210), (211), (222), (320), (321), (400), (420), (421), (520), (521), (440)	0.52941
VD Nb_3Sn-Nb(111)	(200), (210), (211), (222), (320), (321), (400), (420), (421), (332), (520), (521), (440)	0.52959
VD Nb_3SN-Nb(211)	(200), (210), (211), (320), (321), (400), (420), (421), (332), (520), (521), (440)	0.52879

Sample	A15 X-Ray Reflections Used to Calculate Lattice Parameters	Average a_o (nm)
9141-D-100	(200), (210), (211)	0.52974
9141-D-110	no A15 peaks	
9141-D-111	(200), (210), (211), (222), (320), (321), (400)	0.53033
9141-D-211	(200), (210), (211), (320), (321), (400)	0.52960
9152-D-100	(200), (210), (211), (320), (321), (400), (520), (521)	0.52957
9152-D-110	(200), (210), (211), (320), (321), (400)	0.52920
9152-D-111	(200), (210), (211), (222), (320) (411), (420), (520)	0.52993
9152-D-211	(200), (210), (211), (420)	0.52989

Sample	A15 X-Ray Reflections Used To Calculate Lattice Parameters	Average a_o (nm)
9192-D-100	(200), (211), (320), (321), (520), (440)	0.52896
9192-D-110	(200), (210), (211), (320), (400), (420)	0.52897
9192-D-111	(200), (210), (211), (320), (321) (520)	0.52969
9192-D0211	(200), (210), (211), (320), (321) (420), (421), (332)	0.52938
9197-D-100	(200), (210), (211), (320), (321)	0.52732
9197-D0110	(200), (211), (320), (321), (400), (440)	0.52647
9197-D-111	(200), (210), (211), (320), (321)	0.52870
9197-D0211	(200), (210, (211)	0.52725

APPENDIX 2 -- X-Ray Pole Figure Analysis of Disc Samples

A back-reflection Laue photographic method was used to examine the samples. With monochromatic Cu radiation (see Chapter III for specific voltages, currents, and exposure times), four to six Debye rings of relatively uniform intensity and all indexable to A15 crystal planes, were generated. The fiber texture nature of the samples (grains oriented normal to the sample surface) is precisely what causes the full rings; broken rings or arcs would normally imply preferred orientation. Thus, the back-reflection Laue photographs confirmed the presence of A15 phase material in the samples and the presence of a fiber texture, but gave no other preferred orientation information.

As mentioned in Chapter II, a pole figure is a stereographic projection, with a specified orientation relative to the specimen, that shows the variation of pole density with pole orientation for a selected set of crystal planes. A pole is the intersection of a plane normal with a reference sphere which is centered on the specimen. The pole of a plane represents, by its position on the sphere, the orientation of that plane. The pole figure analysis of a given sample then gives information concerning the existence and degree of any preferred orientation, as well as details of the specific orientations involved.

The unique nature of the disc samples in this study (i.e., having flat, sheet-like surfaces with apparent fiber textures)

suggested that analysis by direct X-ray pole figure techniques might be particularly informative concerning preferred orientation. Thus, both sheet texture and wire (or fiber) texture investigations were undertaken.

Initially, the samples were studied using the Schulz reflection method.[93] The specimen was mounted in a Siemen's texture diffractometer with θ and 2θ set at the proper angles to observe the maximum intensity of the A15(200) reflections. The A15(200) reflections were used to generate the pole-figure capable of more convenient interpretation. The specimen holder rotates the sample in its own plane about an axis normal to the sample's flat surface while simultaneously tilting the specimen about a horizontal axis. The great virtue of the Schulz method is that no absorption correction is required for values of the tilt angle between 90° and 40° (90° corresponds to having the flat surface of the sample in the plane of the diffractometer axis). Thus, the intensity of the diffracted beam is directly proportional to the pole density.[94]

The strip chart recorder output appears as a periodic variation of intensity maxima and minima corresponding to the changing positions of the reflecting A15 (200) planes. The strip chart data is reduced by determining the intersection of iso-intensity lines (after corrections are made for background intensities and geometric defocusing effects) with the recorded diffraction intensities and plotting these points on a sterographic

projection. The points will fall on a spiral determined by the rotating and tilting motion of the sample during the run. The specific locations and magnitudes of the plotted pole densities on the stereographic projection are associated with the specific orientation and degree of any sample texturing.

The author attempted to investigate the disc-shaped diffusion layer samples with the Schulz reflection method using both a finely collimated "microbeam" and a more diffuse beam designed to bathe the sample in X-rays. The combination of a finely collimated beam and the small sample size did not generate sufficient diffracted intensities to give useful data. The diffuse beam resulted in a low intensity output combined with high extraneous background radiation, making interpretation of the data unfeasible.

Because the texture of the samples is a fiber texture (i.e., columnar grains randomly oriented about an axis normal to the sample surface), a plot of the pole densities on a stereographic projection should be the same for any given angle of rotation about the sample normal. Thus, a texture diffractometer scan along a radial path of the sterographic projection should give intensity maxima corresponding to tilt angles at which the monitored planes [Al5(200) in this case] are reflecting. This is a modification of the Field and Merchant method of examining wire textures.[95] It was unsuccessful for the samples in this study due again to insufficient diffracted intensities of the small samples.

The author's conclusion as a result of these efforts is that pole figure analysis of diffusion layer samples can be successfully completed only if the sample size is increased.

APPENDIX 3 -- Initial Analysis of Nb_3Sn Diffusion Layers Fabricated on Polycrystalline Nb Foils

Research carried out this summer by L. D. Clark centered on X-ray analysis of Nb_3Sn diffusion layer fabricated on annealed and unannealed polycrystalline Nb foils. The current status of this work follows.

A 1.2 cm by 3.2 cm rectangular strip of commercial grade niobium was cut with scissors from a .13mm thick niobium sheet which had been neither chemically or physically processed after arriving from Wah Chang Albany Co. The strip was examined by X-ray diffractometer runs and texture diffractometer runs before and after reacting it with Sn to fabricate a ~17 μm thick layer of Nb_3Sn by the experimental procedure described in Chapter III. The texture diffractometer runs were performed on a Siemans texture diffractometer utilizing the Schulz reflection method described in Appendix 2. The resulting diffractometer scans and the Nb_3Sn (200) pole figure all indicate intense (100) [011] and (211) [110] texturing of the niobium strip. This texture is commonly found in heavily cold-rolled bcc materials.

Another 1.2 cm by 3.2 cm strip was cut from the same sheet and examined the same way as the above strip except that before fabrication of Nb_3Sn, this second strip was annealed. This anneal was done in a quartz tube at approximately 1090°C while being pumped on by a diffusion pump. After two hours, the tube was removed and quenched in room-temperature air. The resulting Nb_3Sn (200) pole

figure arising from the layer fabricated on this annealed Nb strip shows that most of the original Nb texture was removed.

Although each strip was subjected to a texture diffractometer run, there were many problems with small sample width, background counts, and geometric defocusing determinations so that the resulting pole figures are really of undetermined reliability. The cause of these difficulties is under investigation. Consequently a peak height analysis of diffractometer scans is a more reliable method for determining the actual texture of the Nb_3Sn. Peak height analysis showed that the Nb_3Sn on the annealed Nb sheet has a higher percentage of (200), (222), and (320) orientations than the Nb_3Sn on the unannealed niobium sheet. The Nb_3Sn on the unannealed niobium sheets contains a higher percentage of (211) and (321) orientations than does the Nb_3Sn on the annealed niobium sheet. These results suggest both that the natural growth direction of Nb_3Sn on annealed Nb sheet is (200) and also that Nb_3Sn (111) is more likely to grow on annealed niobium sheet than on unannealed, textured niobium sheet.

Each reacted strip was examined with an X-ray scanning diffractometer utilizing a 3° incident slit: this means that the whole strip is sampled by the X-ray beam, not just a small area. The resulting diffractometer peaks indicate that each strip contains niobium, Nb_3Sn, Nb_6Sn_5 and β-tin. The peaks also show that the unannealed strip has a higher (Nb_3Sn): (Nb_6Sn_5) ratio than does the

annealed strip. Judging from peak height, the unannealed strip's (Nb_3): (Nb_6Sn_5) ratio is approximately 2.5 to 3 times higher than that of the annealed strip.

A set of six diffractometer runs with a 0.4° incident slit were performed on the center and each end of each strip. A 0.4° incident slit samples only a small area of the strip, enabling a strip region of interest to be positioned for examination. The resulting diffractometer peaks show that the end of the unannealed strip close to the tin well during fabrication has only a small quantity of Nb_6Sn_5. (It should be noted that the unannealed strip was itself closer to the well than was the annealed strip.) Its (Nb_3Sn): (Nb_6Sn_5) ratio is higher than at the center or other end of the strip or at any place examined on the annealed strip. At the center of the unannealed strip, the (Nb_3Sn): (Nb_6Sn5) ratio is lower than at either end. The (Nb_3Sn):(Nb_6Sn_5) ratios at all three regions examined of the unannealed strip are higher than those at any region examined on the annealed strip across which the ratio is fairly constant.

No distinct variations in the (Nb_3Sn): (Nb_6Sn_5) ratio were noted on the annealed strip. This correlates with the physical appearance of the strips: the annealed strip was covered with dark-grey material from end to end, while the unannealed strip had only an area of dark-gray material on its center, less dark-grey material on the end further from the tin well, and no dark-grey material on its

end nearer the tin well. These observations indicate that the dark-grey material is most likely Nb_6Sn_5. An attempt to examine by X-ray analysis some amount of this material to confirm this conjecture was unsuccessful due to the small amount of material collected. However, the attempt pointed out that the strips also differ in the amount of effort it takes to dislodge the dark-grey material from the layer: a light touch is enough to dislodge material from the unannealed strip, but more effort, such as a surgical blade, is required to dislodge material from the annealed strip. This suggests that Nb_6Sn_5 amy be more likely to form on and adhere to unannealed niobium sheet than on unannealed, textured niobium sheet.

REFERENCES

1. J.E. Kunzler, E. Buehler, F.S.L. Hsu, J.E. Wernick, Phys. Rev. Lett. 6, 89 (1961).

2. W.A. Fietz, IEEE Trans. Magn. MAG-15, 67 (1979).

3. C.C. Koch, J. Phys. Chem. Solids 34, 1445 (1973).

4. R.D. Blaugher, R.E. Hein, J.E. Cox, R.M. Waterstrat, J. Low Temp. Phys. 1, 539 (1969).

5. J. Hanak, K. Strater, G.W. Cullen, RCA Review 25, 342 (1964).

6. P.R. Sahm, R.V. Pruss, Phys. Lett. 28A, 707 (1969).

7. B. Muhlschegel, Z. Phys. 155, 313 (1959).

8. L.R. Testardi, J.H. Wernick, W.A. Royer, Solid State Commun. 15, 1 (1974).

9. K. Hechler, G. Horn, G. Otto, E.J. Sauer, J. Low Temp. Phys. 1, 29 (1969).

10. S. Foner, E.J. McNiff Jr., T.H. Geballe, R.J. Wilkens, E. Buehler, Physica 55, 534 (1971).

11. D. Dew-Hughes, Cryogenics 15, 435 (1975).

12. S. Foner, E.J. McNiff Jr., J.R. Gavaler, M.A. Janocko, Phys. Lett. 97A, 485 (1974).

13. E.C. Van Reuth, R.M. Waterstrat, Acta. Crystallogr. B24, 186 (1968).

14. J. Muller, R. Flükiger, A. Junod, F. Heiniger, G. Susz, Low Temperature Physics - LT13, Vol. 3: Superconductivity, edited by K.D. Timmerhaus, W.J. O'Sullivan, E.F. Hammel (Plenum Press, N.Y., 1972) p. 446.

15. M. Ashkin, J.R. Gavaler, J. Low Temp. Phys. 31, 285 (1978).

16. Y. Tarutani, M. Kudo, J. Less-Com. Met. 55, 221 (1977).

17. A.H. Dayem, T.H. Geballe, R.B. Zubeck, A.B. Hallak, G.W. Hull Jr., Appl. Phys. Lett. 30, 541 (1977).

18. A.H. Dayem, T.H. Geballe, R.B. Zubeck, A.B. Hallak, G.W. Hull Jr., J. Phys. Chem. Solids 39, 529 (1978).

19. T. Ohtsuka, Anisotropy Effects in Superconductors, edited by H.W. Weber (Plenum Press, N.Y., 1977) p. 27.

20. J. Bostock, M.L.A. MacVicar, Anisotropy Effects in Superconductors, edited by H.W. Weber (Plenum Press, N.Y., 1977) p. 213.

21. E.J. Kramer, G.S. Knapp, J.Appl. Phys. 46, 4595 (1975).

22. S. Foner, E.J. McNiff Jr., Phys. Lett. 58A, 318 (1976).

23. S. Foner, E.J. McNiff Jr., Appl. Phys. Lett. 32, 122 (1978).

24. J. Boisvert, S.B. Thesis, M.I.T., Dept. of Physics, 1979, unpublished.

25. C.C. Koch, D.S. Easton, Cryogenics 17, 391 (1977).

26. A.G. Jackson, M.P. Hooker, Structure and Chemistry of Solid Surfaces, edited by G. Somorjai (John Wiley and Sons, Inc., N.Y., 1969) p. 73-1.

27. K. Togano, K. Tachikawa, R.M. Rose, J. Appl. Phys. 49, 5218 (1978).

28. K. Togano, K. Tachikawa, J. Appl. Phys. 50, 3495 (1979).

29. V. Diadiuk, Sc.D. Thesis, M.I.T., Dept. of Physics, 1978, unpublished.

30. D.S. Easton, D.M. Kroeger, IEEE Trans. Magn. MAG-15, 178 (1979).

31. S.F. Cogan, D.S. Holmes, R.M. Rose, to be published.

32. G. Arnolds, R. Blaschke, H. Piel, D. Proch, IEEE Trans. Magn. MAG-15, 27 (1979).

33. G. Arnolds, R. Blaschke, H. Piel, D. Proch, IEEE Trans. Magn. MAG-15, 613 (1979).

34. P. Kniesel, O. Stolz, J. Halbritter, IEEE Trans. Magn. MAG-15, 21 (1979).

35. P. Kniesel, H. Kupfer, W. Schwarz, O. Stolz, J. Halbritter, IEEE Trans. Magn. MAG-13, 496 (1977).

36. J. Bardeen, L.N. Cooper, J.R. Schrieffer, Phys. Rev. 106, 162 (1957); 108, 1175 (1957).

37. J.R. Schrieffer, D.J. Scalapino, J.W. Wilkens, Phys. Rev. 148, 263 (1966).

38. G.J. Eliashberg, Sov. Phys. JETP 11, 696 (1960).

39. W.L. McMillan, Phys. Rev. 167, 331 (1968).

40. W.L. McMillan, J.M. Rowell, Superconductivity, edited by R.D. Parks (Marcel Dekker, N.Y., 1969) p. 561.

41. J. Bostock, K.H. Lo, W.N. Cheung, V. Diadiuk, M.L.A. MacVicar, Superconductivity in d- and f-Band Metals, edited by D.H. Douglass (Plenum Press, N.Y., 1976) p. 369.

42. J. Bostock, V. Diadiuk, W.N. Cheung, K.H. Lo, R.M. Rose, M.L.A. MacVicar, Phys. Rev. Lett. 36, 603 (1976).

43. G. Gladstone, M.A. Jensen, J.R. Schrieffer, Superconductivity, edited by R.D. Parks (Marcel Dekker, N.Y., 1969) p. 665.

44. J.P. Charlesworth, I. MacPhail, P.E. Madsen, J. Mat. Sci. 5, 580 (1970).

45. M. Weger, J. Less-Com. Met. 62, 39 (1978).

46. J.A. Gregory, Sc.D. Thesis, M.I.T., Dept. of Mat. Sci. and Eng., 1979, unpublished.

47. A.I. Braginski, J.R.Gavaler, G.W. Roland, M.R. Danield, M.A. Janocko, A.T. Santhanam, IEEE Trans. Magn. MAG-13, 300 (1977).

48. J.R. Gavaler, M. Ashkin, A.I. Braginski, A.T. Santhanam, Appl. Phys. Lett. 33, 359 (1978).

49. H. Teichler, Anisotropy Effects in Superconductors, edited by H.W. Weber (Plenum Press, N.Y., 1977) p. 65.

50. A.M. Campbell, J.E. Evetts, Adv. Phys. 21, 199 (1972).

51. A. DasGupta, C.C. Koch, D.M. Kroeger, Y.T. Chou, Philos. Mag. B 38, 367 (1978).

52. A.J. Arko, D.H. Lawndes, F.A. Muller, L.W. Roeland, J. Wolfrat, A.T. van Kessel, H.W. Myron, F.M. Mueller, G.W. Webb, Phys. Rev. Lett. 40, 1590 (1978).

53. L.R. Testardi, R.R. Soden, E.S. Greiner, J.H. Wernick, V.G. Chirba, Phys. Rev. 154, 399 (1967).

54. M. Levinson, D. Zahradnik, R. Bergh, M.L.A. MacVicar, J. Bostock, Phys. Rev. Lett. 41, 899 (1979).

55. E. Nembach, K. Tachikawa, S. Tokano, Philos. Mag. 8, 869 (1970).

56. B.N. Kodess, V.B. Kurithzin, B.N. Tretjakov, Phys. Lett. A 37, 415 (1971).

57. B.D. Cullity, Elements of X-Ray Diffraction (Addison-Wesley Publishing Co., Inc., Reading, Mass., 1978) p. 295.

58. J.W. Matthews, Epitaxial Growth, Part B, edited by J.W. Matthews (Academic Press, N.Y., 1975) p. 560.

59. M.S. Abrahams, Crystal Growth and Characterization, edited by R. Ueda, J.B. Mullin (North-Holland Publishing Co., Amsterdam, 1975) p. 180.

60. J. Strozier, D.L. Miller, O.F. Kammerer, Myron Strongin, J. Appl. Phys. 47, 1611 (1976).

61. B.E. Jacobson, R.H. Hammond, T.H. Geballe, J.R. Salem, J. Less-Com. Met. 62, 59 (1978).

62. T. Luhman, M. Suenaga, IEEE Trans. Magn. MAG-13, 800 (1977).

63. T. Luhman, M. Suenaga, D.O. Welch, K. Kaiho, IEEE Trans. Magn. MAG-15, 699 (1979).

64. H.W. Schadler, L.M. Osika, G.P. Salvo, Mrs. V.J. DeCarlo, Trans. Met. Soc. AIME 230, 1074 (1974).

65. B. Hillenbrand, H. Martens, H. Pfister, K. Schnitzke, G. Ziegler, IEEE Trans. Magn. MAG-11, 420 (1975).

66. B. Hillenbrand, H. Martens, J. Appl. Phys. 47, 4151 (1976).

67. B. Hillenbrand, H. Martens, H. Pfister, K. Schnitzke, Y. Uzel, IEEE Trans. Magn. MAG-13, 491 (1977).

68. G. Arnolds, D. Proch, IEEE Trans. Magn. MAG-13, 500 (1977).

69. H. Pfister, Cryogenics 16, 17 (1976).

70. J.F. Bussiere, V.T. Kovacher, J. Appl. Phys. 49, 2526 (1978).

71. M. Suenaga, C. Klamut, J.F. Bussiere, IEEE Trans. Magn. MAG-13, 436 (1977).

72. J. Halbritter, Primarbericht, 08.02.02 p.010 Institut fur Kernphysik, Nov., 1978.

73. V. Diadiuk, J. Bostock, M.L.A. MacVicar, IEEE Trans. Magn. MAG-15, 610 (1979).

74. J.M. Dickey, Myron Strongin, O.F. Kammerer, J. Appl. Phys. 42, 5808 (1971).

75. J.H. Brophy, R.M. Rose, J. Wulff, The Structure and Properties of Materials, Vol.II (John Wiley and Sons, Inc., N.Y., 1964) p. 93.

76. C.F. Old, I. MacPhail, J. Mat. Sci. 4, 202 (1969).

77. B.D. Cullity, Elements of X-Ray Diffraction (Addison-Wesley Publishing Co., Inc., Reading, Mass., 1978) p. 297.

78. J. DeBroux, V. Diadiuk, J. Bostock, M.L.A. MacVicar, 3rd Conference on Superconductivity in d- and f-Band Metals, unpublished.

79. B.D. Cullity, Elements of X-Ray Diffraction (Addison -Wesley Publishing Co., Inc., Reading, Mass., 1978) p. 86.

80. B.D. Cullity, Elements of X-Ray Diffraction (Addison-Wesley Publishing Co., Inc., Reading, Mass., 1978) p. 303.

81. L.C. Skinner, R.M. Rose, Second Int. Conf. on Electron and Ion Beam Science and Technology, edited by R. Bakish (Gordon and Breach, N.Y., 1966) p. 207.

82. M.L.A. MacVicar, Sc.D. Thesis, M.I.T., Dept. of Met. and Mat. Sci., 1967, unpublished.

83. K. Lo, Ph.D. Thesis, M.I.T., Dept. of Mat. Sci. and Eng., 1975, unpublished.

84. O. Johari, G. Thomas, Techniques of Metals Research, Vol. IIA, edited by R.F. Bunshah (John Wiley and Sons, Inc., N.Y., 1969).

85. J. Yasaitis, private communication.

86. Izv. Akad. Nauk. SSSR Neorg. Mater. 7, 1490 (1971).

87. H.H. Farrell, G.H. Gilmer, M. Suenaga, J. Appl. Phys. 45, 4025 (1974).

88. ASTM Index to Powder Diffraction File, ASTM, Philadelphia, USA.

89. E. Bauer, Techniques of Metals Research, Vol. II, Part 2, edited by R.F. Bunshah (John Wiley and Sons, Inc., N.Y., 1969) p. 501.

90. F. Reif, Fundamentals of Statistical and Thermal Physics (McGraw-Hill, Inc., N.Y., 1965) p. 305.

91. J. VanderSande, private communication.

92. C.A. Neugebauer, J. Appl. Phys. 35, 3599 (1964).

93. L.G. Schulz, J. Appl. Phys. 20, 1033 (1949).

94. B.D. Cullity, Elements of X-Ray Diffraction (Addison-Wesley Publishing Co., Inc., Reading, Mass., 1978) p. 309.

95. M. Field, E.M. Merchant, J. Appl. Phys. 20, 741 (1949).